

Development of Heuristic Model-Based Predictive Control Strategies for an Institutional Net-Zero Energy Building

Emil Jalilov

A Thesis  
in  
the Department  
of  
Building, Civil and Environmental Engineering

Presented in Partial Fulfillment of the Requirements  
for the Degree of  
Master of Applied Science (Building Engineering) at  
Concordia University  
Montreal, Quebec, Canada

November 2021

© Emil Jalilov, 2021

**Concordia University**  
**School of Graduate Studies**

This is to certify that the thesis prepared

By: Emil Jalilov

Entitled: Development of Heuristic model-based predictive control strategies for an institutional net-zero energy building

and submitted in partial fulfillment of the requirements for the degree of

**Master of Applied Science (Building Engineering)**

complies with the regulations of the University and meets the accepted standards with respect to originality and quality.

Signed by the final Examining Committee:

_____	Chair
Dr. Liangzhu Wang	
_____	Examiner
Dr. Liangzhu Wang	
_____	Examiner
Dr. Mohamed Ouf	
_____	Supervisor
Dr. Andreas Athienitis	

Approved by

\_\_\_\_\_

Dr. Mazdak Nik-Bakht, Graduate Program Director

November 25, 2021

\_\_\_\_\_

Dr. Mourad Debbabi, Dean of Faculty

# ABSTRACT

## Development of Heuristic Model-Based Predictive Control Strategies for an Institutional Net-Zero Energy Building

Emil Jalilov

This thesis presents the development of heuristic model-based predictive control strategies for an institutional NZEB building archetype with the Varennes Library selected as a case study. A heuristic model-based predictive control strategy is applied to a radiant floor heating system. Depending on anticipated weather scenarios, developed near-optimal heating temperature setpoint profiles are selected. A generalized methodology for building energy model development to be used by model predictive control (MPC), demonstrating a step-by-step approach of more details addition to the model, is presented. The resulting explicit finite difference 10<sup>th</sup> order lumped parameter resistance-capacitance (RC) thermal network model is used to describe the dynamic behaviour of the building. The selected model is validated using on-site measurements.

The thesis then develops an approach for generalizing the heuristic predictive control strategies. The proposed strategy showed the possibility of 25% energy saving on an extremely cold sunny day. Another strategy emphasizing energy flexibility displaces nearly 100 % of heating power during the morning peak and approximately 80% of the heating power during the evening peak demand event once the one-day ahead notification from the utility is received. Acceptable indoor

thermal conditions recommended by ASHRAE Standard 55 are maintained under proposed strategies.

Finally, the thesis analyzes the building-integrated photovoltaic/thermal (BIPV/T) system installed in the library as a potential solution to increase energy flexibility and energy efficiency, proposes subsystem data-driven control-oriented model development and evaluates the possible enhancements of the installed system both in terms of design and control perspective.

## ACKNOWLEDGEMENTS

I want to take a moment to thank my supervisor Professor Andreas K. Athienitis for his invaluable guidance and supervision. 2 years ago, I was a kid with a dream to enter the field of sustainable energy. Still, I seemed to be in the wrong domain without a relevant degree (Petroleum Engineering). However, Professor Athienitis's trust and vision allowed me to embark on this journey. His further training and leadership enabled me to stay motivated every day, for which I can never thank him enough.

I want to thank my parents, my father and mother. I have a special bond with my father. He has been an unbelievable supporting force throughout my life; I am lucky to have a best friend, mentor, teacher, and inspirational figure in his face. My passion for everyday learning primarily stems from his successful academic path. His lessons on the rock-based foundation of dedication and hard work preached to me from a young age. The sacrifice of my mother, of course, can never be fairly appreciated.

I want to thank Dr. Jose Candanedo for involving me in an IEA EBC Annex 81 mission, which exposed me to the field's leading-edge innovators and allowed me to be part of those super exciting projects that define the industry for many years ahead.

I appreciate the financial support from NSERC/Hydro-Québec Industrial Research held by Dr. Athienitis and the technical support from Hydro-Quebec Laboratoire des Technologies de l'Energie Shawinigan research center under NSERC/Hydro-Québec IRC. Without financial support, I would never have had a chance to enter this field, which genuinely exceeded my expectations above and beyond what I could ever imagine.

I want to thank my sister and nephew for their unconditional support and good memories. I can't say I had a rough journey since I sincerely enjoyed and embraced every bit of it, and that's mainly owing to my colleagues at the CZEBS and their contagious high energy, support, different perspectives, productive and fun times in the office, which, unfortunately, was cut short with the pandemic. Special thanks go to Efstratios Rounis for the training and guidance in the Solar Simulation Lab and continuous reminding to take things slowly while staying hungry. I particularly thank Matin Abtahi for his endless enthusiasm to help everyone in the lab. Big thanks to Anna-Maria Sigounis and Anthony Maturo for their time and efforts to review my thesis.

I thank all my friends and relatives in Azerbaijan, both in Baku and in my village Ashagi Qishlaq in Nakhchivan.

# Dedication

*In the dear memory of*

*Polad Hashimov*

# Contents

<b>List of Figures</b> .....	x
<b>List of Tables</b> .....	xv
<b>Nomenclature</b> .....	xvi
<b>Chapter 1</b> .....	1
Introduction .....	1
1.1 Motivation .....	2
1.1.1 The role of Buildings in Climate Change and Grid Regulation.....	2
1.1.2 Demand-Side Energy Generation and Flexibility.....	3
1.1.3 Enhancement of energy flexibility opportunities in buildings.....	7
1.2 Objective .....	10
1.3 Thesis outline .....	11
<b>Chapter 2</b> .....	13
Literature review .....	13
2.1 State-of-the-art in the building controls .....	13
2.1.1 Rule-based predictive controls.....	15
2.1.2 Model Predictive Control (MPC).....	18
2.1.3 Research needs and methodology.....	22
2.2 Developments in BIPV/T .....	23
2.2.1 BIPV as a predecessor of BIPV/T technology.....	23
2.2.2 Historical development of BIPV/T .....	23
2.2.3 Advantages and limitations of BIPV/T.....	25
2.2.4 Thermal enhancement techniques.....	27
2.2.5 Practical applications .....	28
2.2.6 The role of BIPV/T in energy flexibility .....	29
2.2.7 Research needs and methodology.....	30
<b>Chapter 3</b> .....	31

Varennnes Library as an Institutional Net Zero Energy Building Archetype.....	31
3.1 Overview .....	31
3.2 Operational Sequence.....	35
3.2.1 Ventilation.....	35
3.2.2 Heating / Cooling.....	37
3.3 Conclusion.....	38
<b>Chapter 4</b> .....	39
Modelling methodology and heuristic MPC .....	39
4.1 Modelling approach.....	39
4.2 Numerical approach .....	42
4.2.1 State-space representation.....	42
4.2.2 Explicit representation .....	44
4.3 Physics-based approach – towards white-box modelling .....	49
4.4 Predictive control strategies .....	54
4.4.1 Prediction uncertainties and high-level controls.....	56
4.4.2 Sunny days .....	58
4.4.3 Cloudy days .....	61
4.4.4 Intermediate days and general algorithm.....	63
4.4.5 Key Performance Indicators .....	65
4.5 Results and discussion.....	66
4.5.1 Indoor thermal conditions .....	66
4.5.2 Thermal load and load shifting .....	68
4.5.3 Energy Balance and Flexibility Index.....	71
4.5.4 Preheating length analysis.....	75
4.6 Conclusion.....	76
<b>Chapter 5</b> .....	78
BIPV/T Modeling, Design and Optimization .....	78
5.1 Archetype system overview .....	78
5.2 Control-oriented model development .....	87
5.3 Design and control suggestions .....	94
5.4 Conclusion .....	99
<b>Chapter 6</b> .....	100

Conclusion.....	100
6.1 Summary and future work.....	100
6.2 Contributions.....	103
<b>References</b> .....	<b>105</b>
<b>Appendix</b> .....	<b>118</b>
A .....	118
B .....	122
C .....	123
D .....	127
E .....	128
F.....	143

# List of Figures

Figure 1-1: Power market scenario in Germany; addition of renewables and inflexible conventional power plants led to a negative power price (The Causes and Effects of Negative Power Prices, 2018). .....	4
Figure 1-2: Estimate of Quebec's average hourly electricity demand (Delcroix et al., 2014). .....	5
Figure 1-3: Varennes Library, energy system schematic (Amara, 2019). .....	8
Figure 1-4: Principles to be adopted by buildings during design and operation to maximize flexibility that building can provide to the grid (Grid-Interactive Efficient Building, 2019). .....	8
Figure 3-1: Varennes Library, exterior view (top); energy systems cross-sectional view (bottom) (Amara, 2019). .....	32
Figure 3-2: Architectural plan view with yellow area highlighting hydronic radiant slab (Dermardiros, 2020). .....	34
Figure 3-3: The mechanical layout of the supply, return and BIPV/T air streams. ....	36
Figure 3-4: Fan coil unit provides both ventilation and heating/cooling demand (left). The hydronic radiant slab is the main system for heating/cooling (right) .....	37
Figure 4-1: The variation of the area-weighted average indoor air temperature between upper and bottom zones (top); south and north zones (bottom).. .....	40
Figure 4-2: Thermal network of the library. Each zone is represented by nodes indicating wall (6 & 15), conventional slab surface (7 & 16), hydronic radiant slab surface (2 & 11), interior hydronic radiant slab (3, 4 & 12, 13), bottom of the conventional slab (8 & 17), bottom of hydronic radiant slab (5 & 14). .....	42
Figure 4-3: Simulation of the average indoor temperature with 16 <sup>th</sup> order (formally 6 <sup>th</sup> order) model represented in a state-space form. ....	44
Figure 4-4: 6 <sup>th</sup> order model, indoor air temperature simulation represented in an explicit form with nominal physical parameters. January 13, 2018. ....	45
Figure 4-5: Performance of explicitly represented 6 <sup>th</sup> order model calibrated with hybrid Surrogate Optimization + Pattern Search solvers in terms of the area-weighted average of indoor temperature. First floor (top) and second floor (bottom). Training data; January 25-26, 2018....	47

Figure 4-6: Performance of explicitly represented 6 <sup>th</sup> order model calibrated with hybrid Surrogate Optimization + Pattern Search solvers in terms of area-weighted average indoor air temperature. First floor (top) and second floor (bottom). Test data; January 3-4, 2018 .....	48
Figure 4-7: Cross-sectional view of Library with upper and lower zones considered.. .....	49
Figure 4-8: 10 <sup>th</sup> order thermal network of the library. Each zone is represented by air node (1 & 10), wall (6 & 15), conventional slab surface (7 & 16), hydronic radiant slab surface (2 & 11), interior hydronic radiant slab (3, 4 & 12, 13), bottom of conventional slab (8 & 17), bottom of hydronic radiant slab (5 & 14).. .....	51
Figure 4-9: Performance of models in terms of average zone air temperature over a typical very cold sunny day in Montreal ( $T_{\text{outside}} < -10^{\circ}\text{C}$ ). January 26, 2018.....	52
Figure 4-10: Performance of 10 <sup>th</sup> order model in terms of average zone air temperature over three typical very cold days. 23-25 January, 2018.....	53
Figure 4-11: High-level control algorithm for very cold days. Initial one-day ahead weather prediction is verified through PV generation at 9 am and at noon. ....	57
Figure 4-12: Near-optimal heating setpoint profile on a sunny day to maximize energy flexibility (top) and energy efficiency (bottom).. .....	59
Figure 4-13: Near-optimal heating setpoint profile on a cloudy day to maximize energy flexibility (top) and energy efficiency (bottom). ....	62
Figure 4-14: Near-optimal heating setpoint profile on a semi-cloudy day to maximize energy flexibility (top) and energy efficiency (bottom). ....	63
Figure 4-15: Low-level control algorithm of selection near-optimal setpoint profile on very cold days. Ramp # indicates the slope. ....	64
Figure 4-16: Control architecture with supervisory control feeding temperature setpoint into the local control loop. ....	64
Figure 4-17: Indoor air temperature on a sunny day under proposed and current control strategies .....	67
Figure 4-18: Indoor air temperature on cloudy (top) and semi-cloudy days (bottom) under proposed and current control strategies. ....	68
Figure 4-19: Thermal loads under proposed and current (measured) control strategies on very cold days. ....	69
Figure 4-20: Thermal load during peak and off-peak demand periods on sunny days.....	70

Figure 4-21: Thermal load during peak and off-peak demand periods on semi-cloudy days. ....	70
Figure 4-22: Thermal load during peak and off-peak demand periods on cloudy days. ....	71
Figure 4-23: Energy balance on a very cold sunny day under proposed energy flexibility strategy; PV production, electrical heating load (top); resultant imported power (bottom); January 26, 2018.....	72
Figure 4-24: Energy balance on a very cold sunny day under proposed energy efficiency strategy; PV production, electrical heating load (top); resultant imported power (bottom); January 26, 2018. ....	73
Figure 4-25: Resultant BEFI % for all 9 cases under energy flexibility strategy. ....	74
Figure 5-1: BIPV/T layout on the south-facing roof of the Varennes Library. ....	79
Figure 5-2: Mechanical arrangement of the BIPV/T and AHU.....	79
Figure 5-3: Cross-sectional view of the air stream from BIPV/T. Air from BIPV/T either enters the AHU or exhausts outside .....	80
Figure 5-4: Direct Normal Irradiance and wind velocity on February 5 (top) and March 20 (bottom).....	81
Figure 5-5: Daily fan state, BIPV/T outlet and outside temperature (°C) on February 5 (top) and March 20 (bottom). ....	82
Figure 5-6: Total ventilation, BIPV/T flowrate (L/s) and average velocity over the channel (m/s) on February 5 (top) and March 20 (bottom). ....	84
Figure 5-7: Temperature of mixed air from BIPV/T outlet and outdoor air before and after passing through thermal wheel (°C) on February 5 (top) and March 20 (bottom). ....	85
Figure 5-8: Heat recovered by the BIPV/T and thermal wheel (kW), heat added to bring the ventilation air to indoor air temperature (kW) and thermal efficiency of the BIPV/T on February 5 (top) and March 20 (bottom).....	86
Figure 5-9: RC thermal network representing the PV later, air channel beneath it and back surface insulation. ....	87
Figure 5-10: Comparison of outlet temperature predictions with different exterior convective heat transfer coefficient correlations with the actual data. ....	91
Figure 5-11: Channel air temperature rise on two consecutive days with variable wind speed but similar irradiance intensity. The impact of wind speed on outlet temperature can be observed..	92

Figure 5-12: Performance of regressive control-oriented model in predicting outlet air temperature from BIPV/T on a test set over four consecutive days. 23-27 January, 2018..	94
Figure 5-13: Alternative design configurations in terms of BIPV/T area coverage.	95
Figure 5-14: The resulting flowrate (L/s) of all cases. “half”, “full” in the legend bar imply the BIPV/T portion of the roof coverage. “T”, “occ” indicate temperature-based control (Strategy 2) and occupancy + temperature-based control (Strategy 1) respectively. 18-19 January, 2018	97
Figure 5-15: The resulting BIPV/T outlet temperature (°F) of all cases. “half”, “full” in the legend bar imply the BIPV/T portion of the roof coverage. “T”, “occ” indicate temperature-based control (Strategy 2) and occupancy + temperature-based control (Strategy 1) respectively. 18-19 January, 2018	97
Figure A-1: 3D model of the Varennes Library built in Sketch-up	118
Figure A-2: Effect of removal of internal wall partition between east and west portions of the envelope on the heating load in the 1-week winter period	119
Figure A-3: Air-source heat pump selection based on heating and cooling loads	119
Figure A-4: Air damper control strategy of the air HP	120
Figure A-5: Performance of air-source HP on 21st February	120
Figure A-6: Power consumption on Summer period with ASHP and the studied effect of motorized shading	121
Figure B-1: Thermal slab; thickness 12.5 cm; thermal load 1011 kWh; T <sub>ambient</sub> ~ -15 – -20 °C	122
Figure B-2: Thermal slab; thickness 8 cm; thermal load 792 kWh; T <sub>ambient</sub> ~ -15 – -20 °C	122
Figure C-1: Energy balance over very cold semi-cloudy day under proposed controls strategies, January 13, 2018	123
Figure C-2: Energy balance over very cold -cloudy day under proposed controls strategies, January 3, 2018	123
Figure C-3: Energy balance over a cold cloudy day under proposed controls strategies, February 10, 2018	124
Figure C-4: Energy balance over cold semi-cloudy day under proposed controls strategies, February 1, 2018	124
Figure C-5: Energy balance over a cold sunny day under proposed controls strategies, February 12, 2018	125

Figure C-6: Energy balance over a mild sunny day under proposed controls strategies, February 26, 2018.....	125
Figure C-7: Energy balance over a mild semi-cloudy day under proposed controls strategies, January 20, 2018 .....	126
Figure C-8: Energy balance over a mild semi-cloudy day under proposed controls strategies, February 20, 2018 .....	126
Figure D-1: Bottom floor-zone details model in Modelica .....	127
Figure D-2: Whole-building level model comprised of two zones and detailed solar irradiance calculations .....	127

# List of Tables

Table 4-1: Parameters identified with hybrid Surrogate Optimization + Pattern Search algorithms. ....	46
Table 4-2: Statistical indices showing model validation against area-weighted average zone air temperature. ....	52
Table 4-3: Resultant control scenarios due to weather prediction uncertainty in the form of a selection matrix. Off-diagonal entries represent an error in the initial prediction. Very cold days are assumed.....	58
Table 4-4: BEFI index in kW electrical load under proposed control strategies. % indicates the BEFI relative to the reference average power demand.....	74
Table 4-5: BEFI at different preheating lengths alongside daily energy consumption, January 3, 2018.....	75
Table 5-1: Alternative design configuration cases of BIPV/T.....	95
Table 5-2: Performance of suggested 8 alternative cases in terms of total recovered heat, useful heat and flowrate. Useful heat assumes heat extracted above 20°C.....	98

# Nomenclature

## Symbols

$T_a$	Inside air temperature, °C
$T_f$	Floor surface temperature, °C
$C$	Thermal node capacitance, J/K
$U$	Conductance, W/K
$PV_{\text{produced}}$	Generated power from PV, kW
$PV_{\text{clear sky}}$	Projected power from PV on clear sky conditions, kW
$c_i$	Clustering group
$Z_i$	Representative vector for types of day obtained from the k-means algorithm
$P_{\text{ref}}$	Average power demand at time $t$ over period $Dt$ under reference strategy. kW
$P_{\text{flex}}$	Average power demand at time $t$ over period $Dt$ under energy flexibility control strategy, kW
BEFI	Mean energy flexibility index at time $t$ over period $Dt$ , kW
BEFIP	Average power reduction relative to the reference, %
$\text{Import}_{\text{measured}}$	Measured imported power to the library from the grid under current control strategy, kW
$\text{Import}_{\text{new}}$	Resultant imported power from the library to the grid under proposed control strategy, kW
$\text{Load}_{\text{measured}}$	Electrical load of the library under the current control strategy, kW
$\text{Load}_{\text{new}}$	Electrical load of the library under the proposed control strategy, kW
$\text{Export}_{\text{measured}}$	Measured exported power to the grid from the library under current control strategy, kW
$T_{\text{outlet}}$	Outlet temperature from BIPV/T, °C

$T_{\text{return}}$	Temperature of the return airstream, °C
$T_{\text{mix}}$	Temperature of the mixture of air from BIPV/T and unconditioned outside air
$Q_{\text{air}}$	Heat gained by air in while passing through the channel of BIPV/T, kW
$\dot{m}$	Mass flowrate of air through the channel, kg/s
$c_p$	Specific heat capacity, J/(K kg)
$T_{\text{exit}}$	Outlet temperature of the air from the BIPV/T channel, °C
$T_{\text{in}}$	Inlet temperature of the air, °C
$S_{\text{PV}}$	Total heat gained by the PV surface, kW
$A$	Area of the PV layer, m <sup>2</sup>
$\sigma$	Stefan-Boltzmann constant, $5.67 \times 10^{-8} \text{ W/m}^2 \text{ K}^4$
$T_{\text{PV}}$	Average PV layer temperature, °C
$T_{\text{ins}}$	Insulation surface temperature in BIPV/T, °C
$T_{\text{amb}}$	Ambient air temperature, °C
$h_{\text{amb}}$	Convective heat transfer coefficients between ambient and PV surface, W/K m <sup>2</sup>
$h_{\text{top}}$	Convective heat transfer coefficients between top surface of the channel and flowing air in the channel, W/K m <sup>2</sup>
$\epsilon_{\text{PV}}$	Total hemispherical emissivity of PV surface
$\epsilon_{\text{ins}}$	Total hemispherical emissivity of insulation

L	Characteristic length of the flow, the diameter of the pipe, m
k	Thermal conductivity of the air, W/K m
Re	Reynolds number
Pr	Prandtl number
$\hat{y}(t)$	Output variable
$v_{\max}$	Maximum speed of the fan, m/s

## Acronyms

AC	Air conditioning
AHU	Air handling unit
ANN	Artificial neural network
ASHRAE	American Society of Heating, Refrigerating and Air- Conditioning Engineers
BAS	Building Automation System
BEPSTN	Building energy performance simulation tool
BIPV	Building-integrated photovoltaic
BIPV/T	Building-integrated photovoltaic/thermal
BMS	Building Management System
BOPTST	Building Optimization Performance Test
CV (RMSE)	Coefficient of variation of the root mean squared error
DALI	Digital addressable lighting interface
DR	Demand response
EBC	Energy in Buildings and Communities
ECM	Electronically commutated motor
EV	Electric vehicle
FCU	Fan-coil unit
FVM	Finite Volume Method

GHG	Greenhouse gas
GSHP	Ground-source heat pump
HVAC	Heating, ventilation and air conditioning
IEA	International Energy Agency
IRENA	International Renewable Energy Agency
KPI	Key performance indicator
LEED	Leadership in Energy and Environmental Design
MPC	Model predictive control
NZEB	Net-zero energy buildings
ODE	Ordinary differential equation
PCM	Phase Change Material
PID	Proportional–integral–derivative controller
PV	Photovoltaics
PV/T	Photovoltaic/thermal
RBC	Rule-based control
RC	Resistance-capacitance
RES	Renewable energy sources
RL	Reinforcement learning
RTP	Real-time prices
SNEBRN	Smart Net-Zero Energy Buildings Research Network
SS	State-space
SWN	Support-vector networks
TES	Thermal Energy Storage
UFAD	Underfloor air distribution
UNEP	United Nations Environment Programme
UTC	Unglazed transpired collector
VAV	Variable air volume
VDC	Variable direct current

# Chapter 1

## Introduction

In the last decade or so, the confluence of the demand for innovation with the necessity for significant reductions in energy usage and greenhouse gas (GHG) emissions in the construction industry altered the way buildings and their energy systems are perceived. The pursuit of an integrated design approach, more efficient envelope and lighting heating, ventilation and air conditioning (HVAC) systems, mass installation of on-site renewable technology, more stringent energy codes, and the emergence of green building certification programs are evidence of this. Nowadays, buildings and grids are independently pushing various energy efficiency innovations; nevertheless, these initiatives are not well integrated enough to fully exploit the new prospects. Combining and managing a varied set of demands from both the building and the local utility requires more controlled, adaptable, and integrated building operations. Many electrical loads in buildings may be handled flexibly and can be regulated to run at specified times and varying output levels using advanced controls. The capacity to implement more complex continuous energy management solutions at the building level can assist utilities in addressing peak demand issues, which are becoming increasingly significant. Therefore, this thesis proposes moving beyond simple grid-integration techniques (such as demand response) to create integrative solutions that result in substantial long-term savings for building owners, grid operators, utilities, and other stakeholders without compromising occupants' comfort.

The reasons for greater demand-side engagement in electric grid operation, the routes via which this may occur, and the role buildings can play are all covered in the introduction chapter.

Following the motivation, the introduction concludes with the thesis' general objectives and structure of this thesis.

## **1.1 Motivation**

### **1.1.1 The role of Buildings in Climate Change and Grid Regulation**

Scientific evidence supporting the occurrence of shifts in global climate trends has accumulated over the previous century. Still, data collected in the last 25 years demonstrates that we are amidst a rapid and globally happening movement toward increasing average temperatures (Houghton et al., 2015). The building industry is the largest source of worldwide greenhouse gas (GHG) emissions; buildings consume around 40% of global energy and produce roughly 30% of GHG emissions (LEED, 2014). If current trends continue, these emissions are expected to double by 2050. (UNEP, 2019). Though statistics vary per building, studies show that over 80% of greenhouse gas emissions occur during the operational phase of buildings to fulfill different energy demands such as air conditioning and lighting, but especially space heating (IEA, 2020). Several measures are being taken in the right direction, even though present policies lack ambition for climate change mitigation to the desired targets. At the international level, the Paris agreement reached at the end of the Conference of the Parties' 21st meeting in 2015 resulted in the framework of an overarching plan of action (UNFCCC, 2015). On 16 November 2020, the Quebec government adopted the 2030 Green Economy Plan (PEV 2030), according to which \$6.7 billion are going to be invested in building and transportation sectors over the next five years targeting the GHG emissions (2030 Plan for a Green Economy, 2020). But it will not be enough. As indicated by its implementation plan, the envisaged results will reduce emissions by just 12.4

million tons (Mt) of the 29 Mt that should be eliminated annually to reach the target of 37.5% under the 1990 level in 2030. It will therefore be necessary to do much more from 2021 to achieve our targets. To do more, building owners must comprehend their buildings' value proposition. There is a necessity for analysis based on reliable data; however, achieving this task has become a challenge in recent years due to federal changes in Canada that impose limitations on the availability, frequency of publication and access to specific critical energy data. Statistics Canada recognizes the challenges present with the data and actively collaborates with its partners to identify possible solutions. Ultimately, a reform of the Statistics Act will need to be carried out to correct these gaps (The state of energy in Quebec, 2021).

### **1.1.2 Demand-Side Energy Generation and Flexibility**

In many countries, renewable energy sources (RES) are growing with the widespread demand for electrification. Hydropower already plays a crucial role in adopting renewable energy in several regions, such as Quebec. Still, it is geographically confined to a few locations where it is already primarily utilized. Solar and wind power are the fastest-growing RES sectors today due to significant cost reductions that have made them cost-competitive with the other fossil or nuclear fuels, resulting in their rapid adoption (IRENA, 2018). However, on the other hand, their intrinsic intermittency poses particular challenges to the grid's stability, increasing supply volatility. Indeed, these two power sources are highly dependent on climatic circumstances, which leads to a mismatch between fluctuating supply and demand when the use of renewable energy sources is widespread. Installing small-scale PV panels or windmills and injecting electricity into the grids allows buildings to affect the energy exchange of the grid and become prosumers. However, the electricity network was not designed to handle unpredictable power flows, and this might cause system congestion. The most famous example of this issue is

California's “duck curve” (Lawrence Berkley National Laboratory, 2017). The impacts of high penetration of renewable energy sources (RES) were also observed in Germany where, according to New York Times (Reed, 2017), the negative pricing due to excess renewable energy supply occurred over 100 times per year in 2017 (Figure 1-1).

In such circumstances, curtailment of RES is a simple and common remedy, although it essentially consists of squandering free available energy resulting in economic and zero-carbon electricity losses.

Going back to the challenges of integrating renewable energy, besides the surplus, the intermittent nature of these sources also means that the output may be inadequate to meet the

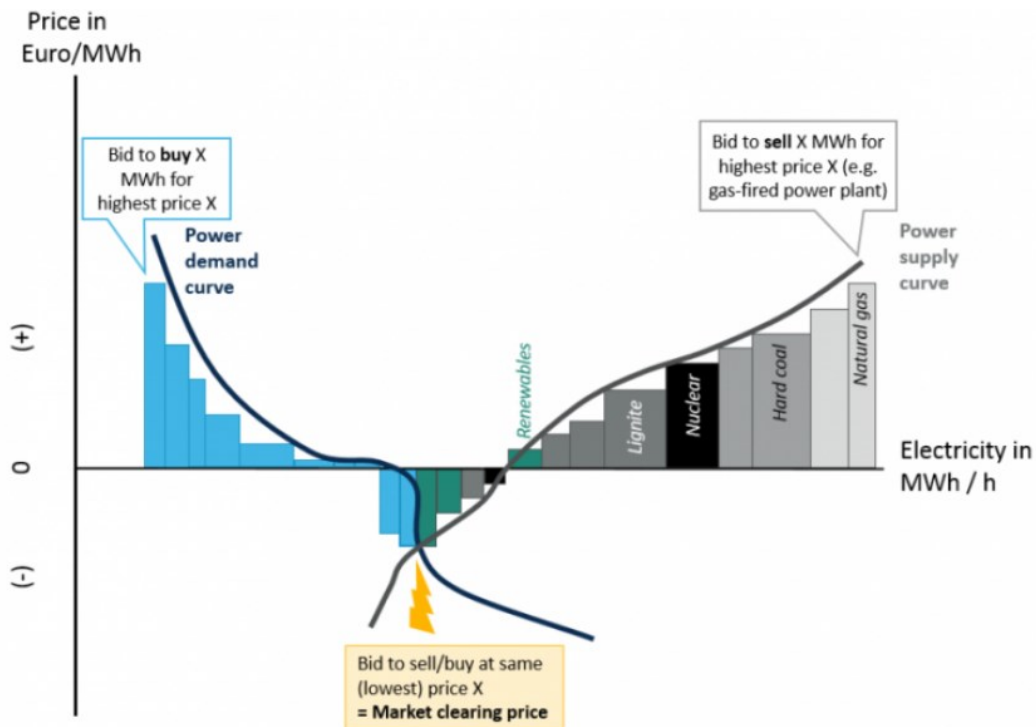


Figure 1-1: Power market scenario in Germany; addition of renewables and inflexible conventional power plants led to a negative power price (The Causes and Effects of Negative Power Prices, 2018).

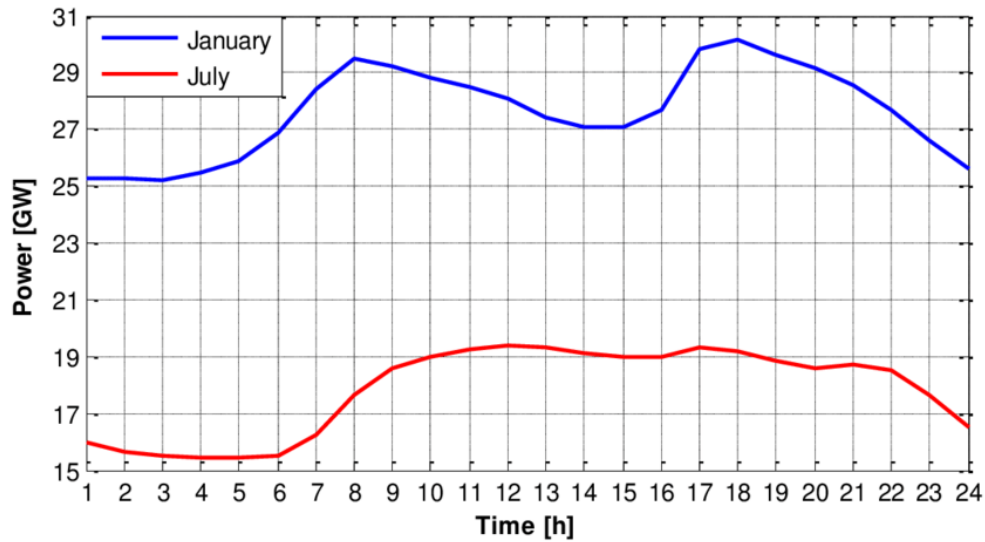


Figure 1-2: Estimate of Quebec's average hourly electricity demand. (Delcroix et al., 2014).

demand, necessitating additional peak power units. These facilities must be easily dispatchable, and their primary energy source is usually natural gas or nuclear. Such peak power facilities must be kept operational all year to ensure that their power capacity is available when solar and wind power output is not enough. Some financial issues arise due to their profitability: they would only be used for a few hours per year when the RESs are not accessible. Or, if the significant baseload power production is nuclear, such as in Ontario or California, it can be challenging to modulate its supply.

The two peak demand periods for the grid in Quebec are shown in Figure 1-2 above. There are several potential solutions to address the mismatch of power generation by RES and building demand. Opportunities exist from both the utility side and consumer side. Exhausting excess generated energy to restore the plant's stability, as discussed above, might not be the optimal solution. To compensate for a shortage of renewable energy output, grid-side flexibility can be used, but it does not make financial sense to maintain those plants only for a little time of use. Building/upgrading new power plants and transmission lines can be economically not warranted either. However, expanding transmission lines to exchange energy between the countries of

different weather conditions (and consequently different available renewable energy sources) is a promising solution for the future. There are ongoing talks between the countries to overcome the political and technical barriers. Electricity surplus can be stored for later use, where batteries, thermal storage, hydrogen systems and aqueous reservoirs are popular solutions. However, these solutions remain not cost-effective, and significant research breakthrough is required for their profitability. Now, what about the flexibility from the prosumer, such as, building side?

Buildings are essential to energy management since they constitute approximately 40% of the total end-use of energy globally and 32% in Quebec (The state of energy in Quebec, 2021).

In recent years, a substantial amount of research has focused on improving the flexibility of buildings through optimal controls and demand management. One of those is the proposal of the new research annex by the International Energy Agency's (IEA) Energy in Buildings and Communities (EBC) Program "Annex 67 — Energy-flexible buildings". Experts in this project described buildings' energy flexibility as the “capacity to regulate their requirement and generation under local climatic circumstances, user demands and network requirements” (IEA, 2017). Various aspects of a building can be considered as a source of flexibility. Thermal mass, such as gypsum board or a thick radiant floor, can act as passive thermal storage and be utilized to shift the energy demand without impacting indoor thermal comfort significantly. Onsite renewable energy generation sources, such as solar systems, must be addressed as well, both in terms of design and operation and finding synergies with ventilation, heat pumps, and thermal storage systems. Electric vehicles and batteries can also provide the building's energy flexibility. Furthermore, the Building Management Systems (BMS) for commercial buildings provide coordinated, supervisory management of all systems in the building, allowing for effective demand management while providing adequate services to occupants and guaranteeing system

functioning within operating constraints. Consistent model development must be deployed to assist in estimating potential energy flexibility available to the grid from buildings (Date et al., 2020).

### **1.1.3 Enhancement of energy flexibility opportunities in buildings**

Buildings can provide considerable flexibility services to the grid by an integrated design and control of their thermal and electrical energy systems. Given that buildings are the highest energy consumers globally, the trend for enhancing energy flexibility in the building sector is rising. Considering the general issue of global warming and energy conservation, more and more incentives and programs are being proposed to promote the construction of high-performing buildings that achieve nearly Zero Energy Buildings (nZEB) or Net-Zero Energy Building (NZEB) status, which implies a net-zero energy consumption in a yearly balance. While these buildings are designed to be energy-efficient and require much less energy import from the grid than traditional buildings, given the generation and storage systems integrated within their design, they are also potentially a significant source of energy flexibility. The majority of zero energy buildings have some form of energy storage in the form of active, passive thermal systems or/and batteries, on-site renewable generation systems such as solar power, wind power and bioenergy; efficient HVAC systems such as heat pumps and heat recovery and Building Automation Systems (BAS) which allow implementation of sophisticated control logic, data collection and remote control. One of such typical buildings studied in this thesis as an archetype example is the Varennes Library – the first institutional Net-Zero Energy Building in Canada. The library, inaugurated in 2015 and located in Varennes, Quebec, Canada, comprises the majority of technologies discussed above, some of which, as shown in Figure 1-3 below, serves as an excellent archetype for non-residential buildings with similar performance.

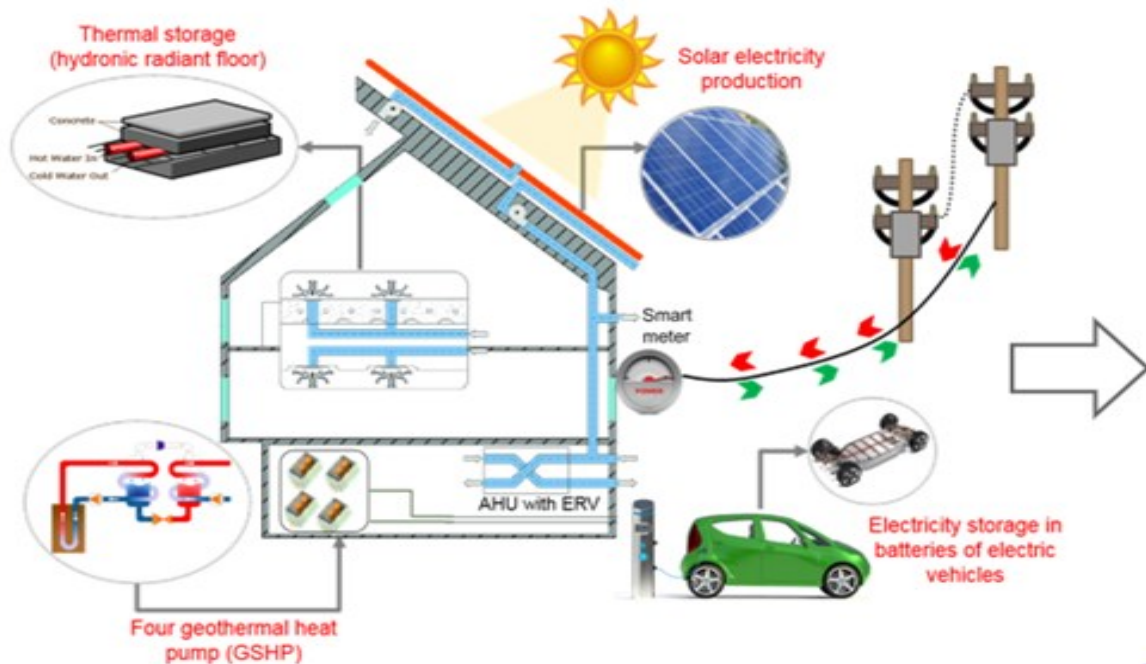


Figure 1-3: Varennes Library's energy system schematic (Amara, 2019).

The building is described in detail in Chapter 3, but it is worth noting it comprises building-integrated photovoltaic/thermal (BIPV/T) and building-integrated photovoltaic (BIPV) for electricity and heat generation, passive and active thermal storage in the form of the concrete floor exposed to south-oriented windows, radiant hydronic pipes embedded in the floor structure, electrical storage through 2 EV charging stations, ground source heat pump (GSHPs) for heating/cooling and operable windows for free cooling and more. These are only the potential

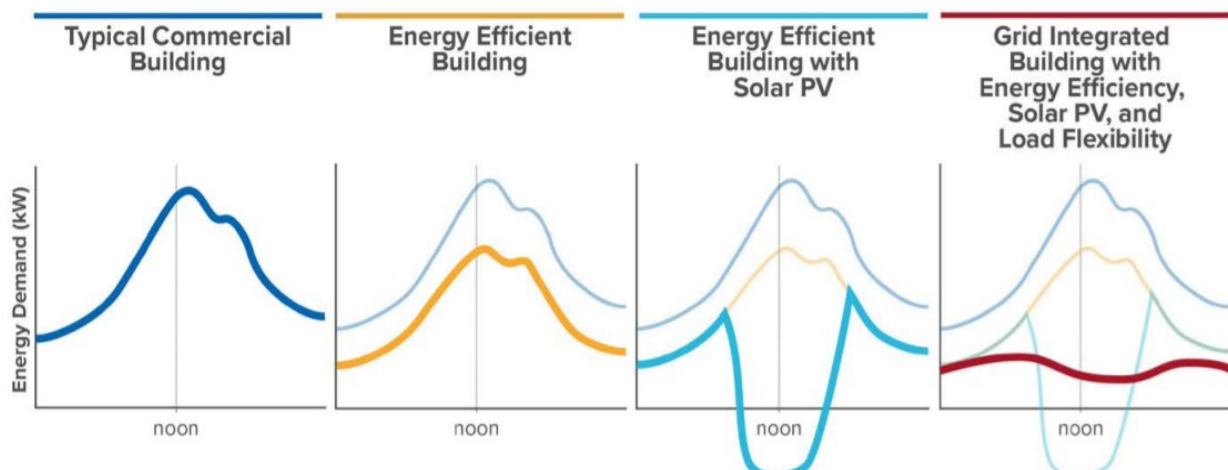


Figure 1-4: Principles to be adopted by buildings during design and operation to maximize flexibility that building can provide to the grid (Grid-Interactive Efficient Building, 2019).

sources of energy flexibility, and optimal operation with further design enhancements are required to activate and maximize that potential.

There are three step-by-step principles, as shown in Figure 1-4, that building owners and utilities must undertake to conserve energy and to enhance the energy flexibility in buildings:

- 1) Design an energy-efficient building. Reduction of energy consumption and demand charges requires considering the building as a whole integrated system utilizing the advantages of the surrounding nature from the concept design phase and integrating the storage in its structure.
- 2) Adding on-site intermittent renewable energy generation sources. Solar PV is the most popular option, it reduces loads around noontime, but it also leads to steep load ramping and grid modulation issues. In cold climates like Quebec, peak energy demand occurs when solar energy is not available. Simply installing rooftop solar panels does not provide many benefits, if not creates more problems to the grid unless step 3 is undertaken.
- 3) The net load curve is successfully flattened by shifting load to periods of high renewable energy supply, as shown in Figure 1-4, resulting in a reduced daily peak and a more consistent demand profile. A smoother demand profile with less daily peaks implies that a surge in demand above reference loads would be smaller and have less impact on the grid. Lower peak demand means less frequent use of inefficient, expensive, and polluting power plants. Load matching alongside other techniques adjusts building loads to match generation, smoothing peak loads. It improves energy efficiency and reduces demand charges while ensuring grid stability and resilience. Having the capacity to respond to demand during grid peak scenarios generates additional income.

The Varennes Library, selected as an institutional NZEB archetype for this study, is currently implementing the first two principles of an energy-efficient design and generation; this thesis will mainly focus on the application of the last principle to increase the energy flexibility of the building through predictive controls and design.

## 1.2 Objective

The discussion above highlights the need for optimal operation in buildings to exploit the possible sources of flexibility. We must establish a coordinated power usage strategy. This coordination must consider future or anticipated demands, flexibility availability, and restrictions, which may vary depending on tenant activity, schedules, weather and a grid's state. Most research proposes solutions through model predictive controls to achieve an optimal integrated operation, especially in complex structures with a large quantity of integrated thermal storage (Vallianos et al., 2019; Finck et al., 2019; Saberi & Athienitis, 2021). The common practice to reduce the peak demand in urgent situations in buildings is the demand response (DR) strategy, which is an expertise-driven rule-based technique. However, when considering such strategies, several challenges arise, each with its own set of obstacles to resolve. Thus, this thesis aims to quantify and utilize the energy flexibility potential of institutional/commercial buildings that can be provided to the grid based on an institutional Net-zero energy building (NZEB) archetype example through predictive controls by resolving issues of modelling and limited availability of data. The objectives can be summarized as follows:

1. Develop and validate a generic step-by-step control-oriented modelling methodology that is fast to develop to estimate the building's indoor air and concrete slab temperature.

2. Develop a heuristic MPC methodology to maximize energy efficiency and/or the flexibility potential of the library, where the latter aims to reduce the demand during the two daily peak winter periods for the grid in Quebec.
3. Design and control study of enhancing the energy efficiency of the building through a BIPV/T system.

## 1.3 Thesis Outline

The thesis is structured in chapters in the following way:

**Chapter 1** briefly introduces the role of buildings in climate change, the downsides of taken initiatives, the challenge of obtaining the data, and the concept of energy flexibility concerning building-grid interaction.

**Chapter 2** consists of two parts. The first part reviews the literature and current state-of-the-art control methods tailored to the need for predictive control and energy flexibility. The second part examines the current knowledge and developments in the BIPV/T systems as a possible solution to increase energy flexibility in buildings, their large-scale application and the existing challenges towards wide-scale adoption. Both parts of the literature review wrap up with the research needs and methodology.

**Chapter 3** describes the institutional NZEB archetype, its role in providing energy flexibility services to the grid, and the steps required to achieve it. Key architectural and mechanical features, as well as operational sequences, are also overviewed.

**Chapter 4** introduces the step-by-step approach for model development of institutional NZEB for heuristic predictive control strategies. The methodology is generic and can be applied to other buildings with significant thermal mass. This is followed by the introduction and development of

the heuristic MPC control strategies with an objective to maximize energy flexibility and/or energy efficiency. Performance of different scenarios is analyzed and compared with the baseline data.

**Chapter 5** starts with a detailed overview of the BIPV/T system, its mechanical integration with AHU and controls. Exploratory data analysis is performed based on an example of two typical clear days. Then control-oriented data-driven modelling of the BIPV/T is introduced for whole-building and subsystem MPC, followed by the evaluation of alternative design and control options.

**Chapter 6** concludes with the final remarks, the contribution of this thesis and direction towards expected future work.

# Chapter 2

## Literature review

Energy flexibility studies at the whole building scale can be separated into two phases: design and operation. During the design stage, the general objective is modelling and parametric design analysis to achieve the best synergies between the generation and storage systems and a building design. Maximizing energy flexibility at the operational phase includes predictive control strategies evaluations. These strategies can be optimal or heuristic, model-based or model-free and be implemented online or offline.

The literature review consists of two major parts, each concluding with its own research needs and methodologies. The first part covers the operational phase to address the energy flexibility in buildings through predictive control practices and demand-side management. The second part deals with the flexibility at the design phase, covering the design, thermal enhancements and large-scale applications of BIPV/T systems, which besides the generation of electrical energy, provides energy flexibility through the generation and in-place storage of thermal energy.

### 2.1 State-of-the-art in the buildings control

The control functions in the building system can be divided into two parts: local level and supervisory level. Local controls' fundamental and automation tasks enable the building systems to work correctly and offer appropriate services. Local control may be further split into two divisions being process control and sequencing control. While sequencing control determines the logic of which the system components should operate (such as open outdoor air damper when the

fan is energized, shut off the valve when the fan is off, timeclocks, and so on), process control modifies the controlled variables to achieve specified process objectives. Most of the existing building process control algorithms are based on simple feedback loops; once the error signal is detected, that is, when the measured output (feedback) deviates from a reference value, corrective action is taken (PID controller). The control action of these local controllers is inherently reactive, configured to provide an adequate minimal service by following the provided setpoints and usually, are not optimal or energy efficient. The majority of large commercial and institutional buildings are slow-responding systems accommodating concrete slabs, electrical and thermal storage systems and other technologies with significant time constants where reactive controls fail (Dermardiros, 2020).

Supervisory control is responsible for the overall system monitoring and control of the local subsystems. It aims to reduce or maximize an objective function by selecting variable values within acceptable ranges directly. Supervisory control of building systems strives to provide pleasant interior comfort and a healthy indoor environment with the least energy input or running cost possible, considering the constantly changing indoor and outdoor conditions and pricing schemes and demand charges. From a supervisory control point of view, there is a need for control strategies that can use the building's thermal inertia to increase energy flexibility. Incorporating weather and occupancy behaviour prediction patterns can help to take preventative measures to maximize energy efficiency and flexibility.

Most buildings nowadays utilize rudimentary rule-based control techniques (RBC), which provide limited energy efficiency (Privara et al., 2013). However, the uprise of the digital age provides increased opportunities in computation and data collection, unleashing the potential application of complex control strategies, such as model predictive control (MPC) (Athienitis,

A., & O'Brien, W. 2015). MPC has been a dominating control methodology in research on smart buildings in the previous decade. While RBC and MPC have their own merits, they come with limitations discussed in the following sections.

### **2.1.1 Rule-based predictive controls**

The use of rules and heuristics-based expertise and best practices can be used to derive easy-to-apply supervisory control strategies. It is common practice in the BAS to develop a series of if-then-else rules to implement near-optimal operating points for the system. RBC techniques are usually realized by manipulating temperature setpoint or schedule, such as pre-conditioning, optimal start/stop, temperature reset for supply air, and so on. Albeit rule-based approaches are simple and can find only near-optimal operation points, they can achieve a substantial energy efficiency if correctly applied (Mařík et al., 2011). Besides the ease of practical implementation, the other advantages of RBC are logic with a distinct physical meaning and flexibility to be modified for a specific sub-type of the system component. Furthermore, if a rule cannot be used owing to a lack of sensors, a simpler rule (requiring simpler or virtual sensors) can be applied. However, customized solutions are implemented on a project-by-project basis, with methodology needed to make them more general and reproducible.

The rule-based approach is typically used to compute better setpoints and/or better scheduling (optimal start/stop, pre-cooling, and so on.). When the building operators aim to attain a particular objective beyond comfort, they generally specify specific goals to achieve. These targets are not usually clearly defined in RBC, but an implicit objective can be determined most of the time.

The most common form of rule-based control to maximize energy flexibility is expertise-derived load shifting with fixed scheduling. For example, Carvalho et al. (2015) turned off a heat pump

over peak heating hours from 9:00 to 10:30 and from 18:00 to 20:30, saving up to 34 % on energy costs. Lee et al., (2015) modulated set points during peak evening demand hours, reducing the energy consumption by 80 % in cooling and 64 % in heating during that period. De Cornick et al. (2013) used RBC schedule to charge a thermal energy storage tank optimally. Given that heat pumps operate more efficiently when the source and sink temperatures are closest, he charged the tank with a heat pump from 12:00 to 19:00, including raising setpoint until 16:00 and achieved better results than other standard expertise-based controls. Rule-based controls were also used for peak shaving strategies in several studies (Dar et al., 2014; de Salis et al., 2014; Halfmann et al., 2017; Hida et al., 2010; Lu et al., 2021; Moghimi et al., 2016). In these instances, the building's power transaction with the utility is tracked, and power import and export cutoff can be set. When the thresholds are exceeded, the controller acts to halt or activate the operation of the specific parts, such as mechanical systems, batteries and others, in order to keep peak demand below the predetermined level. In a NZEB with a photovoltaic system, for example, Dar et al., (2014) established an import restriction of 2.5 kW and an export limit of 5 kW, whereas (De Coninck et al., 2010) proposed alike “grid-load” approach with 3.5 kW import and export cutoff. Some control techniques are aimed at lowering end-user energy expenses. These techniques, in general, rely on time-varying energy costs, with the controller aiming to operate energy-consuming equipment during low-price times or avoid them during high-price ones. Identification of the low and high-price thresholds is one of the most critical aspects of these RBC methods. Schibuola et al., (2015) used a predictive rule-based approach, where based on the forecasted electricity price for the next 12 hours, a controller responded to the price. He achieved cost savings of around 15%. Clauß et al., (2019) studied three rule-based predictive control strategies to reduce cost, CO<sub>2</sub> and energy usage during peak demand hours in a

lightweight timber residential building in Norway. He reported that in all three cases, the potential cost savings for the proposed strategies were outweighed by the increased heating electricity usage. The schedule-based control, where the temperature setpoint was raised for heating 3 hours before the peak demand, proved to be the most efficient strategy for load shifting.

A model-based approach was presented by Athienitis et al., (1988), who developed a predictive control algorithm for heating massive buildings with high solar gains in the frequency domain. The amplitude of a half-sinusoidal curve for solar radiation and the amplitude of a sinusoidal curve for temperature were determined using temperature and clearness index predictions for the following days. These predictions were then applied to the building's linear model. Five different setpoint ramps were developed, and the one that provided the least energy consumption was selected for the day.

While RBC is relatively simple to develop, it does not consider weather and occupancy behaviours predictions in most cases. They are usually model-free and rely purely on supervisory control expertise. Therefore, it is challenging to guarantee that the comfort constraints on the control output will always be maintained. An expert system is used as a supervisory controller may identify energy-efficient or cost-effective control settings for a near-optimal HVAC system operation based on the current working conditions. These energy or cost-effective control settings are discovered using a mix of knowledge-based rules and data from BAS. An expert system's knowledge base is generated from one or more humans' specialized expertise. Based on the knowledge base, an expert system may replicate human thinking to make judgments for a specific working situation. It is also capable of deducing appropriate solutions from incomplete data collection. It is simple to set up and maintain; however, because the rules are static, the

depth of the knowledge database affects the application of an expert system, posing a considerable risk of mistakes. Other alternative techniques do not employ a model in the decision-making, such as reinforcement learning, where a controller tries to improve the operation based on the outcomes of past actions. However, making the controller “learn” requires an excessive amount of time and data collection. Many aspects influence the controller's performance, including the state-action selection and learning settings.

### **2.1.2 Model Predictive Control (MPC)**

Another growing field of research in predictive control strategies to maximize building energy flexibility is Model Predictive Control (MPC). As the name suggests, these controllers require a building model for the whole building and/or its subsystems to forecast thermal behaviour such as energy loads or thermal comfort. The type of modelling approach is usually classified into three categories: white-box, grey-box and black-box. White box models, or physics-based models, are developed from the first principles and implemented widely in building energy modelling (BEM) tools such as DOE-2, EnergyPlus and IES-VE. In general, they comprise energy balance equations applied to each surface and zone in a detailed geometry which yields comprehensive analysis of the model for the design decision and retrofitting purposes. The disadvantages of these models are the time and cost required to build them and the need for complete knowledge of buildings physics which is not always available. Thus, they are rarely used for controls, although there are some applications in the literature where offline MPC uses such models (Gomez-Romero et al., 2019; Kontes et al., 2018). Since white-box modelling of subsystems is computationally cheap, they are frequently used to model certain components within a building (Mirakhorli & Dong, 2018). On the other hand, black-box modelling methods do not model buildings using physics laws and are entirely data-driven. Developing these models

requires large and rich datasets, capturing a large variety of conditions throughout the whole season. This is, usually, the biggest challenge in deploying black-box models. When dealing with big datasets with numerous features (variables or sensors in this example), feature evaluation and selection become crucial in developing an accurate and efficient model. Data-driven building models used to estimate energy flexibility range from the simple regression models (Yin et al., 2016) to the artificial neural network (ANN) and the support-vector networks (SWN) (Kara et al., 2014). There is also a combination of first-principle and data-driven models, called grey-box modelling. The most common form of those models is Resistance-Capacitance (RC) thermal network models. Depending on the resolutions, the parameters can be determined either from the measured data through system identification techniques or meaningful physics-based parameters can be used. Prívarva et al., (2013) studied a method for developing and selecting a predictive control model that focused solely on the grey-box approach. He concluded that the performance of semi-physical models worsens as a building becomes more complex, proposing a black-box subspace alternative as a viable solution. The advantages of grey-box models are cited in the literature as the ease of interpretation of the model parameters and some of the underlying physical processes that describe building behaviour.

MPC often formulates an online convex optimization problem to determine the optimal reference input for lower-level controllers and uses a model to do so. Reduced-order models have been used in most research, with state-space formulation being the most prevalent. State-space models have a well-established theory and are widely utilized in MPC applications in many fields, including the process industry. A state-space (SS) formulation is a collection of first-order differential equations (possible for an RC network) that describes the relationship between input, output, and state variables. One of the most significant advantages of MPC is the explicit

definition of the objective function, which is absent in RBC. Objective functions are commonly defined in cost or energy consumption while specifying the comfort constraint (usually maintaining a specified temperature range). The efficacy of the pricing signal is critical in activating and encouraging the use of a building's energy flexibility. Ruusu et al., (2019) used MPC to determine the most efficient operation of a building's energy system in order to reduce operational energy costs. The flexibility included optimal management of local renewable energy sources by using battery and thermal energy storage. He concluded that MPC had a better performance than a conventional rule-based approach with no forecast. Pedersen et al., (2017) utilized thermal mass for the MPC with the objective to minimize the cost of space heating and compared the performance with a conventional controller. The MPC strategy resulted in cost savings of up to 6% and a power shift from peak load periods of 2 kWh/m<sup>2</sup> of heated area. By combining real-time prices (RTP) and economic model predictive control (E-MPC) of an AC unit in a single residence, Avci et al., (2013) reported a 13 % cost reduction and a 23.6 % reduction in peak-hour energy consumption when compared to a baseline controller. Vrettos et al., (2013) used predicted upcoming prices in MPC to study the energy flexibility potential of a residential house. Compared to a rule-based controller, the energy consumption was reduced by 20%, and the cost was reduced by 28%.

MPC controller usually requires a linear model due to the convexity of the optimization problem; however, some researchers also examined nonlinear building models. A totally linear model usually yields poor performance in buildings partly due to the non-linear behaviour of convective heat transfer in spaces with substantial temperature differences. The challenges of model development for MPC prompted researchers to look at data-driven methods that preserve MPC's predictive power without the cost of significant computation efforts.

Over the last several years, there has been an increase in black-box techniques targeted at capturing building thermal dynamics. These comprise decision tree learning, k-means, Gaussian processes, and reinforcement learning (RL) algorithms. Some of the approaches maintained the optimization problem linear, for example, through the Fourier variable separation technique (Behl et al., 2016; Bünning et al., 2020; Jain et al., 2016), while others addressed the non-linearity by using heuristic search algorithms, such as Genetic Algorithm (GA) (Reynolds et al., 2018).

Chen et al. (2020), Yamaguchi et al. (2015), Dermardiros et al. (2019) Also investigated the application of "reinforcement learning" algorithms, which combine an ANN with algorithms that extract information from the system's operation to develop an optimal control strategy in real-time. Instead of using a model, the cost of each control action was determined by the system's operation. The penalty of each control action was assigned through the system's operation rather than using a model. The RL approach's limitation is the large availability of data to train the agents, which requires a lot of time.

Overall, the MPC strategies are usually superior to RBC. They incorporate a building model that considers the synergy between building dynamics and HVAC by utilizing thermal mass and exogenous inputs such as weather and occupancy. May-Ostendorp et al., (2011) managed to reproduce the common heuristic rules such as pre-heating of spaces and demand response but did so in an automated, more optimal and cheaper manner than expertly-derived supervisory-level controls. The most significant disadvantage of the MPC technique lies in its requirement of a simple yet accurate model, which is costly to build, train and monitor. Furthermore, extra hardware is needed to accommodate MPC calculations and automatically access the day-ahead

electricity prices and weather forecast. Smart meters must be implemented to enable communication between the grid and end-customer (Péan et al., 2019).

### **2.1.3 Research needs and methodology**

While RBC strategies can significantly enhance building energy flexibility, they are usually model-free and do not incorporate weather predictions. On the other hand, MPC strategies can formulate the objective explicitly and utilize the incorporated model to derive optimal control action. However, the cost of the stringent modelling requirement and extra hardware are among the main barriers to its wide-scale adoption. This thesis proposes combining both approaches, which inherits the benefits of numerical MPC for using building model and RBC for practicality and cost-effectiveness of implementation, leading to the introduction of the heuristic MPC concept. The study will focus on developing model-based rule-based predictive control strategies applied to the radiant floor heating system of the institutional NZEB. Depending on anticipated weather scenarios, the pre-developed optimal room temperature setpoint profiles will be selected to save energy and/or increase the building energy flexibility by reducing power demand during the two critical periods for the grid in the heating season. The uncertainties associated with predictions are addressed using the data from on-site PV production and ambient temperature in the last 3 hours.

## **2.2 Developments in BIPV/T**

### **2.2.1 BIPV as a predecessor of BIPV/T technology**

Building-integrated photovoltaics (BIPV) are photovoltaic modules that are aesthetically and functionally incorporated into the building envelope, substituting standard and/or premium building materials, including roof shingles, wall cladding, windows, and overhangs (Yang & Athienitis, 2016). BIPV, as opposed to rack-mounted PV systems, is a multipurpose technology. BIPV can therefore serve as a weather and noise barrier, generate usable heat (BIPV/thermal – BIPV/T) and allow daylight transmission (semitransparent BIPV), potentially converting up to roughly 80% of incoming solar radiation into usable energy in the form of electricity, heat, and daylight (Athienitis & O'Brien, 2015). As it can be used to cover large roof and façade surfaces, BIPV is projected to be a primary technology for generating on-site power in high-performing buildings. On-site energy generation by BIPV may fulfill a portion of daily electricity demand in commercial and institutional building applications while avoiding grid distribution losses associated with transferring the same amount of electricity across large distances from the power plants. It can also assist in minimizing power demand during peak demand events when precooling or preheating the space.

### **2.2.2 Historical development of BIPV/T**

To assure energy sustainability, supply of expanding power demand and reduce environmental concerns of GHG, replacing the polluting fossil fuel sources with eco-friendly counterparts is a critical task. As a result, tremendous efforts have been focused in recent decades on developing innovative renewable energy solutions. The photovoltaic system can convert incoming solar

irradiation into electrical power with a restricted efficiency of roughly 11–20%, based on geographical and design factors (Agrawal & Tiwari, 2010; Lamnatou & Chemisana, 2017). By January 2020, the worldwide accumulative capacity of installed PV amounted to approximately 627 GW, with the capacity expected to increase to 1,520 GW by 2030 and 4,274 GW by 2050, accounting for more than 15% of global energy generation (IRENA, 2019). The part of incident solar energy not transferred to electrical power progressively accumulates as thermal energy raising the temperature of the PV cells and consequently reducing their electrical efficiency (Chowdhury et al., 2020). Therefore, it is necessary to develop PV module technologies that improve long-term electrical efficiency by lowering the temperature of the surface through a cooling medium. This also extends the life of solar modules by reducing silicon degradation due to overheating (Sathe & Dhoble, 2017). As a result, PV/T systems using various mediums, mostly air or water, were developed to absorb and recover the lost solar energy collected in PV modules, leading to a considerable increase in electrical efficiency and module's life expectancy in addition to an extra heat recovery (Rounis et al., 2018; Waqas & Jie, 2018; Liu & Yang, 2018). A lot of efforts in the literature were made to analyze the design options and efficiency of those systems. In the last ten years, PV/T systems achieved a substantial upgrade through the various design configurations. The photovoltaic/thermal system (PV/T) can be integrated into residential and non-residential buildings serving multiple functions. Effectively integrating the PV/T into the building envelope, which results in building-integrated photovoltaic-thermal (BIPV/T) systems, requires early collaboration and communication efforts at the building concept design phase.

### **2.2.3 Advantages and limitations of BIPV/T**

Environmental consequences such as greenhouse gas (GHG) emissions and noise are reduced and partially mitigated by locating power plants away from the metropolitan regions and cities and more towards the countryside. This, nevertheless, leads to energy losses during power transmission and distribution, which significantly influences the price of electricity (O'Brien & Athienitis, 2015). Applying BIPV/T systems reduces the need for electrical energy transmission across large distances, potentially lowering investments in grid infrastructure and its operation (Gholami et al., 2020). Overall, the advantages of BIPV/T solutions in the building can be summarized as follows:

1. Onsite electrical energy production: reduced transmission losses, reduced the building's carbon and land footprint and diminished the heat island effect.
2. On-site heat generation: increased HVAC efficiency, better equipment performance (reduced thermal demand).
3. Enhanced energy flexibility: integration with electrical and/or thermal storage, thermal storage in manifolds.
4. Provision of aesthetics, enhancement of building envelope function and structural integrity.
5. Increase in the building value.

Nevertheless, there are some barriers to widespread BIPV/T adoption, including thermal integration difficulties, overheating issues, dust and snow accumulation on module surfaces, reliability concerns, and a mismatch in the life duration of BIPV/T systems and the underlying architectural elements, such as the roof (Gautam & Andresen, 2017).

Despite the abundance of data supplied by the research, most studies are focused on PV/T systems, which are small-scale or stand-alone systems that do not represent a complete picture of the integration of BIPV/T and operation. More research is also required to design simulation software that can accurately model the energy behaviour of BIPV and BIPV/T systems and optimize their performance. As a result, the biggest challenge to the widespread adoption of the BIPV/T system is the lack of expertise, planning, operating and maintenance, standardized technologies, and commissioning.

Rounis et al., (2021) examined the state-of-the-art and listed the following major challenges in the research of BIPV/T technology:

- Deficiency in the practical consideration of the designs, thermal improvements, and experimental performance in their integration to building envelope and mechanical systems and the inconsistent testing conditions between experiments.
- Lack of critical review of BIPV/T modelling, specifically, the lack of equations accurately describing the convective heat transfer phenomena appropriate for BIPV/T.
- The need for creating a common testing methodology for PV/T and BIPV/T systems.

Therefore, narrowing down the system assumptions to practical considerations is critical for improved design and operation.

Another challenge preventing the increase in BIPV/T adoption is the lack of systematic modelling. Wind-driven convection accounts for most of the system energy balance, and despite the abundance of proposed correlations in the literature, no single equation can accurately predict that effect. The most commonly used equations used to characterize the wind-driven convective

phenomena include, but are not limited to correlations developed by Sharples & Charlesworth (1998), McAdams (1954), Palyvos (2008) and Duffie & Beckman (1994).

## **2.2.4 Thermal enhancement techniques**

Air-based BIPV/T systems are preferable to water-based systems for envelope integration due to technical considerations such as avoiding leaks, which could be detrimental to the building envelope. However, they are less effective at heat extraction. There is extensive literature on strategies to improve the thermal performance of air-based configuration applied either on customized prototypes or PV/T systems. Most approaches incorporate control optimization, design alternative, or attachment of material components, such as fins, to increase a heat transfer. The addition of several air inlets along the collector's channel is a relatively modern method for thermal enhancement, proposed by Yang & Athienitis (2012). This approach is based on breaching the thermal boundary layer and exploiting the resultant entry effects. By adjusting the flow distributions to each inlet, the convective heat transfer from the PV layer to the channel increases, and more uniform module temperatures may be attained. The advantages of multi-inlet systems are numerous and studied experimentally by Yang & Athienitis (2015). Due to entry effects, the convective heat transfer coefficient increases near the intake along the flow cavity below the PV layer, which improves heat transfer from the PV to the air. In a traditional BIPV/T system, the PV panel warms both air beneath the channel and free air on top of its surface, where the latter is usually lost to ambient. The addition of extra inlets increases the chance to draw the heated air into the channel that otherwise would have been lost to ambient unless an inward wind direction prevails. In addition, cold air enters the channel near the PV panel, resulting in a larger temperature differential between the air and the PV than in the traditional single-inlet systems. As a result of the temperature differential, the BIPV/T may extract more heat. The performance

of a two-inlet system was simulated using convective heat transfer correlations derived from the testing of an experimental single-inlet prototype inside a solar simulator facility by Yang & Athienitis (2012). The installation of a second intake enhanced the system's thermal efficiency by 5-7%, lowered the maximum PV temperatures and slightly improved the electrical efficiency. Rounis et al., (2016) developed a flow distribution model to simulate the performance of multiple-inlet BIPV/T and compared its performance with the traditional one-inlet system in office space conditions. Results showed improved electrical and thermal efficiencies (approximately 1% and 20%) and more uniform PV surface temperatures.

## **2.2.5 Practical applications**

Large-scale practical applications of the BIPV/T have been investigated experimentally in residential and commercial /institutional buildings. Ahmed-Dahmane et al., (2018) experimentally investigated the integration of BIPV/T with an air handling unit (AHU) under both cold ( $T_{\text{ambient}}$  around 15°C) and hot weather ( $T_{\text{ambient}}$  around 30°C) conditions in Algeria. In cold weather, the output from the BIPV/T system would be used to preheat the ventilation air, whereas in hot weather, instead of ambient air, cold air from the building's conditioned areas was used to cool the PV cells. When exhaust air at 24 °C was used as a coolant for the PV, the temperature of the PV cells was reduced by 5 °C. Chen et al., (2010) investigated an air-based open-loop BIPV/T system installed at EcoTerra house, a high-performing prefabricated home in Quebec, Canada. The system was connected to a vented concrete slab, allowing warm air from the BIPV/T system to flow via a tubing within the slab, preheating it and using concrete's thermal storage capacity. A finite-difference model was created for this system, and field tests were used to validate it. The temperature of the PV panels was discovered to be substantially lower, and that the system can dramatically contribute to space heating. Athienitis

et al., (2011) designed a prototype system where he used an appropriate attachment mechanism to integrate specifically designed photovoltaic modules to the unglazed transpired collector (UTC), which constituted approximately 70% of PV panels and BIPV/T system on the side. Combining unglazed transpired collectors with connected photovoltaic panels on facades can be a promising solution for building applications with a substantial requirement to heat ventilation air in the winter. This BIPV/T prototype was built as a demonstration project at Concordia University's John Molson School of Business building.

Another well-known full-scale application of BIPV/T is the Solar XXI office building in Portugal (Aelenei & Gonçalves, 2014). The fundamental concept of the building is to maximize thermal efficiency via the use of passive heating and cooling systems, as well as energy efficiency through the use of renewable energy technologies. BIPV/T and BIPV panels cover most of the building's south-facing facade, producing around 12 MWh/year, about 67% of the primary energy and 70% of total power demand.

Agrawal & Tiwari (2010b) carried out energy and exergy analysis on BIPV/T used as the rooftop of an experimental laboratory at the Centre for Sustainable Technology, Indian Institute of Science Bangalore, with an effective area of 65 m<sup>2</sup>.

### **2.2.6 The role of BIPV/T in energy flexibility**

BIPV/T systems are promising low-grade heat recovery solutions, which is an added benefit to the primary purpose of electricity generation. Besides displacing heating/ventilation loads and enhancing the energy efficiency of the buildings, these technologies are also a potential source of energy flexibility. When optimally controlled, the recovered heat can be stored and utilized at times of peak demand. Integrating BIPV/T systems with an air-source heat pump and TES or

PCM is another possible solution; when controlled in a predictive manner, the power demand at peak periods can be reduced. However, there is still a lot of work to be done to turn these ideas into viable, scalable design alternatives. While BIPV/T is a relatively new technology, there is a need for consistent control-oriented modelling, large-scale practical applications for data collection and optimal controls to optimize the recovery fan operation.

### **2.2.7 Research needs and methodology**

While BIPV/T systems can generate a significant amount of electric and thermal energy, the lack of standardized technology, expertise, and commissioning are the main barriers to faster adopting this technology. Most of the literature on BIPV/T is based on the lab-scale PV/T prototypes, where assumptions lack practical consideration. The deficiency in simulation technology is also part of the challenge, partially due to ambiguity in the systematic modelling of convective heat transfer coefficients.

This thesis analyzes the configuration and the collected data of one of the first large-scale installations of BIPV/T, proposes a control-oriented data-driven modelling approach and lastly, suggests alternative design and control options that can potentially increase the building energy flexibility and meet the enhanced ventilation demands cost-effectively in buildings to mitigate the spread of viruses.

# Chapter 3

## Varenes Library as an Institutional Net Zero Energy Building Archetype

### 3.1 Overview

The NZEB concept encourages the exploitation of the grid as an effective energy storage medium in buildings. NZEBs rely significantly on the energy transfers with the grid in order to maintain their annual zero balance. However, the grid's energy import and export capacity may be limited; it can simultaneously accommodate only a certain amount for such buildings. Fortunately, besides energy conservation, the NZEBs also have the potential to provide substantial flexibility services to the grid by managing their thermal and electrical energy loads intelligently since a design principle incorporates a wide range of storage and on-site energy generation capabilities. One of such institutional buildings chosen as an archetype example in this study is the Varenes Library, the first institutional Net-Zero Energy building in Canada, which will be analyzed in terms of further design and control perspectives to estimate and maximize the available energy flexibility. The library is an excellent choice for the study since it represents the typical high-performing institutional building with vast available energy flexibility sources installed in places such as building-integrated photovoltaic-thermal (BIPV/T) and building-integrated photovoltaic (BIPV) for electricity and heat generation, passive and active thermal storage in the form of exposed concrete and hydronic radiant slab, thermal storage through BIPV/T manifold, electrical storage through 2 EV charging stations, high-efficient ground source heat pumps for heating/cooling, operable windows for free cooling and a BAS for

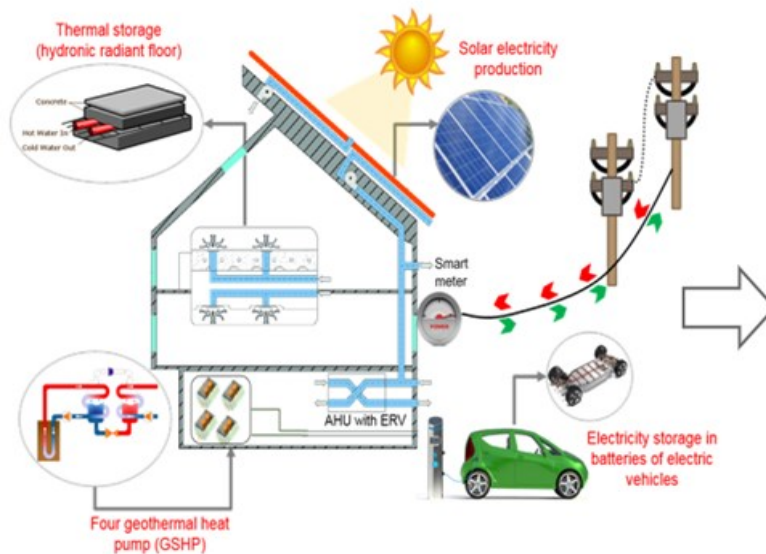


Figure 3-1: Varennes Library, exterior view (top); energy systems cross-sectional view (bottom) (Amara, 2019).

remote supervisory control and data collection. Some of those technologies are shown in Figure 3-1. Constructed in 2014 and inaugurated on May 16, 2016, the library received LEED Gold certification alongside many other awards (Dermardiros et al., 2019). The library’s mass has dimensions of 54.9 m x 19.1 m x 6.8 m in (length x width x depth). It is considered highly well-insulated, spanning two floors and covering a total area of 2100 m<sup>2</sup>.

The library's design was carried out in close collaboration among many specialists, including architects, engineers in various disciplines, and solar engineering experts, due to the necessity for an integrated approach.

A team from Concordia University represented the Smart Net-Zero Energy Buildings Research Network (SNEBRN), which guided the creation of the energy concept for the library. A key aspect of the building is its integrated approach in the design and adoption of a wide range of technologies that substantially reduced the energy demand of the library and enabled it to be the first net-zero institutional energy building in Canada.

From the concept design phase, it was decided to spread the library across two levels, providing for the optimum light penetration and cross ventilation due to its long-form and narrow depth.

The form is oriented to provide the fenestration and roof surfaces with the optimal southern exposure to maximize the incoming solar gains in winter. The roof's southern side has an extensive area of 711 m<sup>2</sup>, accommodating 425 solar photovoltaic panels pitched at 37° with a total capacity of 110.5 kW. 60% of the PV area, or 428 m<sup>2</sup>, is vented naturally through a gap of 150 mm between the PV panels and the roof membrane to prevent overheating and maximize electrical efficiency. The remaining 40% are actively vented with a fan through an air gap of only 70 mm. An area of 173 m<sup>2</sup> (66 panels) of the total BIPV area is BIPV/T that actively recovers heat through the outdoor air intake, controlled by variable-speed fans. The heat is recovered during the heating demand period only and is exhausted outside in the summer.

The building's heating and cooling needs are supplied from four ground-source heat pumps (GSHP) connected to eight 152 m deep boreholes, with a total cooling capacity of 105 kW and a heating capacity of 80 kW. Electric heating coils with a capacity of 20 kW are also available on



Figure 3-2: Architectural plan view with yellow area highlighting hydronic radiant slab (Dermardiros, 2020).

demand. Space heating and cooling are distributed by hydronic radiant slabs on the southern perimeter of the building, as shown in Figure 3-2, supplemented by 18 fan-coil units (FCUs).

The library operates on a different fixed schedule on weekdays and weekends. When occupied, the heating setpoint temperature is set at 22 °C and switched to 18° C on an unoccupied period. Underfloor air distribution (UFAD) systems are used for the air distribution at the building's upper floor and overhead diffusers on the ground floor. The ventilation is demand-based, controlled with a CO2 setpoint of 850 ppm.

The building's fenestration is designed to take full advantage of natural light. Low-e double- and triple-glazed windows with high insulation were installed. Occupancy sensors are installed in

each zone for lighting control. A weather station is also mounted on the roof to provide data on outdoor illumination levels to a centralized DALI (digital addressable lighting interface) management system, allowing lighting fixtures to be controlled based on daylight availability. The majority of the energy consumption accounts for fans and pumps (40%), followed by the heating/cooling (29%) and lighting (25%) applications. A control system monitors the solar photovoltaic panels' energy usage and power output in real-time and displays the data on a screen at the library entrance.

## **3.2 Operational Sequence**

### **3.2.1 Ventilation**

The schematic of the dedicated outdoor air system, located 3.3 m below the ground, is shown in Figure 3-3. The general ventilation system supplies fresh air to VAV terminal boxes which feed 18 fan-coil units in the building. After being fully conditioned in the fan-coil units, the fresh air is supplied to the space through diffusers. The fresh air is distributed to the first floor by overhead diffusers, while the second floor is predominantly by an underfloor air distribution system (UFAD). However, several overhead diffusers exist also on the second floor as well. The ventilation air is preheated by the heat recovered from the building-integrated photovoltaic/thermal (BIPV/T) system and by heat from the thermal wheel. Supply fans shut off when windows are open, enabling natural ventilation. Supply temperature set point is readjusted between 13 °C and 18 °C depending on the average demand of the rooms. The heating/cooling coil located after the thermal wheel is activated when the supply temperature to the FCUs deviates from this setpoint boundary. In winter, the return air temperature sensor sequentially modulates the thermal wheel and the heating coil valve. When the air from BIPV/T is directed to

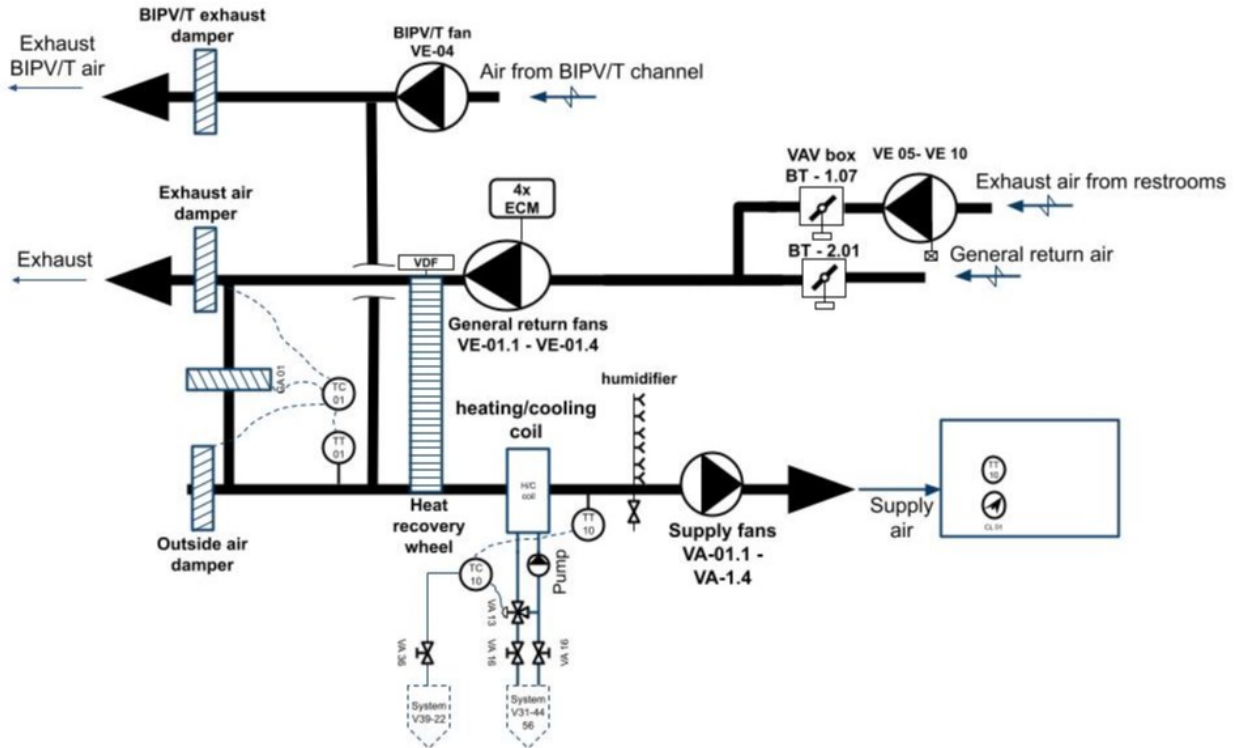


Figure 3-3: The mechanical layout of the primary and BIPV/T air streams.

the system, the BIPV/T fan provides at least the same flow rate as the general supply fans. Supply and exhaust fans are equipped with an ECM motor and can be modulated directly by a 0-10 VDC signal. The supply pressure is maintained by starting the four supply fans in sequence and modulating them to ensure the flow to all the fresh air terminal boxes so that the most open one is at a minimum of 90%. The room humidity set point is maintained to a minimum of 30 %; however, a high limit in the supply set to 85% turns off the humidifier to prevent condensation. The speed of the BIPV/T recovery fan is modulated sequentially between 33% and 80% to maintain the BIPV/T outlet temperature below 25 ° C. When the outlet temperature of air from BIPV/T is above 25 ° C for more than 60 minutes, the fan will switch its speed from 80% to 33%. The fresh air supplied to the fan-coil unit is controlled between the minimum and the maximum by the CO<sub>2</sub>, with the highest threshold set to 850 ppm in the room. When the fan coil

unit is stopped, or the library is unoccupied, the fresh air damper is closed. BIPV/T system's operation and configuration are discussed in more detail in Chapter 5.

### 3.2.2 Heating / Cooling

The zones are heated and cooled by fan coil units, and a hydronic radiant slab (both shown in Figure 3-4) supplied with cold water at 9.4 °C and hot water at 37.2 °C by the GHPs. In all cases, heating or cooling is prioritized by the radiant floor; FCUs are either condition the ventilation air (followed by VAV box terminals) or assist the radiant slab in keeping the temperature in the room within the setpoint. The position of the coil valves is sequenced according to the demand.

On a call for heating, the cooling outlet valve closes so that simultaneous heating and cooling are avoided. Upon a call for closure, the supply valve can modulate. For the radiant floor, however, the action on the valve changes depending on whether the water supplied is hot or cold. The maximum floor temperature measured by the sensors, located approximately 4 cm below the surface, is limited to 32°C (so the maximum surface temperature is limited to around 29°C by ASHRAE Standard 55.1) and the minimum temperature to 18°C. The radiant slab serves 11 zones and is controlled by the zone air temperature only. The ground floor has five zones and a hydronic slab area of 240.61 m<sup>2</sup>, whereas the upper floor comprises six zones with a total area of

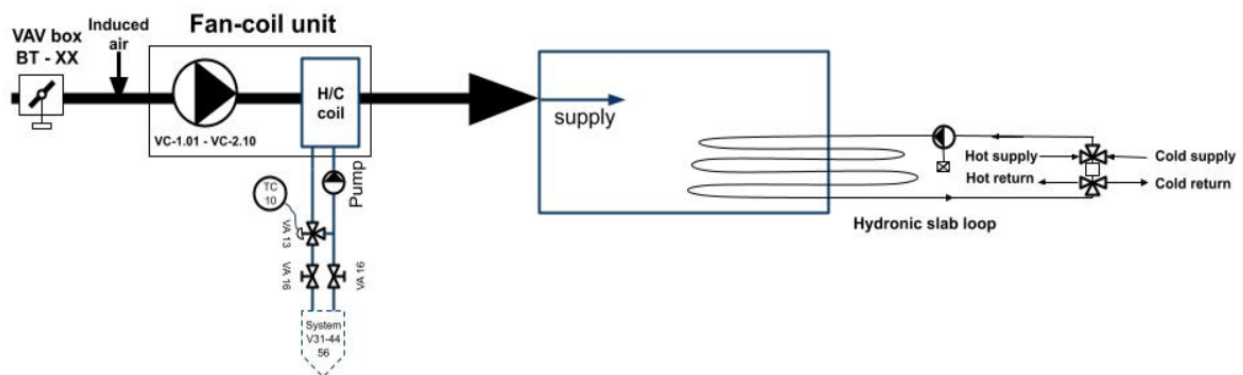


Figure 3-4: Fan coil unit provides both ventilation and heating/cooling demand. Hydronic radiant slab is the main system for heating/cooling (right)

hydronic slab of 433 m<sup>2</sup>. In each room, the zone air temperature sensor continuously controls the 6-way valve of the radiant floor and the fan-coil unit at two-stage, to maintain the heating set point at 22°C in winter and the cooling setpoint at 25°C in summer. The zone supply fan speed is adjusted between the minimum of 10% and the maximum according to the higher of the two inside temperature or CO<sub>2</sub> signals to satisfy the greatest demand. Fans will stop in areas outside of offices if there is no CO<sub>2</sub> demand or the temperature setpoint is met. In an unoccupied period, the heating setpoint is lowered to 18°C, and the air conditioning is stopped. The library is also equipped with motorized windows for natural ventilation, which open automatically in the cooling season when the outside temperature is between 13°C and 22°C. During unoccupied periods, only the motorized windows located in the upper part of the building can be opened. Windows are automatically closed upon the detection of the rain.

### **3.3 Conclusion**

To conclude, the Varennes library is intelligently designed in an integrated manner comprising renewable generation systems and efficient HVAC and storage systems that allow it to achieve a net-zero energy balance yearly. However, in a grand scheme of electrification and accommodation of larger scale of renewables mission, the timing of net energy balance is more valuable than the absolute amount. NZEBs must be optimized with anticipated operation in mind, resulting in a grid impact that is mainly predictable and manageable. With this objective, the next chapter will focus on optimizing the current baseline operation by shifting the power from the two peak demand periods of the grid and maximizing self-consumption.

# Chapter 4

## Modelling methodology and heuristic MPC

This chapter is structured as follows: First, a step-by-step control-oriented model development and calibration methodology for heuristic MPC in the NZEB are proposed. Both data-driven and physics-based parameter identification approaches are evaluated and verified with the measured data. This is followed by developing heuristic model-based predictive control strategies to maximize energy efficiency and/or energy flexibility with the approach of handling uncertainties in weather forecasts from the collected data. The performance of proposed control strategies is assessed and compared with the current baseline, followed by the conclusion.

### 4.1 Modelling approach

For control-oriented models, there is always a trade-off between the requirements for adequate detail of the processes, precision in the modelling and a high time resolution alongside minimizing the number of inputs and maximizing the ease of use, reliability, and the model's computational efficiency. Thermal Resistance-Capacitance (RC) network models based on the heat balance equation usually meet those criteria and are often used for control-oriented modelling. Due to the computational requirements above, low-order models are often proposed, which parameters are identified through various system identification techniques. This subchapter discusses the methodology to develop a grey-box RC capacitance model for the heuristic MPC in the Varennes library. Although we live in the era of data analysis and data-driven methodologies, the lack of availability of monitored data in buildings is one of the issues hindering the full potential of applying traditional MPC in buildings. Instead, the availability of

extensive BAS databases in buildings, such as the Varennes library, provides an opportunity to develop and verify different building modelling approaches.

The first step is to identify zone arrangements and structure of the model that would capture the average thermal behaviour in the whole building. For this purpose, measured indoor temperature data is analyzed, and variation in the area-weighted average indoor temperature between zones exposed to the most different conditions: south and north orientations and 1<sup>st</sup> and 2<sup>nd</sup> floors are

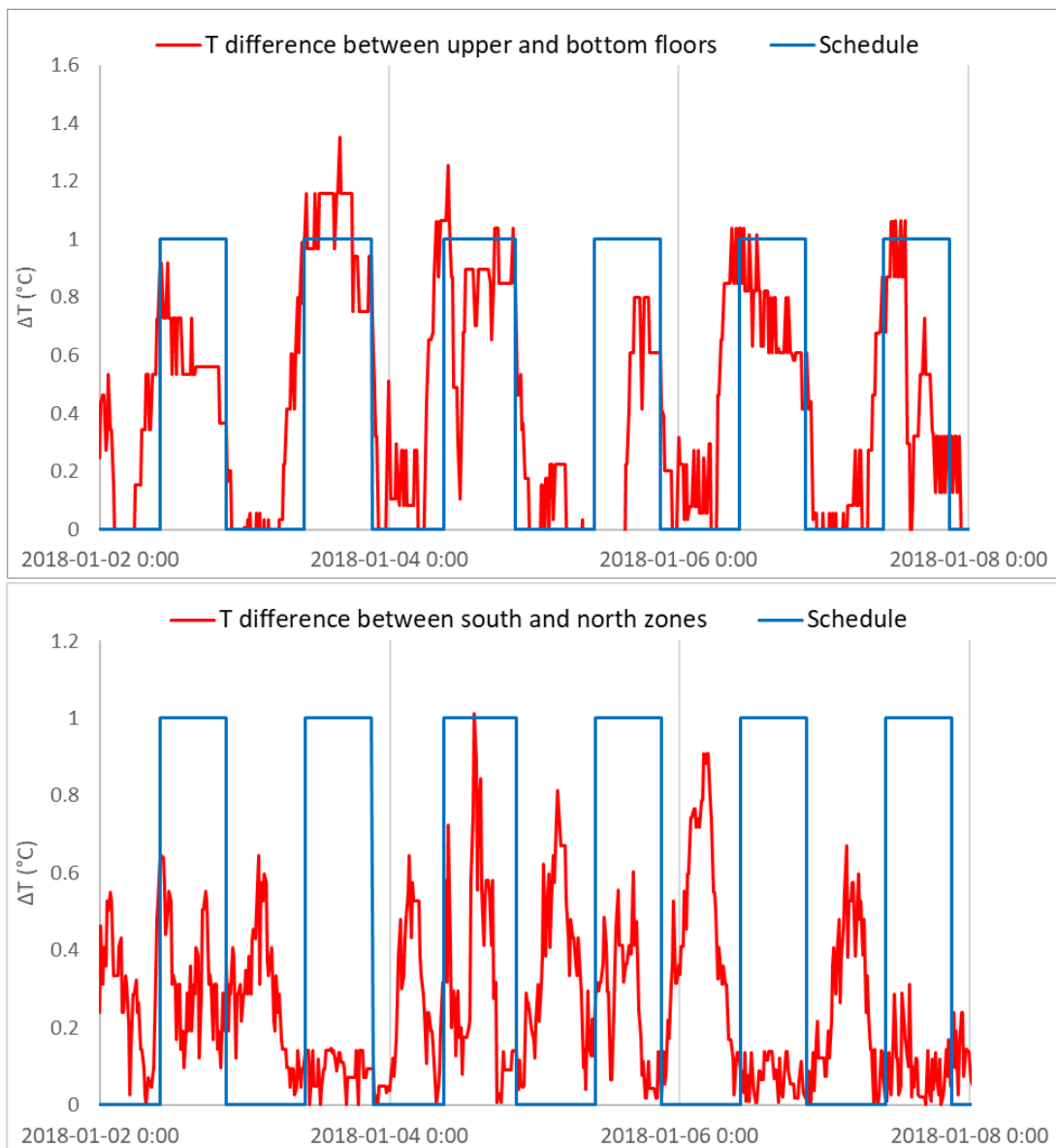


Figure 4-1: The variation of the area-weighted average indoor air temperature between upper and bottom zones (top); south and north zones (bottom).

calculated and shown in Figure 4-1. The data indicates a higher variation in indoor temperature between the top and bottom zones than the south and north zones. This can be explained by the open space interior design, underfloor air distribution system, ceiling fans installed in the library, and buoyancy effects. Following this analysis, a 6<sup>th</sup> order model zoned on the floor level basis is initially proposed. The heuristic MPC, which will utilize the developed model, can accept higher-order models than the traditional MPC since it does not require solving the optimization problem in real time. Thus, it is decided to start with a 6<sup>th</sup> order model to avoid excessive simplification so that close to meaningful parameters can be used, but, at the same time, simple enough to capture the dynamic behaviour of a building to the desired degree in a short time resolution. The structure of the initially proposed base case 6<sup>th</sup> order model is shown in Figure 4-2. It has 24 parameters, 6 of which represent the capacitances of the floor at two levels. Two capacitances model the part of the floor slab incorporating hydronic radiant tubes and once capacitance conventional concrete slab. The following are some of the critical assumptions used to build simplified RC thermal networks:

- Each surface is isothermal.
- Each zone has an even air distribution, and the air temperature is uniform (represented by one node).
- Air is transparent to radiation.
- For the windows, parallel heat flow paths are assumed for the framing and the glazing.
- The floor absorbs 70 % of incoming solar radiation and the remaining 30 % by the other surfaces.

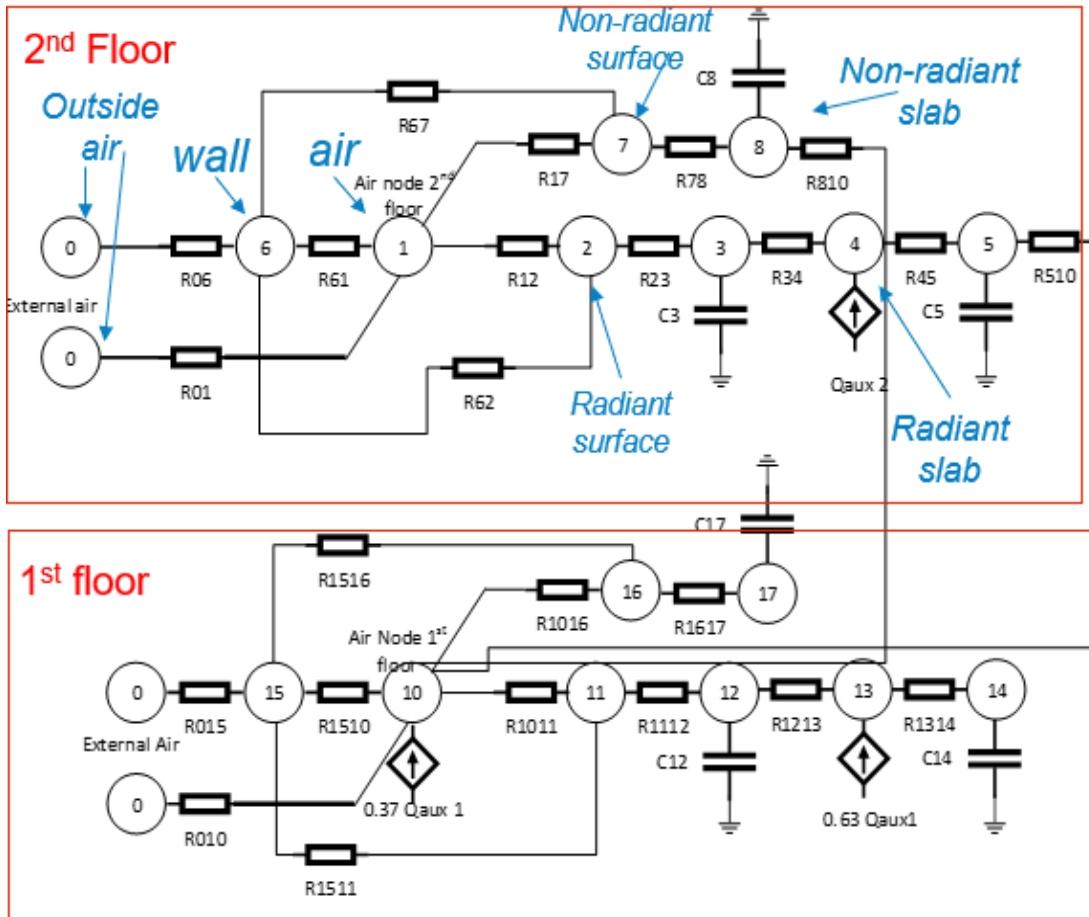


Figure 4-2: Thermal network of the library. Each zone is represented by nodes indicating wall (6 & 15), conventional slab surface (7 & 16), hydronic radiant slab surface (2 & 11), interior hydronic radiant slab (3, 4 & 12, 13), bottom of the conventional slab (8 & 17), bottom of the hydronic radiant slab (5 & 14).

Two approaches have been undertaken and compared to identify model parameters: numerical approach and physics-based approach (closer to white-box).

## 4.2 Numerical approach

### 4.2.1 State-space representation

The common way to describe systems of linear differential equations is through compact state-space representation to facilitate a mathematical treatment of a problem. One of the drawbacks of this form is that it cannot contain algebraic differential equations; that is, all state variables have

to be in the form of linear ordinary differential equations (ODEs). Thus, to describe the suggested 6<sup>th</sup> order model discussed above in canonical state-space shape, all the temperature nodes must be assigned with some negligible capacitance, which increases the intended model complexity. Another disadvantage of this method is the inability to incorporate nonlinearities. As will be seen later, the nonlinearities will significantly affect the performance of the physics-based model. The state-space representation of this model can be found in Appendix E.

**System Identification.** The area-weighted average zone air and slab surface temperature data, available from the Varennes Library, were used as a reference output for the model. First, the linear grey-box model estimation function – “greyest” in the MATLAB Model Identification Toolbox was used to identify model parameters. The ‘fmincon’ search method was chosen. The solver did not even run, claiming the model is “unstable”. The same error was encountered when using another function in the Model Identification Toolbox for estimation of state-space model with structured parametrization – “ssest”.

After a series of errors, it was decided to define the optimization problem explicitly. The difference between the measured reference outputs and the output from the proposed state-space RC thermal model was quantified by the 2-norm operator:  $\|T - \check{T}\| = \sqrt{\sum_{i=1}^K [T(i) - \check{T}(i)]^2}$ . The

cost function was quantified as follows:

$$J(P) = 2\|T_{1,a} - \check{T}_{1,a}\| + 2\|T_{2,a} - \check{T}_{2,a}\| + \|T_{1,f} - \check{T}_{1,f}\| \|T_{1,f} - \check{T}_{2,f}\|$$

Where subscripts denote: “a” – air, “f” – floor, “1” – 1<sup>st</sup> floor, 2 – 2<sup>nd</sup> floor.

The parameters to be identified are the following: U12, U17, U1011, U1016, C3, C5, C8, C12, C14 and C17 (the notations could be found in Figure 4-2 above). The search space of parameters

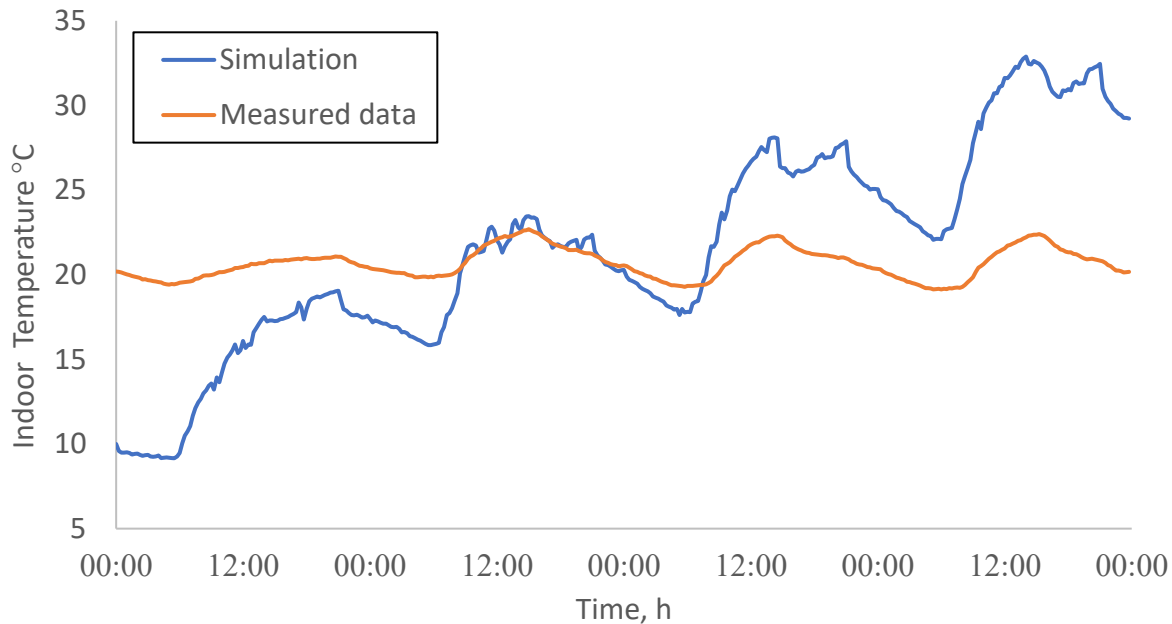


Figure 4-3: Simulation of the average indoor temperature with 16<sup>th</sup> order (formally 6<sup>th</sup> order) model represented in a state-space form.

is constrained so that the maximum allowable capacitances are nominal capacitances increased by a factor of 10 and conductivities by a factor of 3. The minimum allowable capacitances are nominally divided by 10 and for conductivities divided by 3. The other 10 extra capacitances that were added due to state-space representation were defined with extremely small values to ignore the effects. However, as a result, the intended 6<sup>th</sup> order model was simulated as 16<sup>th</sup> order. Due to increased model complexity, simulation was taking too long, and a fit was extremely poor.

Figure 4-3 shows the simulation result with calibrated parameters. On the second day, there is an accumulating effect of extra ten capacitances; the dynamic behaviour is not captured. One of the reasons is that as infinitely small capacitances have been assigned to the additional nodes, the time step of simulation became extremely small due to decreased critical time constant. So even a very small timestep can lead to a significant change in T, leading to errors in the solver.

## 4.2.2 Explicit representation.

In this case, all algebraic-differential equations describing the thermal behaviour of the model were written in an explicit form. It resulted in a reasonable response in terms of time constant and led to a faster solution of the cost function. The dynamic behaviour of the building was captured to a better degree, as shown in Figure 4-4 below. To minimize the cost function defined above, ‘fmincon’ – a local nonlinear optimization solver available in MATLAB Optimization Toolbox was used. The results showed improvement in the fit; however, estimated parameters were very close to the initial guesses. Due to model complexity and non-smoothness of the function, the solutions stuck in attraction basins when using local solvers like “fmincon”. To solve this complex constrained non-linear optimization problem, the Surrogate Optimization algorithm from MATLAB Global Optimization Toolbox was first used to assist in setting up the initial guesses, which were fed to the Pattern Search algorithm in order to avoid local minima. Pattern Search is essentially a grid search algorithm on the parameters where an initial guess is

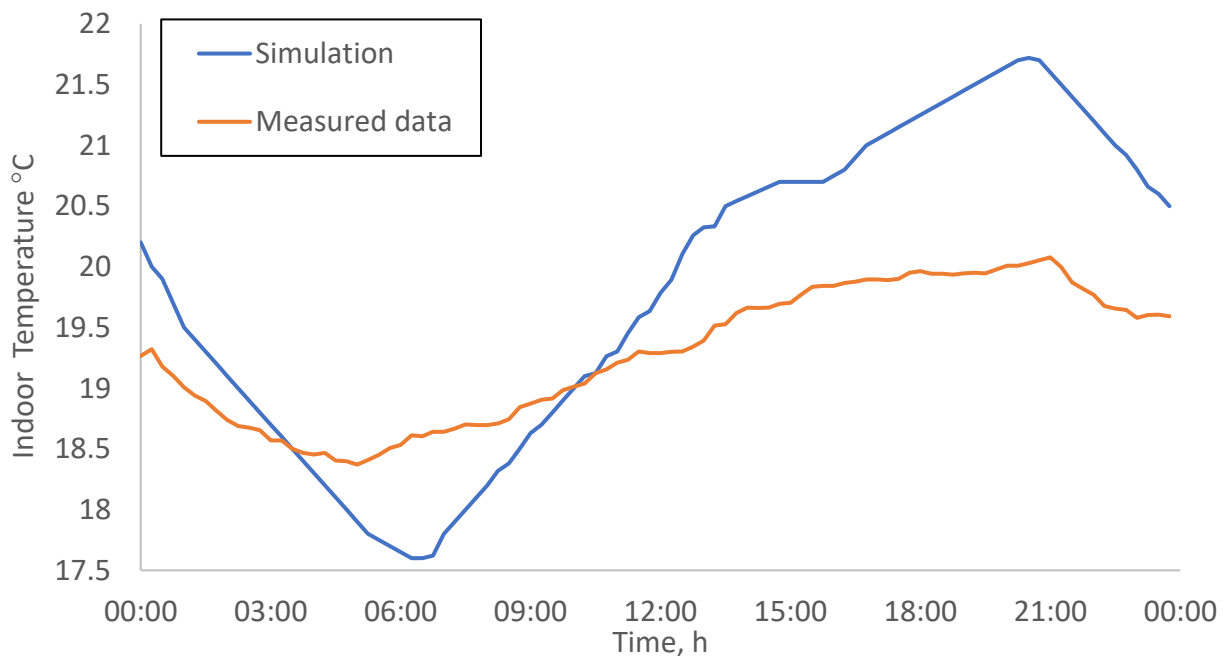


Figure 4-4: 6<sup>th</sup> order model represented in an explicit form with nominal physical parameters; indoor air temperature simulation. January 13, 2018.

made, and points in a grid around the guess are evaluated for a more optimal solution. The algorithm continues to search in the grid until no more optimal solutions can be found, and it reduces the size of the grid and searches locally around the current most optimal solution identified by the larger grid. The identified parameters are shown in Table 4-1 below. The performance of calibrated model both for training and test data for the consecutive periods of 2 very cold days (outside Temperature  $\sim -20$  °C) is shown in Figures 4-5 and 4-6, respectively.

Table 4-1: Parameters identified with hybrid Surrogate Optimization + Pattern Search algorithms.

<b>Parameter</b>	<b>Nominal</b>	<b>Calibrated</b>
C3 (J/K)	5e+7	2.3e+8
C5 (J/K)	5e+7	3e+7
C8 (J/K)	1.25e+7	2e+9
C12 (J/K)	2.8e+7	3e+8
C14 (J/K)	2.8e+7	3e+7
C17 (J/K)	1.7e+8	8.4e+8
U01 (W/K)	670	543
U010 (W/K)	714	795
U12 (W/K)	5012	8312
U1011 (W/K)	2904	9320

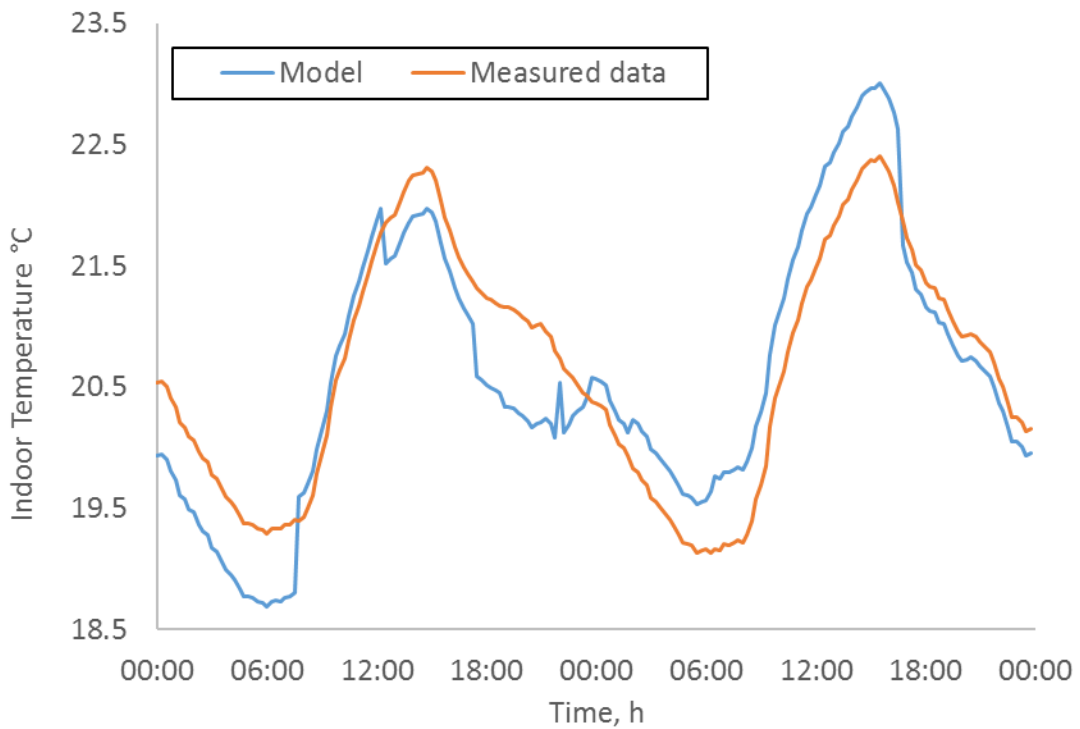
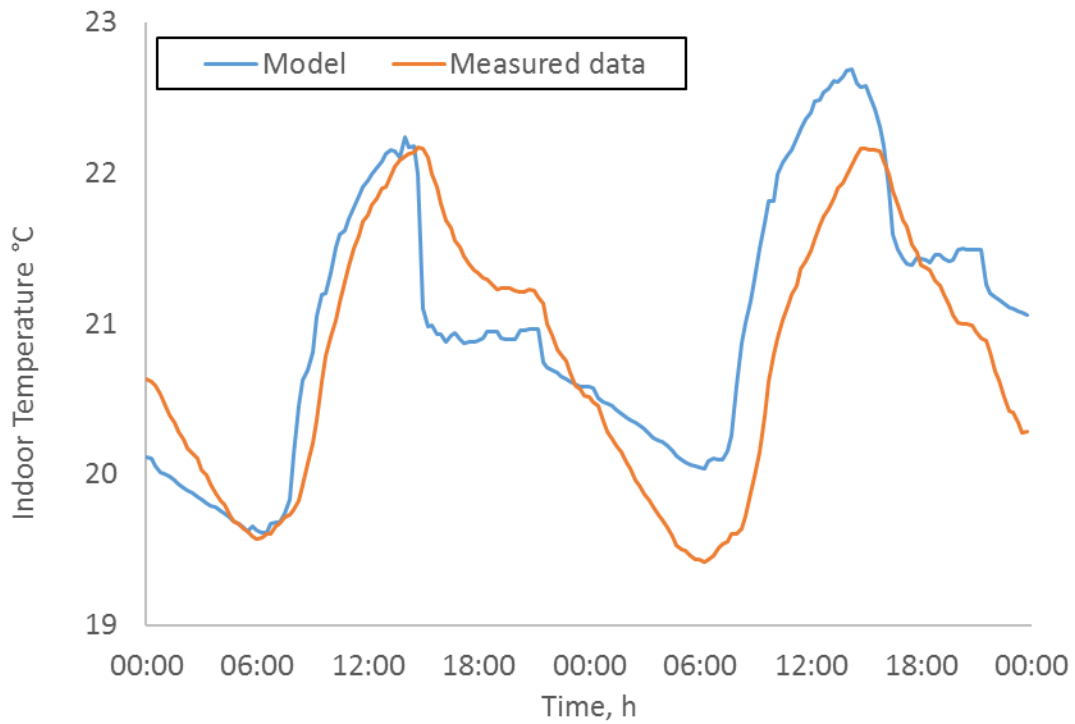


Figure 4-5: Performance of explicitly represented 6<sup>th</sup> order model calibrated with hybrid Surrogate Optimization + Pattern Search solvers in terms of the area-weighted average of indoor temperature. First floor (top) and second floor (bottom). Training data; January 25-26, 2018.

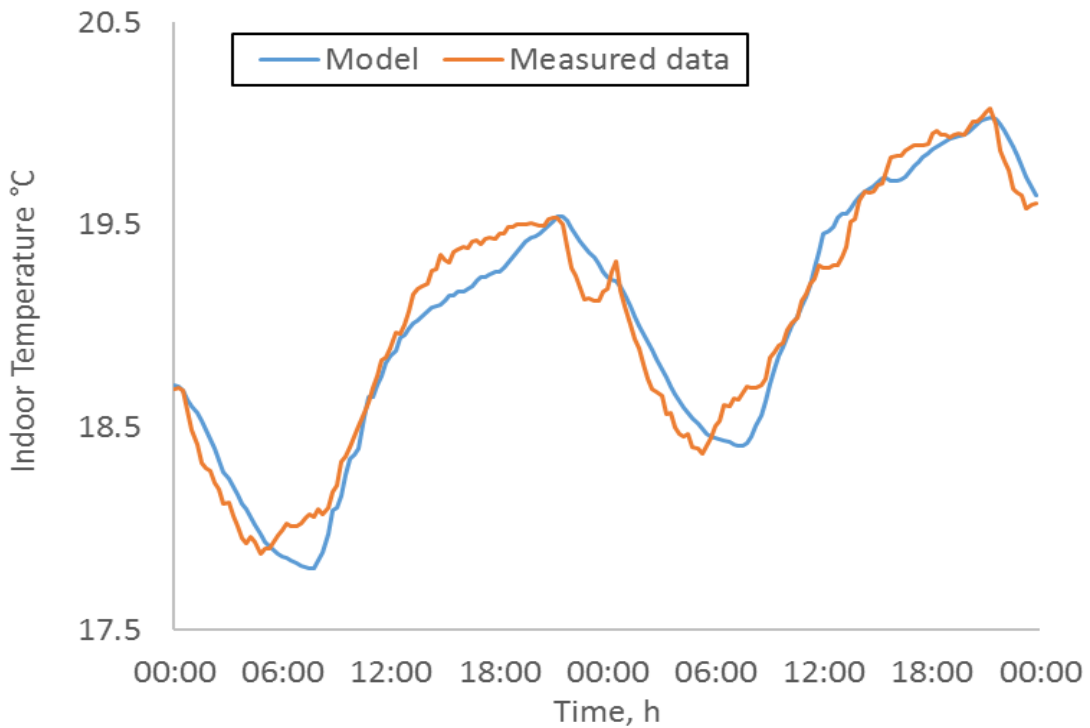
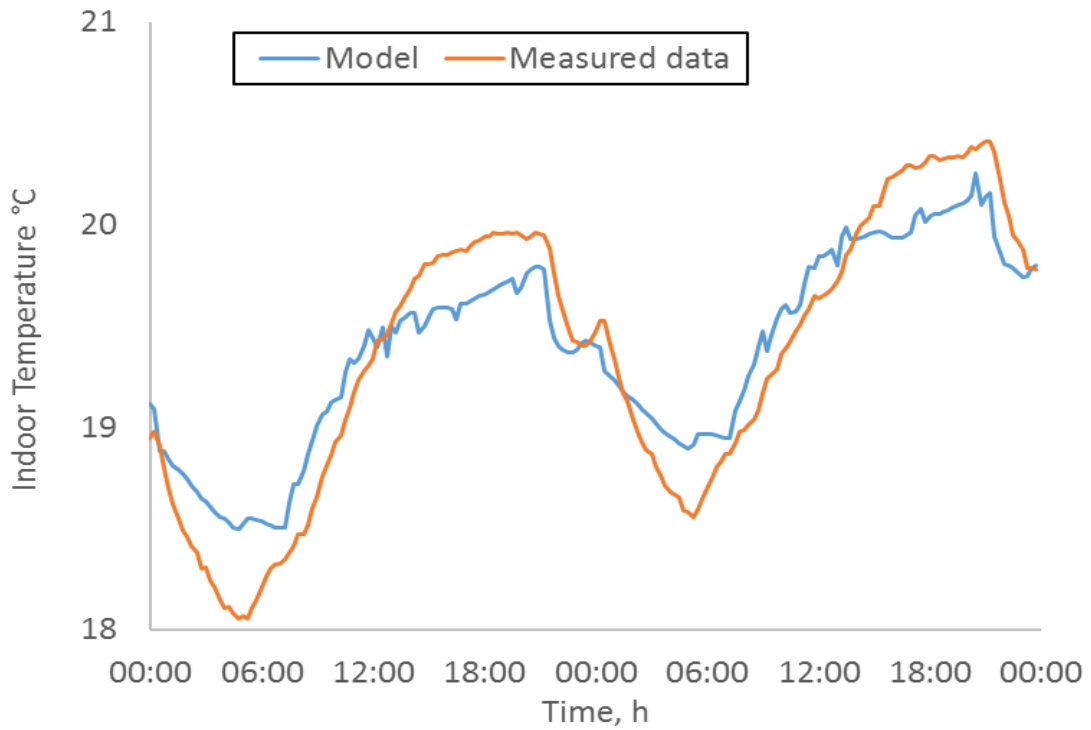


Figure 4-6: Performance of explicitly represented 6<sup>th</sup> order model calibrated with hybrid Surrogate Optimization + Pattern Search solvers in terms of area-weighted average indoor air temperature. First floor (top) and second floor (bottom). Test data; January 3-4, 2018.

### 4.3 Physics-based approach – towards white-box modelling

While the model remains the main limitation of MPC, this subsection provides a solution through a close-to-white-box physics-based model. As was mentioned, the heuristic MPC proposed in the next section does not simulate the incorporated building model in real-time to find optimal control action. Thus, the model can be several orders of higher complexity with parameters derived from the first principles. The arrangement of zones of the west partition of the library is shown in Figure 4-7 below. The upper zone's dimensions are 17.1 m by 4 m by 3.2 m, the bottom zone's 17.1 m by 4 m by 2.8 m.

The step-by-step procedure used to select the level of resolution and to calibrate the model is as follows:

- **Baseline model (Case 1): 6<sup>th</sup> order model**, a hydronic radiant slab in each floor is represented by two capacitances, conventional slab with one, resulting with a total of three capacitance in each zone. A key feature of the model is that the conductance

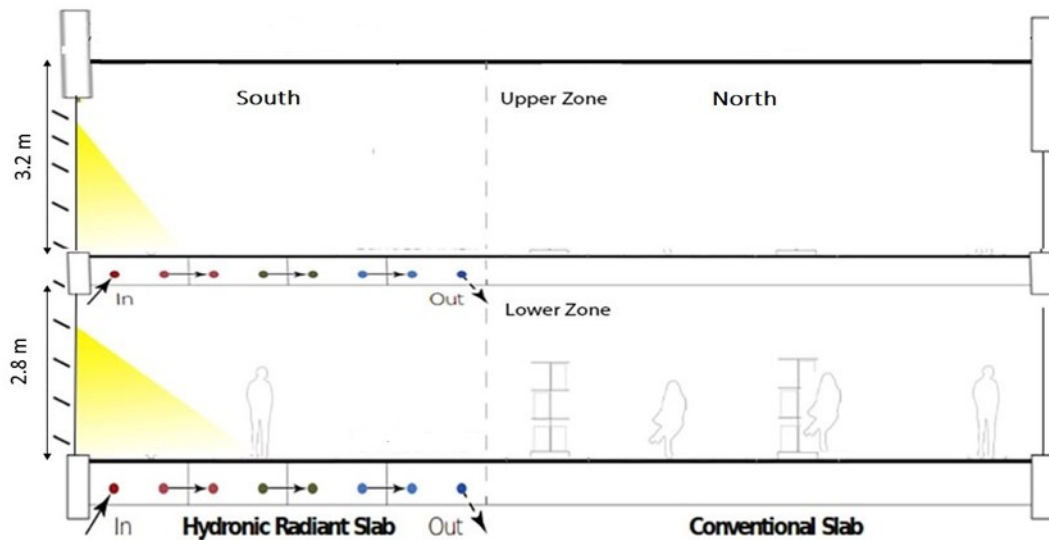


Figure 4-7: Cross-sectional view of the Library with upper and lower zones considered.

associated with radiative and convective heat transfers are combined and constant. The baseline model does not integrate the thermal mass present in the walls made of gypsum board, assuming that these effects would not significantly impact the model's dynamics and accuracy since the thermal capacity of these walls is much less than the concrete.

- **Case 2: 6<sup>th</sup> order model**, conductance associated with radiative and convective coefficients are nonlinear and time-variant as a function of respective temperatures. All the capacitances are increased by 20% representing “effective” thermal capacitance, essentially accounting for thermal capacitance in walls and furniture. The idea of “effective” capacitance is usually suggested and applied to use a low-resolution model while still achieving sufficient accuracy predictions. This hypothesis is based on the idea that it is possible to increase the precision of a low-order model by assuming that the substance has a higher capacitance than the physical (Date, 2016). It is important to note that this does not represent any alternation in the material; it is just a modelling approximation.
- **Case 3: 8<sup>th</sup> order model\_1**. It incorporates the capacitance of the gypsum board present in walls.
- **Case 4: 8<sup>th</sup> order model\_2** Same as Case 2, but the “effective” air node capacitance is included. The capacitance of air was increased by a factor of 20 to account for books, book stands, furniture and other objects which store heat. The factor of 20 is found through the numerical calibration with the collected data set. The iterative calibration approach yielded similar results.

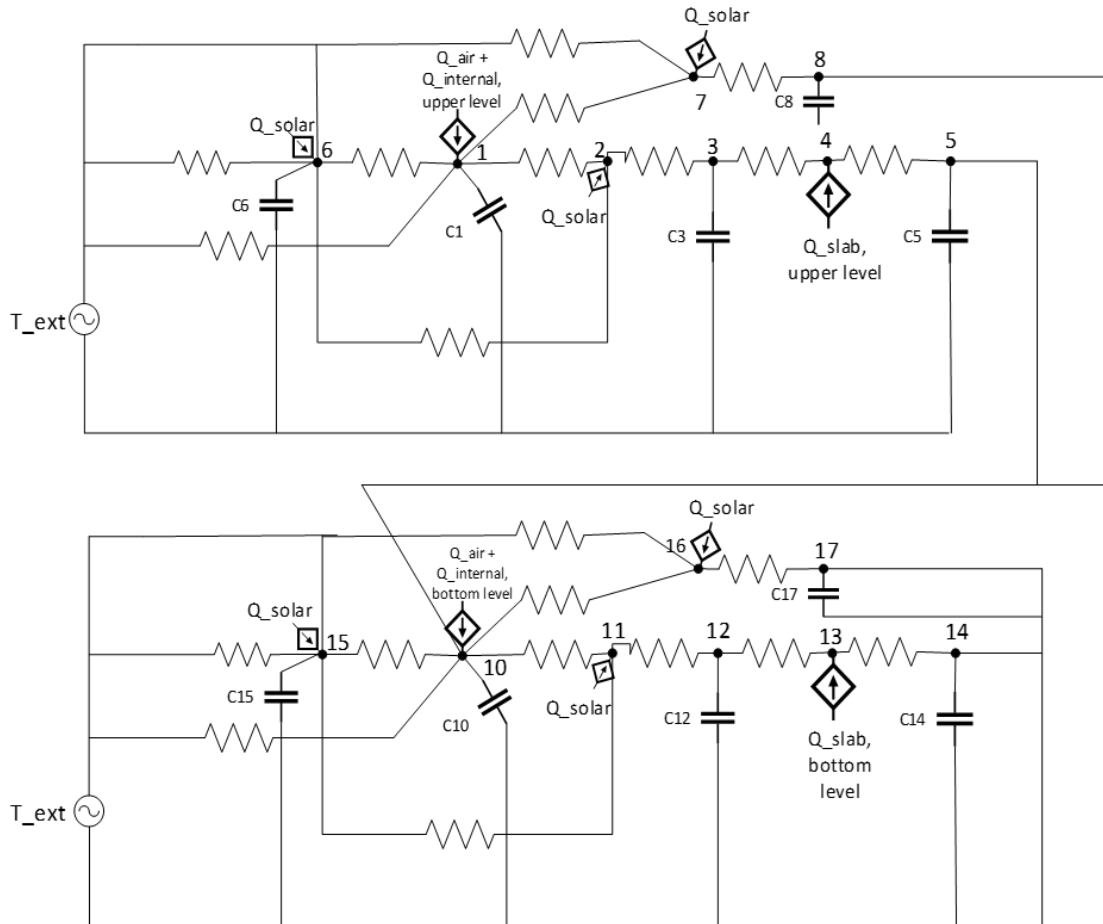


Figure 4-8: 10<sup>th</sup> order thermal network model of the library. Each zone is represented by air node (1 & 10), wall (6 & 15), conventional slab surface (7 & 16), hydronic radiant slab surface (2 & 11), interior hydronic radiant slab (3, 4 & 12, 13), bottom of conventional slab (8 & 17), bottom of hydronic radiant slab (5 & 14).

- **Case 5: 10<sup>th</sup> order model.** Combination of Case 3 and Case 4 – both “effective” air and wall capacitance are included. The detailed thermal network model for this case is shown in Figure 4-8.

The heat and weather input from the collected data and the resulting indoor air temperatures are used to analyze and compare the performance of proposed models. Figure 4-9 shows the performance comparison of all 5 models on a typical cold day in winter. Case 5 (10<sup>th</sup> order model) and Case 4 (8<sup>th</sup> order model with “effective” air capacitance) achieve significantly better performance in predicting indoor air temperature compared to other considered cases.

For model validation, the statistical indices CV (RMSE) and NMBE were calculated. ASHRAE Guideline 14 (ASHRAE Guideline 14-2014) recommends CV (RMSE) and NMBE values to be below 30% and 10% on an hourly basis, respectively, for a calibrated model to be satisfactory. To take a more conservative approach, Table 4-2 compares these indices calculated on a 15-minute basis for the proposed 5 model cases on the typical cold sunny day. It can be observed as the model's detail increases, the correlation between data and model increases. The 10<sup>th</sup> order

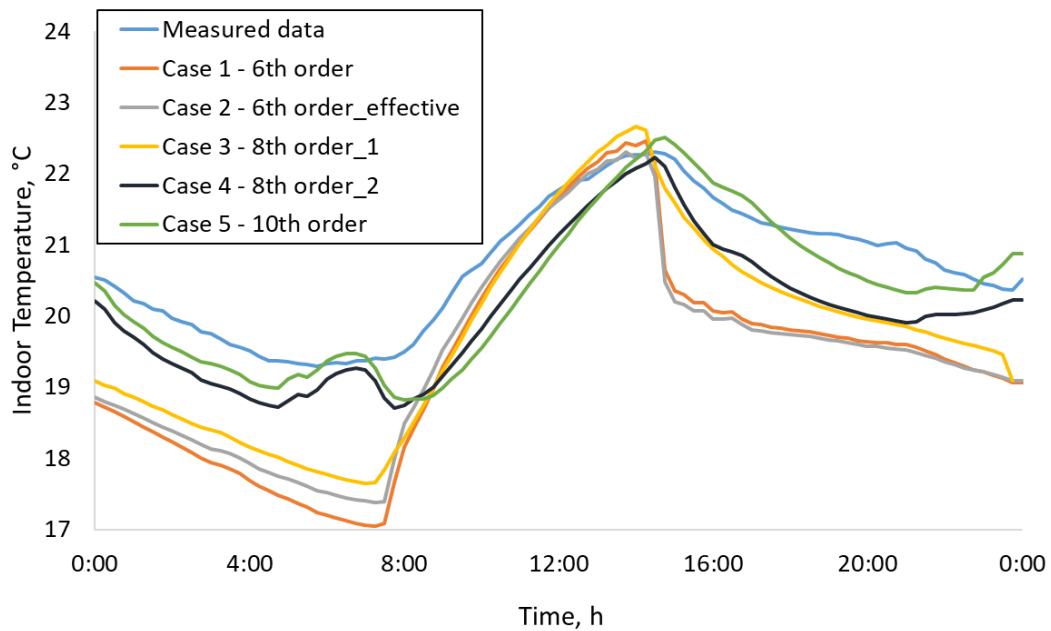


Figure 4-9: Performance of models in terms of average zone air temperature over a typical very cold sunny day in Montreal ( $T_{\text{outside}} < -10^{\circ}\text{C}$ ). January 26, 2018.

Table 4-2: Statistical indices showing model validation against area-weighted average zone air temperature. January 23-26, 2018

Model	2 <sup>nd</sup> zone air T		1 <sup>st</sup> zone air T	
	CV (RMSE)	NMBE	CV (RMSE)	NMBE
<b>Case 1 (Baseline)</b>	7%	6.2%	3.3%	2.8%
<b>Case 2</b>	6.7%	5.9%	3.2%	2.6%
<b>Case 3</b>	5.1%	4.5%	5.1%	2.5%
<b>Case 4</b>	3.3%	3%	2.3%	1.8%
<b>Case 5</b>	2.6%	1.6%	2.1%	1.7%

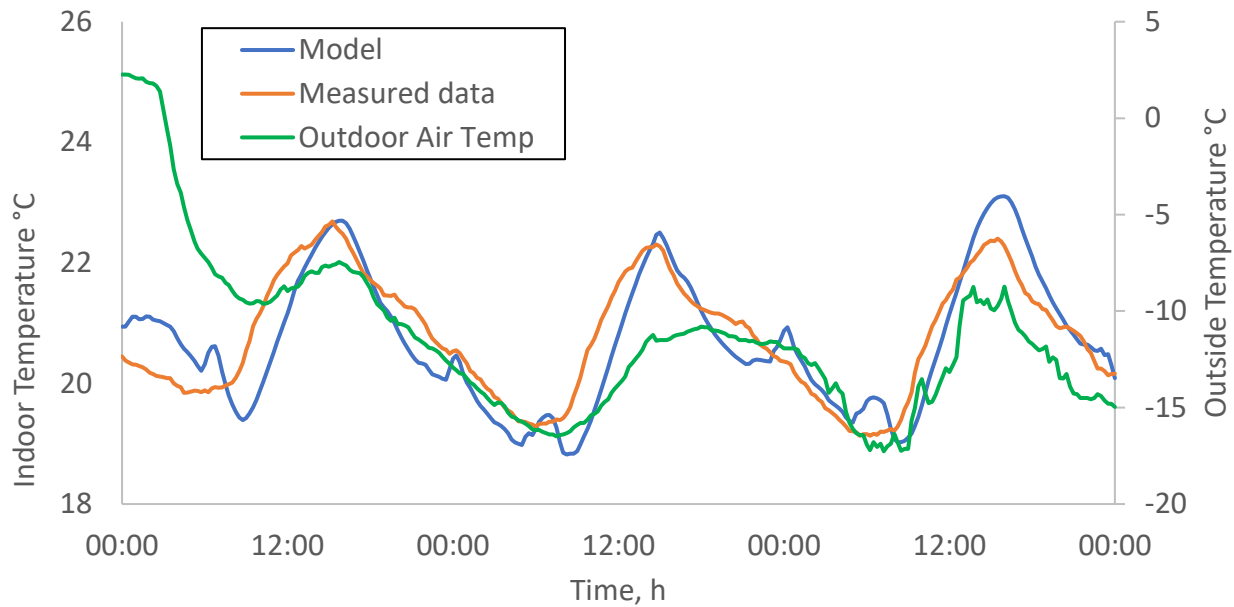


Figure 4-10: Performance of 10<sup>th</sup> order model in terms of average zone air temperature over three typical very cold days. 23-25 January, 2018.

model, which accounts for wall and indoor objects' thermal mass effects, performs significantly better than the 6<sup>th</sup> order baseline.

Both the 8<sup>th</sup> order model accounting for “effective” air node capacitance and the 10<sup>th</sup> order models perform well over a long time horizon; thus, any of those can be chosen depending on the application. The largest effect on the model performance accuracy was the incorporation of ‘effective’ air node capacitance, where CV(RMSE) and NMBE dropped from 7% and 6.2% to 3.3% and 3%, respectively. Thus, a 2-zoned 8<sup>th</sup> order model for institutional buildings like Varennes library can be effectively used for practical applications. As the control strategy proposed in this study can adopt a more complex model, Case 5 – 10<sup>th</sup> order model, which includes air and wall capacitance, is used for further study. Figure 4-10 above shows its performance on the three other very cold days.

## 4.4 Predictive control strategies

The need for rigorous design and operation of a building as an integrated energy system is a core requirement of a high-performance building (Athienitis & O'Brien, 2015). Energy-efficient buildings must be operated in an anticipated manner, leading to a predictable and reasonable grid impact. Predictive control strategies have not been generally implemented on a wide scale, partially owing to a lack of collaboration among the A/E team and facility energy manager, given the prevalence of the design-bid-build project procurement method. In that respect, incorporating the building model and its associated slow responding systems into optimal control strategies has a significant influence on the performance of the buildings. Furthermore, apart from cost savings due to dynamic energy pricing, predictive control strategies may be used to prevent the oversizing of the HVAC capacity, as will be shown in this section on the example of the design day. As a result, both the life-cycle operating and initial cost can be effectively minimized if an integrated approach is taken.

The following sections propose the development of heuristic model-based predictive control strategies for the near-optimal operation of the library's passive and active thermal storage at the supervisory level. The strategies are derived from the physics principles and iterative simulations. Prediction is based on the forecasted next-day outdoor temperature and the sun availability; possible expected weather conditions are clustered into 9 possible scenarios, and 18 daily heating setpoint profiles are developed for each scenario. For each type of day, two sets of predictive controls are developed with targets to maximize: i) Energy-efficiency and ii) Energy flexibility. The energy-efficiency strategy aims to minimize daily energy consumption and reduce daily maximum power demand, whereas the objective of the energy-flexibility case is to shift the load at two peak demand periods in Quebec, given one day ahead of notice. Peak

demand events in the winter period for the grid in Quebec occur from 6 am to 9 am and from 4 pm to 8 pm, and the majority of that accounts for space heating. The uniqueness of each building is recognized, so that developed setpoint profiles may not apply to others, but the main principles can be generalized to other passively designed buildings supplied by a hydronic radiant slab.

Peak demand for the grid in Quebec occurs throughout the winter; thus, very cold days with the mean outdoor temperature between  $-20^{\circ}\text{C}$  and  $-10^{\circ}\text{C}$  are of particular importance. Other days considered in the winter season include cold and mild days with the dry air temperature in the range of  $-10^{\circ}\text{C}$  and  $0^{\circ}\text{C}$  and above  $0^{\circ}\text{C}$ , respectively. These days are further clustered into three subcategories depending on one day ahead sun availability prediction: sunny, semi-cloudy/intermediate and cloudy type of days. Thus, overall there are 9 types of days with 2 strategies to be developed for each. On a local level, heat pumps are controlled through a PI feedback controller as an inner local loop, with the associated deadband acting as an outer closed-loop reset. Ground source heat pumps continuously modulate between 20% and 100%, turning on/off based on the reset. The principle of this reset is the following: if the controller was previously on, heating continues until the difference between the reference setpoint and actual room temperatures reaches zero. Once it is turned off, it remains at an off state until the controlled temperature drops  $1^{\circ}\text{C}$  below the setpoint. The building is thermally massive, and the heat pumps have a wide range of modulation, so short cycling is not expected, as shown in the next section. An important consideration should also be given to selecting the appropriate minimum proportional parameter for a PI controller. As a rule of thumb, for the predictive strategies, the coefficient should be chosen such that room temperature tracks the setpoint increase of ramp slope  $1^{\circ}\text{C}$  within a maximum of 1 hour.

#### 4.4.1 Prediction uncertainties and high-level controls

As noted in the previous section, the optimal setpoint profile is selected based on the predicted outdoor temperature and sun availability. Initially, from 12 am to 9 am, the weather forecast from a reliable weather station is used to select the appropriate setpoint. To address the uncertainties with the initial prediction, at 9 am and 12 pm, verification of the initial prediction based on the actual outdoor temperature and the amount of energy produced from installed building-integrated photovoltaic systems (BIPV) systems in the last 3 hours is performed. The corrections are applied during those times if the initial weather forecast happens to be wrong.

For example, if it is expected to have a very cold sunny day, the setpoint developed for the very cold sunny day (shown in the next section) is initially used. At 9 am, the electricity generation from on-site BIPV and the actual outside temperature are compared against the forecasted value. For example, if the PV production is much less than projected, the profile developed for the cloudy day is selected. If it is close to the predicted value, then the initial weather forecast is confirmed, and the previously selected profile for the sunny day remains unchanged. The projected PV power generation is different for each day and has to be calculated daily, as there are many factors to consider, including, but not limited to, location (latitude & longitude), calendar day (incidence angle) and tilt angle. Various software is available for that purpose. In this study, the projected PV generation is derived from Hottel's clear sky model (Hottel, 1976).

The degree of sun availability in the verification stage is classified through k-clustering (Equation 4-1):

$$c_i = \min_{j=1,2,3} \|x_i - z_j\| \quad (4-1)$$

Where,

$c_i$  is a clustering group,

$x_i$  is the vector  $\frac{PV_{produced}}{PV_{clear\ sky}}$  in the last 3 hours,

$z_j$  is a representative vector for types of days obtained from the k-means algorithm.

The algorithm used to train the  $z_j$  vectors is the following:

1. A preliminary list of representative  $z_{1,2,3}$  vectors with nominal values based on modelling experience are made.
2. The vectors  $x_i$  from the collected 2 months data (from January 1<sup>st</sup> to February 28<sup>th</sup>) are divided into 3 clusters according to the nearest representative vector  $z_j$ .
3. Revise representatives  $z_{1,2,3}$ . For every cluster  $j = 1,2,3$ , update  $z_j$  to be the average of the vectors in cluster  $j$ .

One of the assumptions included in this strategy is that the type of day identified during the verification period will stay constant throughout the rest of the day after 12 pm. This uncertainty



Figure 4-11: High-level control algorithm for very cold days. Initial one-day ahead weather prediction is verified through PV power generation data at 9 am and at noon.

Table 4-3: Resultant control scenarios due to sun availability prediction uncertainty in the form of a selection matrix. Off-diagonal entries represent an error in initial prediction. Very cold days are considered.

<b>Verification outcome at 9 am</b>			
<b>Initial weather prediction</b>	Sunny	Semi-cloudy	Cloudy
	$\frac{PV_{\text{produced}}}{PV_{\text{clear sky}}} \geq 0.7$	$0.25 \leq \frac{PV_{\text{produced}}}{PV_{\text{clear sky}}} < 0.7$	$\frac{PV_{\text{produced}}}{PV_{\text{clear sky}}} \leq 0.2$
Sunny	Scenario 1	Scenario 2	Scenario 3
Semi-cloudy	Scenario 4	Scenario 5	Scenario 6
Cloudy	Scenario 7	Scenario 8	Scenario 9

is alleviated by the high thermal mass of the building and the availability of renewable production for the latter part of the day unless the cloudy day turns out to be a false negative.

The flowchart of the high-level control algorithm under the assumption of the continuous very cold day is shown in Figure 4-11 above. Table 4-3 indicates the resultant possible scenarios for very cold days. The same pertains to warm and mild days.

#### 4.4.2 Sunny days

This subsection discusses the principles used to derive the supervisory heating setpoint strategies to maximize energy efficiency as a first case and maximize energy flexibility as a second while maintaining the minimum thermal comfort conditions. On these days, heat in the form of solar radiation transmits through the window, and a substantial portion of it gets absorbed in the thermal slab. Depending on the temperature profile of the slab and the ambient room temperature, part of absorbed heat penetrates to the bottom of the floor, increasing the interior temperature of the slab and another part is immediately released to the room by convection and radiation means, thus contributing to the short-term indoor temperature rise. Majority of reactive controls which do not anticipate this effect have a high risk of overheating on sunny days. A predictive control strategy can utilize the floor's thermal mass in anticipation of solar gains to

store the energy for future use, thus providing the energy flexibility. In the case of energy efficiency, the strategy is to fully utilize the anticipated solar radiation to displace heating loads by keeping the thermal slab as cold as possible in the early morning. A rapid setpoint change from a night setback to a daytime setpoint is well understood to cause a rise in peak demand. Several studies (Candanedo et al., 2015; Date et al., 2015) explored the impact of using ramps for transition between setpoints. This study, therefore, uses ramps to transition from one setpoint to another.

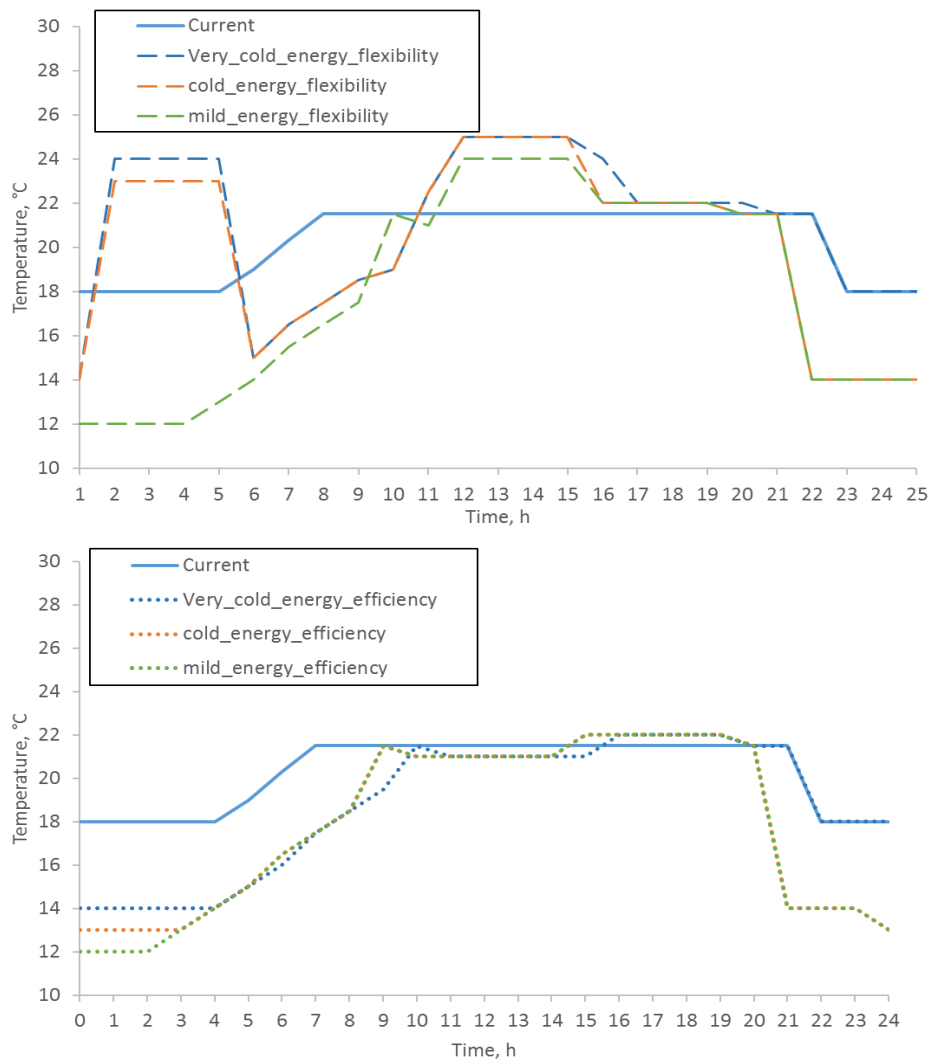


Figure 4-12: Near-optimal heating setpoint profile on a sunny day to maximize energy flexibility (top) and energy efficiency (bottom).

In the energy efficiency case, right after the library is closed, the temperature setpoint on a very cold day is set at a low night setback, to around 14°C, and it is maintained until 4 am. From 4 am to 6 am, the setpoint is increased by using a linear ramp until 16°C. Given the warm floor from the previous day, usually, no heating is expected at this time. Starting from 6 am set the setpoint is linearly raised to 18.5°C by 8 am. At this period, depending on how cold the inside temperature is, heating may or may not start; if it is equal to or higher than 17.5°C, it will not start. Starting from 8 am, the projected room air temperature is between 17-18°C, and solar radiation intensifies. By 9 am the setpoint is increased to 19.5°C, and at this time, the projected zone temperature is between 19°C and 20.5°C.

To mitigate this uncertainty and ensure the library meets the minimum required temperature at 10 am (opening time), the setpoint is increased to 21.5°C from 9 am to 10 am. From 10 am to 2 pm, reference input is lowered to 21°C. This serves multiple purposes considering all possible scenarios. In the first scenario, if heating is on before 10 am, it will try to bring the inside to 21°C as soon as possible, likely in less than half an hour, and then will go off expecting high solar gains and avoiding possible overheating. In the second case, if heating is off, the building is already above 21°C (given the setpoint of 21.5°C from 9 am to 10 am as mentioned above) before 10 am and considering incoming solar radiation, no heating will be initiated. In any case, the heating will continue until 10:30 am maximum, and then the heat pump will turn off. From 2 pm till 5 pm, the solar radiation level generally falls and assuming heating is off before 2 pm, the setpoint is now set at 22°C. Considering the differential deadband discussed above, when the pump is at off state, it will not initiate unless room temperature drops below 21°C. This allows to still effectively use the incoming solar gains for the remainder of the day as a means of space heating. Only when it is not enough to maintain the minimum comfort conditions, the heating

will initiate. This typically will occur after 4 pm, but it may vary on a case-by-case basis. At 8 pm, 1 hour before the building becomes unoccupied, the setpoint is decreased to 21.5°C. The energy flexibility strategy for the clear sunny days utilizes the same principles with slight modification. There is no – to low expected electricity demand in the morning period, and thus 3 hours of preheating is recommended. However, from 10 am to 3 am, the setpoint is set at 24°C and then decreased to 22°C for the peak evening period. On sunny days the preheating of 5 hours instead of 7 is preferred. There are several reasons for that. Firstly, there is a risk of overheating, and due to incoming solar gains, there is already low power demand in the baseline scenario for the second part of the day, which is difficult to fully displace without the risk of overheating. Also, when starting preheating from 9 am, the temperature will reach the setpoint 24°C well before the evening peak demand event (approximately at 12 pm - 1 pm), so the heating will turn off, and due to the deadband, it will stay off until it drops below 23°C. As a result, the displaced load at the peak demand window will be less if preheating was instead continuously 5 hours before the event. After 4 pm, heating will start once room temperature drops below 21°C. Figure 4-12 above shows temperature setpoint profiles for cold and mild sunny days as well.

### **4.4.3 Cloudy days**

These are design days, the days when maximum loads are expected and for which HVAC capacity is designed for. The following section shows that the library is strongly underheated on cloudy very cold days while not continually operating at maximum load. This is one of the cases where even self-tuning reactive controllers can fall short in buildings. The aim of energy efficiency strategy on these days is to bring the inside air temperature to 21°C at 10 am while avoiding high power demands. The strategy for the energy efficiency case is elaborated further.

From midnight the heating setpoint is set slightly higher than usual night setback, at 19°C until 3 am (on very cold days). Depending on the thermal mass of the building and airtightness, heating may or may not start. From 3 am to 8 am, the setpoint is linearly increased up to 20°C. The heat pump is most likely to start at this time frame, and by 10 am, the setpoint is ramped to 22°C. Heating is not expected to stop on a very cold cloudy day, and the setpoint can be kept at 21.5°C till the end of the occupancy. For an energy flexibility strategy, heating should start much earlier to minimize the electricity heating consumption for morning peak demand events. From 11 pm on the previous day till 6 am on the next day, the floor is preheated at a setpoint of 24 °C to increase the demand at the off-peak time and, consequently, shift the load from the peak demand

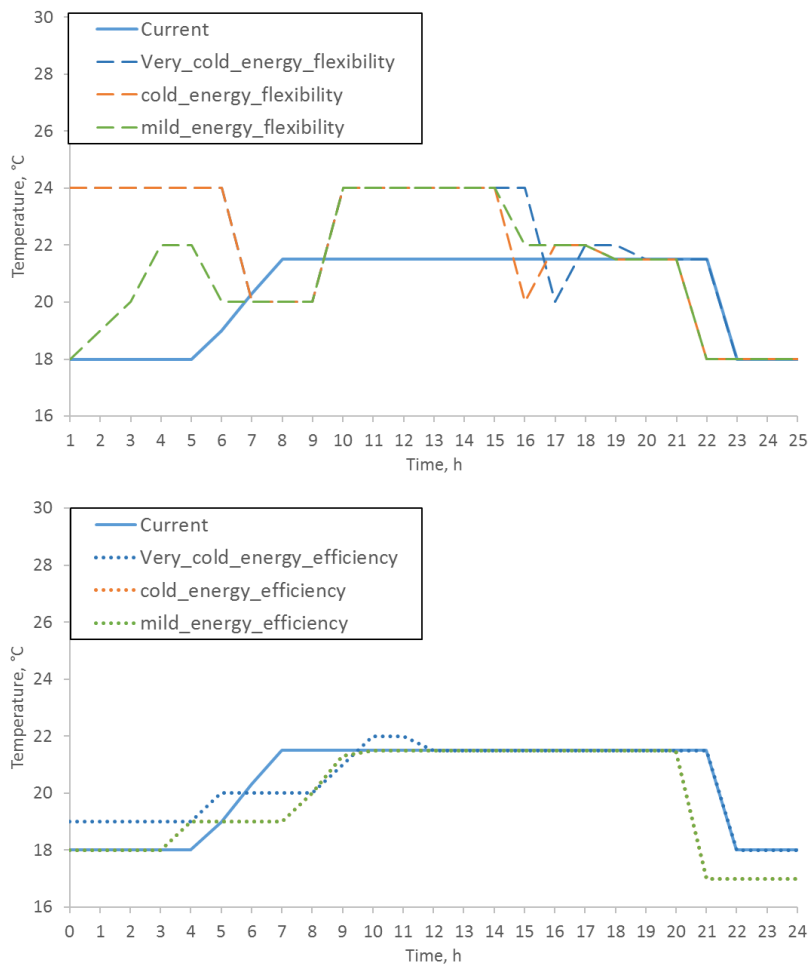


Figure 4-13: Near-optimal heating setpoint profile on a cloudy day to maximize energy flexibility (top) and energy efficiency (bottom).

event. From 6 am to 9 am, the setpoint is decreased to 20°C and ideally, heating stops during this time. Right after this period, the setpoint is adjusted back to 24°C until 3 pm. Afterwards, heating is turned off at 4 pm for one hour by setting a low setpoint, for example, 20°C, and then ramping it back to 23°C so the heating would start only when the inside temperature drops below 21°C. Once the heating turns on, it should operate at a setpoint of 21.5°C. See Figure 4-13 for the setpoint profile developed for cloudy very cold, cold and mild days.

#### 4.4.4 Intermediate days and general algorithm

Intermediate days are the most common days and, for practical purposes, can be subdivided into two further categories: semi-cloudy and semi-sunny. However, for simplicity, in this thesis, only one category for this type of day is considered – intermediate days.

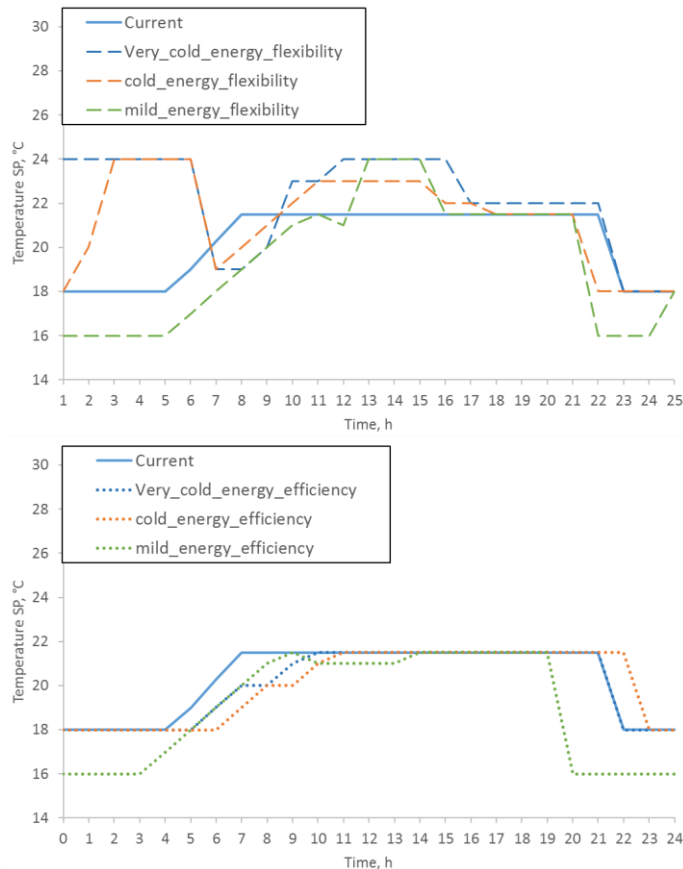


Figure 4-14: Near-optimal heating setpoint profile on a semi-cloudy day to maximize energy flexibility (top) and energy efficiency (bottom).

The proposed near-optimal control strategy for intermediate days is the mixture of principles described above, and the resultant setpoint profile is approximately the average of the clear and sunny days. The profiles targeting both energy efficiency and energy flexibility are shown below in Figure 4-14.

Overall, based on the above discussion, the following low-level implementation algorithm and process schematic for BAS are produced as shown in Figures 4-15 and 4-16 below.

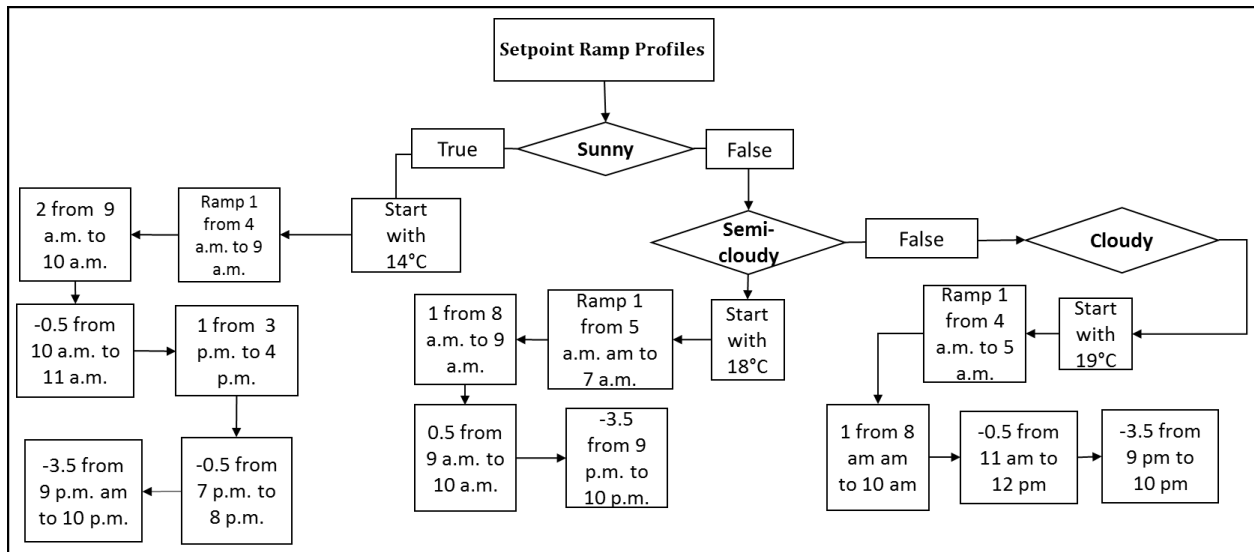


Figure 4-15: Low-level control algorithm of selection near-optimal setpoint profile on very cold days. Ramp # indicates the slope.

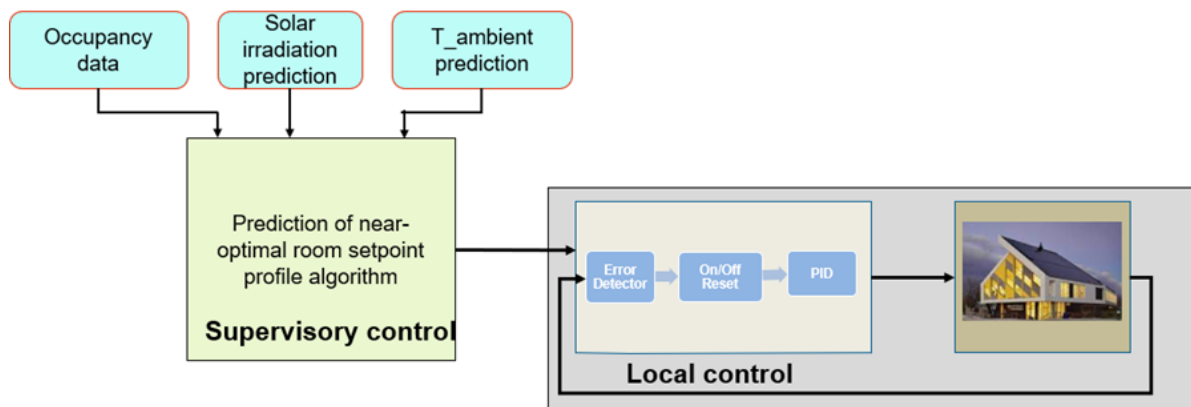


Figure 4-16: Control architecture with supervisory control feeding temperature setpoint into the local control loop.

## 4.4.5 Key Performance Indicators

Several performance metrics are assessed and compared to estimate the effect of proposed control strategies:

- *Thermal energy load for heating [kWh]*. It includes the heating load to be supplied by the geothermal heat pump with a heating capacity of 80 kW and COP of 4 and an auxiliary electric heater with a capacity of 40 kW and COP of 1. It does not include energy consumption associated with distribution fans and circulation pumps.
- *Building Thermal Energy Flexibility Index (BEFI) [kW]*. It quantifies the average available power throughout a specified length of time, usually at times of peak demand, compared to the reference profile. BEFI is calculated as follows defined by Athienitis and Dumont; (2020):

$$\overline{BEFI}(t, Dt) = \frac{\int_t^{t+Dt} P_{ref} dt - \int_t^{t+Dt} P_{flex} dt}{Flexibility\ time\ period} \quad (4-2)$$

Where,

BEFI - the mean energy flexibility Index at time t over period Dt,

$P_{ref}$  – average power demand at time t over period Dt under reference strategy, kW,

$P_{flex}$  – average power demand at time t over period Dt under energy flexibility control strategy, kW.

- *Building Thermal Energy Flexibility Index Percentage (BEFIP) [%]*. Indicates the average power reduction relative to the baseline reference in terms of % (Equation 4-3):

$$\overline{BEFIP}(t, Dt) = \frac{\int_t^{t+Dt} P_{ref} dt - \int_t^{t+Dt} P_{flex} dt}{\int_t^{t+Dt} P_{ref} dt} \quad (4-3)$$

- *Load shifting [kWh]*. The amount of thermal energy displaced over peak demand hours considering indoor thermal comfort as a constraint.

- *Imported electricity power [kW]*. The amount of power imported from the grid under a proposed strategy by calculating the energy balance of the building where the building footprint is the energy boundary. As described in section 2, the building has an installed PV capacity of 110.5 kW, where generated energy displaces building loads with the excess being exported to the grid. The energy balance for new imported power, given the availability of measured imported power, is calculated as follows:

$$\text{Import}_{\text{new}} = \text{Import}_{\text{measured}} - (\text{Load}_{\text{measured}} - \text{Load}_{\text{new}}) - \text{Export}_{\text{measured}} \quad (4-4)$$

Where,

$\text{Import}_{\text{measured}}$  – measured imported power to the library from the grid under current control strategy, kW,

$\text{Import}_{\text{new}}$  – resultant imported power from the library to the grid under proposed control strategy, kW,

$\text{Load}_{\text{measured}}$  – electrical load of the library under current control strategy, kW,

$\text{Load}_{\text{new}}$  – electrical load of the library under proposed control strategy, kW,

$\text{Export}_{\text{measured}}$  – measured exported power to the grid from the library under current control strategy, kW.

## 4.5 Results and discussion

### 4.5.1 Indoor thermal conditions

Monitoring the indoor thermal conditions of the space on the design days is critical to evaluate the effectiveness of the control strategy and sizing of the air conditioning system. Data collected over 2 months span (January-February, 2018) were analyzed, and the indoor temperature on very cold days was selected for further comparison and performance analysis. The air temperature of the zones is

averaged based on weighted areas and presented here as a single variable. Figures 4-17 and 4-18 show the measured and resulting inside temperature under proposed control strategies alongside outdoor thermal conditions. On sunny days (Figure 4-17), the energy-efficiency strategy steadily brings and maintains the space temperature slightly above 21°C throughout the day.

In contrast, the energy flexibility case reaches a peak of 23°C at 2 pm, followed by a gradual decline to the end of the library’s operation. The highest temperature difference is 2.5 °C throughout the day and all strategies, including the current one, satisfy the thermal comfort requirements recommended by ASHRAE 55 (ASHRAE, 2016). Temperature profiles on cloudy and semi-cloudy design days are shown in Figure 4-18. Collected data shows that the library is strongly overheated on both days and current conventional reactive controls fall short. Both proposed predictive control strategies achieve minimum acceptable indoor thermal comfort conditions since the first hour of the library’s operation and maintain it throughout the day.

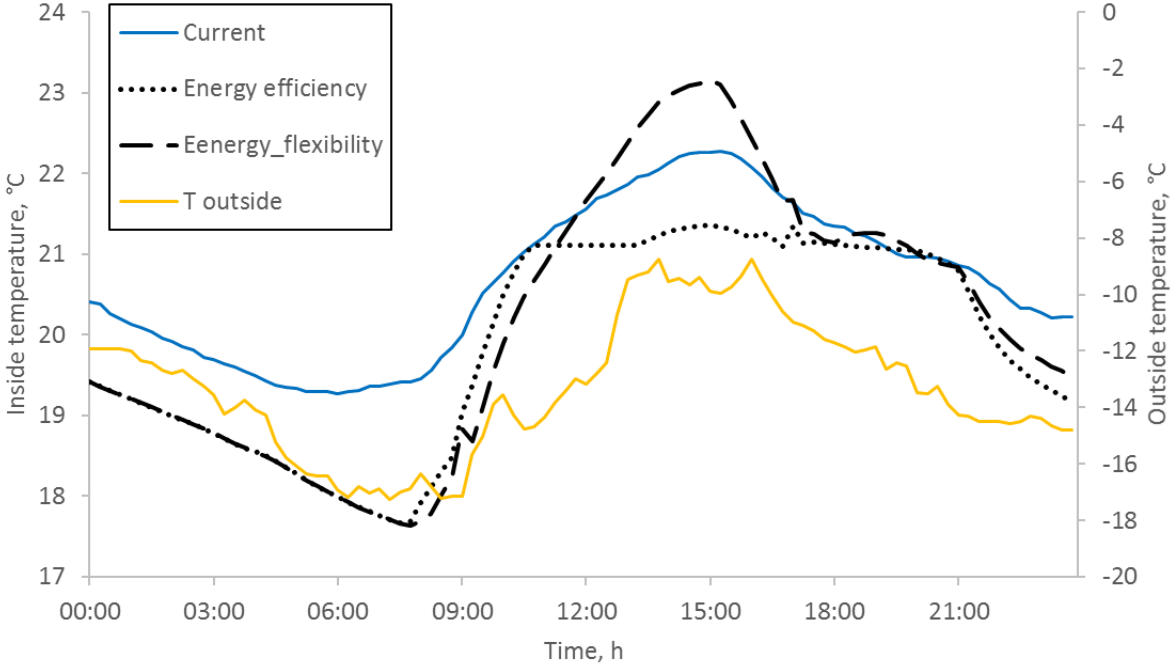


Figure 4-17: Indoor air temperature on a sunny day under proposed and current control strategies.

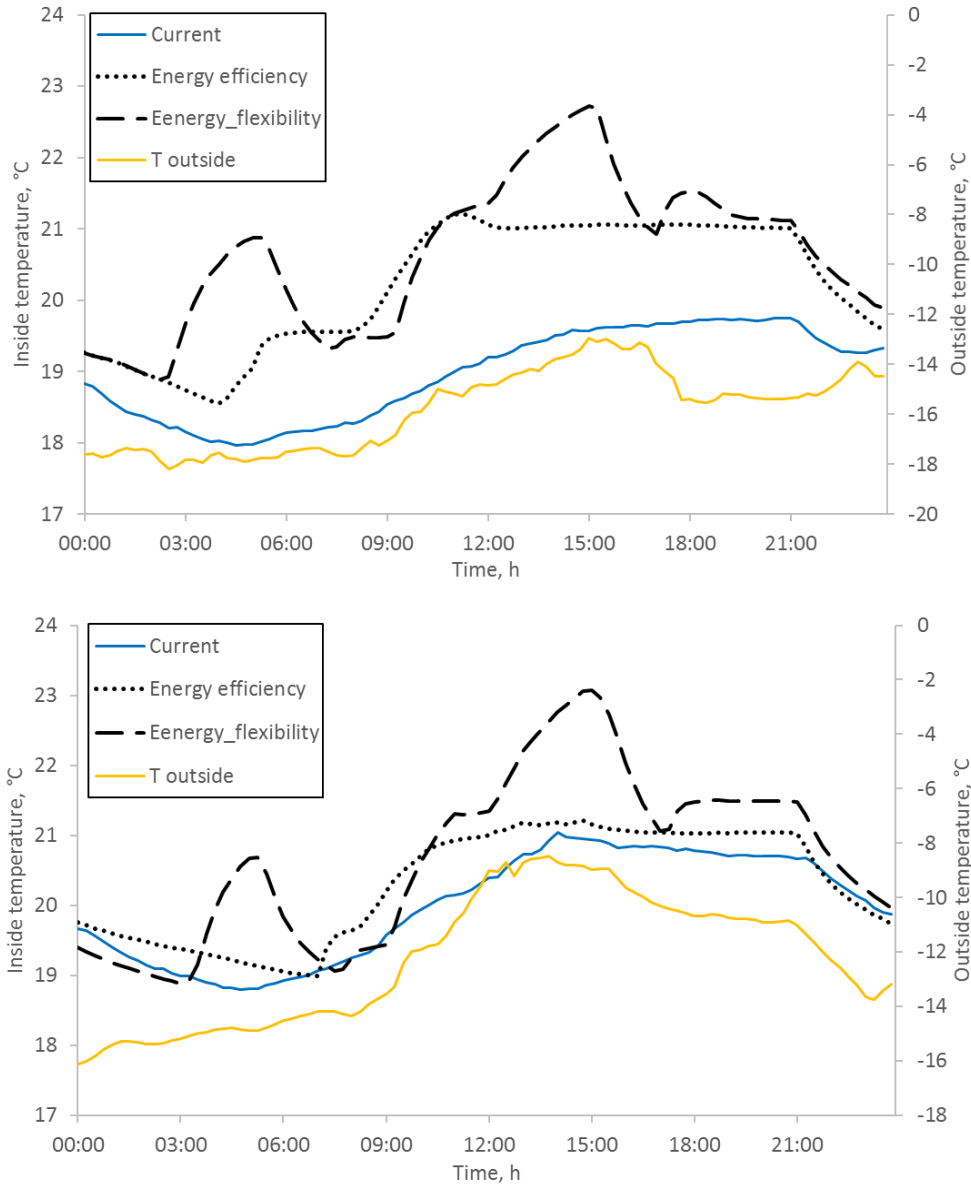


Figure 4-18: Indoor air temperature on cloudy (top) and semi-cloudy days (bottom) under proposed and current control strategies.

## 4.5.2 Thermal load and load shifting

Figure 4-19 illustrates the impact of proposed control strategies on the thermal energy load over 24 hours on extremely cold days. On sunny days, the heating loads are decreased by 25% under the energy-efficiency strategy, whereas the energy flexible case saves only 4% of energy. On

cloudy and semi-cloudy days, energy savings with the energy-efficiency strategy are only 15% and 8%, respectively, but they also satisfy thermal comfort conditions, as was discussed above.

Figures 4-20, 4-21, 4-22 show the load shifting potential from two peak demand periods for all three strategies on sunny, semi-cloudy and cloudy days, respectively. On very cold sunny days, the energy-flexibility strategy shifts on average 68% of load during peak demand events compared to the current and energy-efficiency strategy. However, 100% of the energy demand is shifted from both peak periods on cold and mild sunny days. On a very cold semi-cloudy day, 76 % of the peak energy demand relative to the current baseline strategy and 78 % relative to the energy efficiency strategy is displaced. Similar to sunny days, on cloudy cold and mild days, 100% of demand is displaced. The energy-flexibility strategy is highly effective on very cold cloudy days as well, reducing the power demand by almost 81 % in peak demand events. Like semi-cloudy and sunny days, 100% of demand is shaved at the mild and cold types of days.

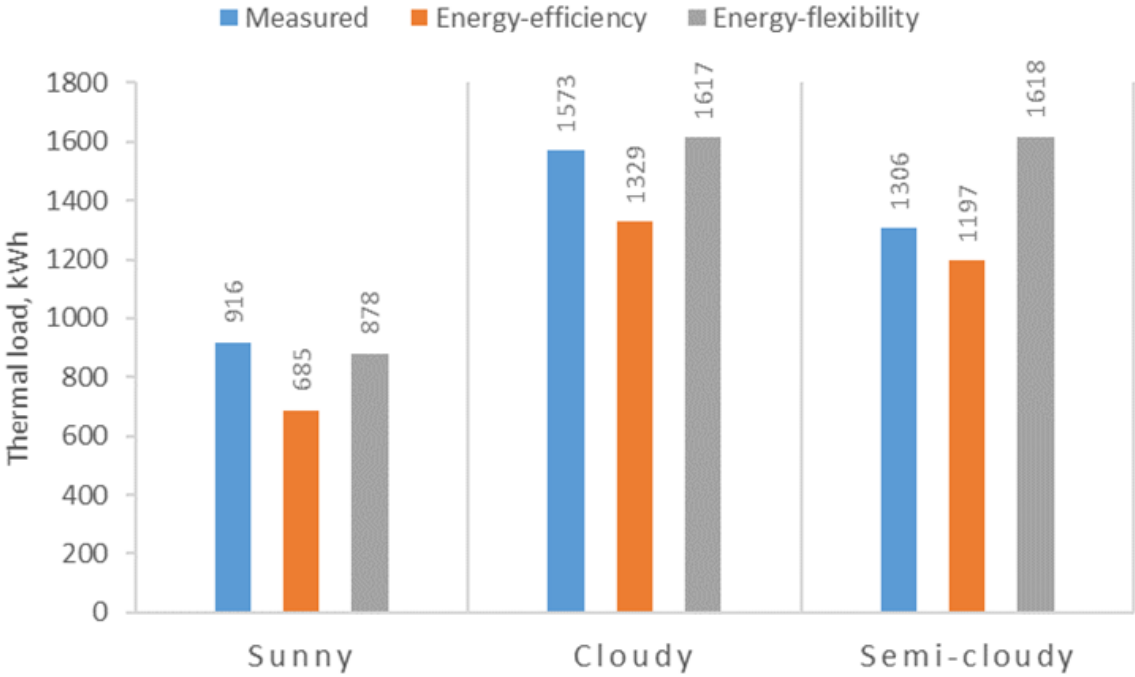


Figure 4-19: Thermal loads under proposed and current (measured) control strategy on very cold days.

Overall, the energy-flexibility strategy leads to a substantial demand decrease in peak hours, between 70% and 100%, while increasing energy use for heating by approximately 30% compared to the energy-efficiency strategy.

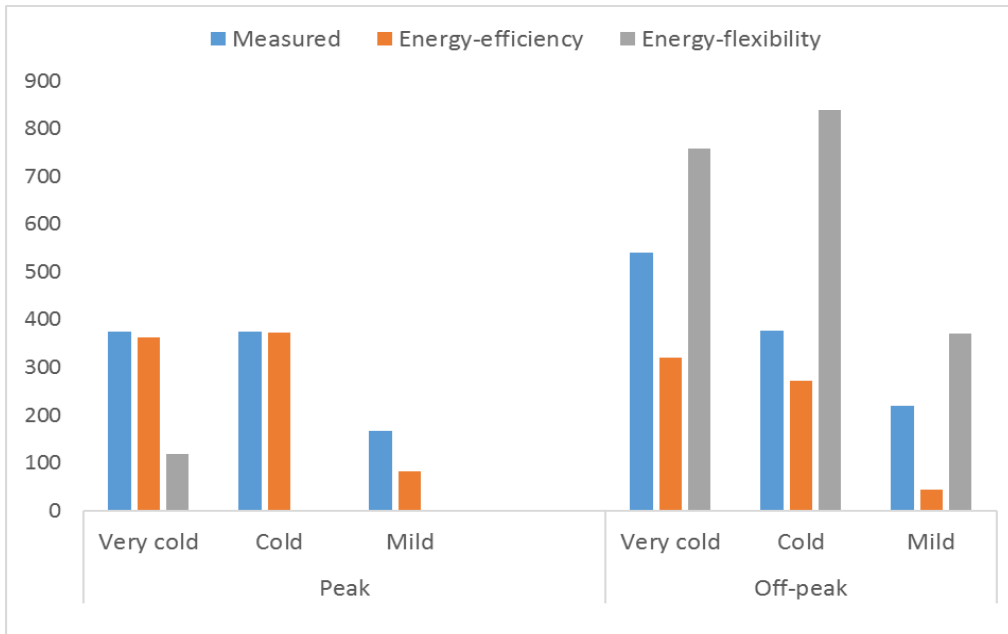


Figure 4-20: Thermal load during peak and off-peak demand periods on sunny days.

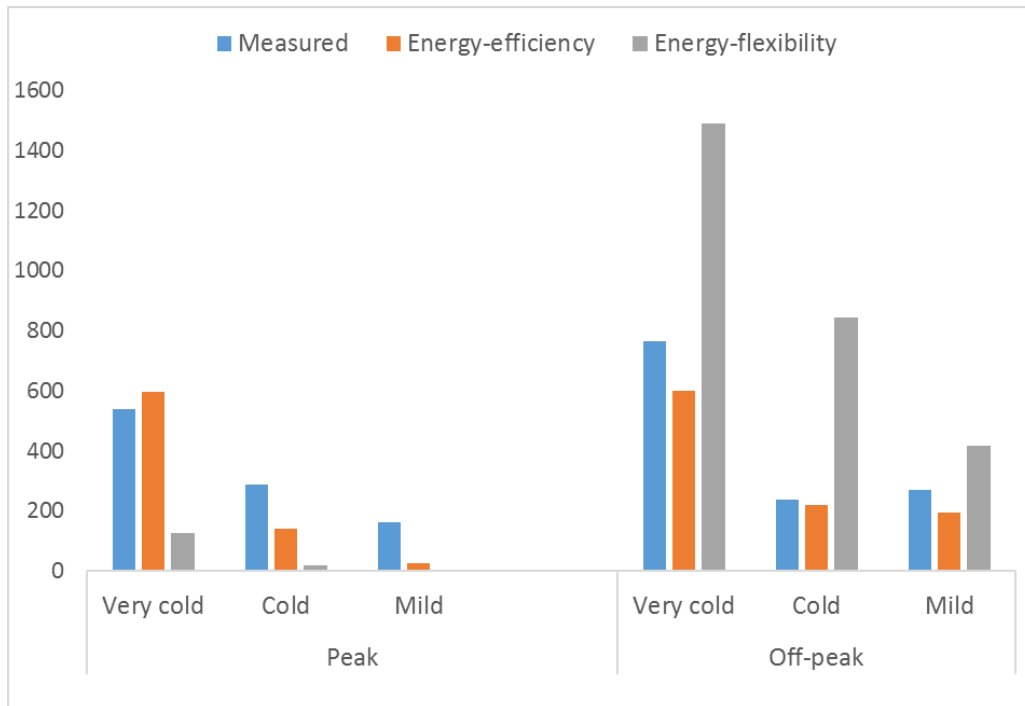


Figure 4-21: Thermal load during peak and off-peak demand periods on semi-cloudy days.

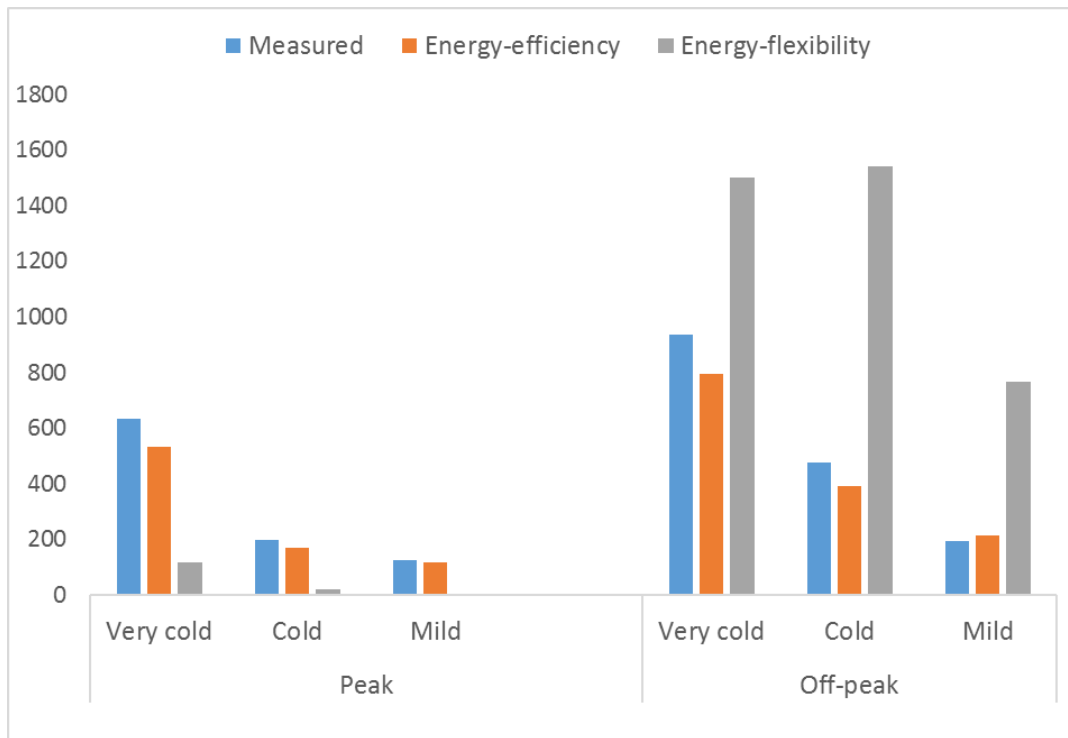


Figure 4-22: Thermal load during peak and off-peak demand periods on cloudy days.

### 4.5.3 Energy Balance and Flexibility Index

Figures 4-23 and 4-24 show the continuous building energy balance profile on a very cold sunny day. The majority of excess energy associated with the energy flexibility strategy is met by on-site renewable electricity production. As a result, the energy-flexibility case has 15% less total energy import from the grid than the measured case. Analogous results for the other 8 types of days are shown in Appendix D. The reason why currently implemented reactive controls fail to achieve thermal comfort on cold cloudy days is now apparent. Although heating is operating continuously and eventually consumes more energy than the predictive energy-efficiency strategy, it is working below the available heating capacity for a continuous period of time. The heat loss at an instantaneous point in time outweighs the required energy input from heating. One of the reasons for this behaviour is that the tuning of the control loop is done in one

condition, which is no longer valid under extreme conditions. Even self-tuning techniques do not always solve the problem as there are challenges associated with disturbances that skew the results when a step test is in progress. Predictive controls overcome this issue by predicting the load based on anticipated exogenous inputs and disturbances and reacting before the event occurs as long as the embedded model is accurate enough.

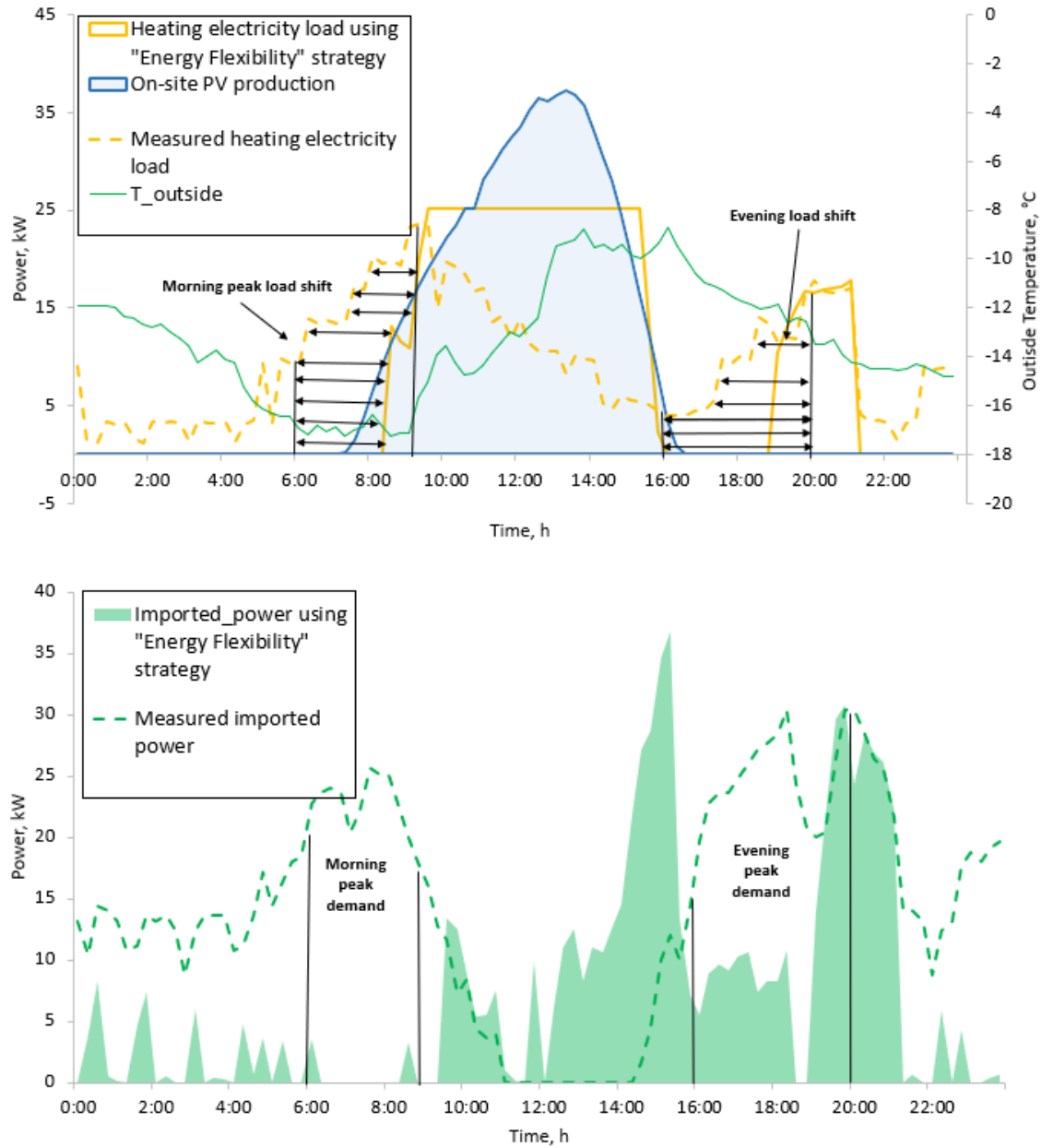


Figure 4-23: Energy balance on a very cold sunny day under proposed energy flexibility strategy; PV production, electrical heating load (top); resultant imported power (bottom); January 26, 2018.

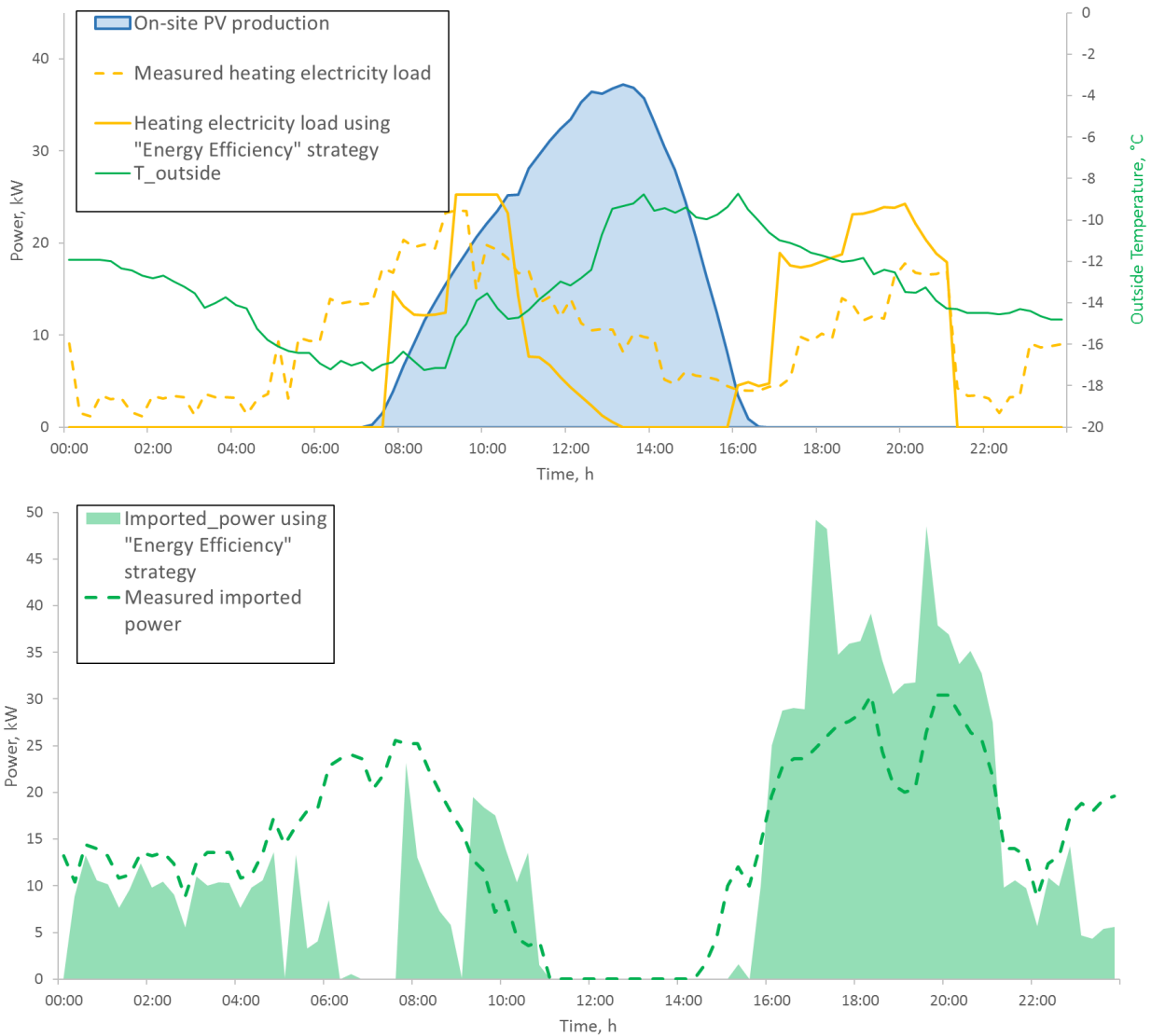


Figure 4-24: Energy balance on a very cold sunny day under proposed energy efficiency strategy; PV production, electrical heating load (top); resultant imported power (bottom); January 26, 2018.

Figure 4-25 below compares the averaged BEFIP of all 9 energy flexible strategies. Evidently, on cold and mild days, it is possible to achieve nearly 100% of BEFIP if the appropriate setpoint profile is chosen. The scenarios of the biggest importance, very cold days, also show promising results by reaching the BEFIP on cloudy and semi-cloudy days 78% and 87%, respectively. On an analogous sunny day, BEFIP is only 65% on average (83% in the morning and 48% in the evening peak period) since there is already a low demand to displace beforehand.

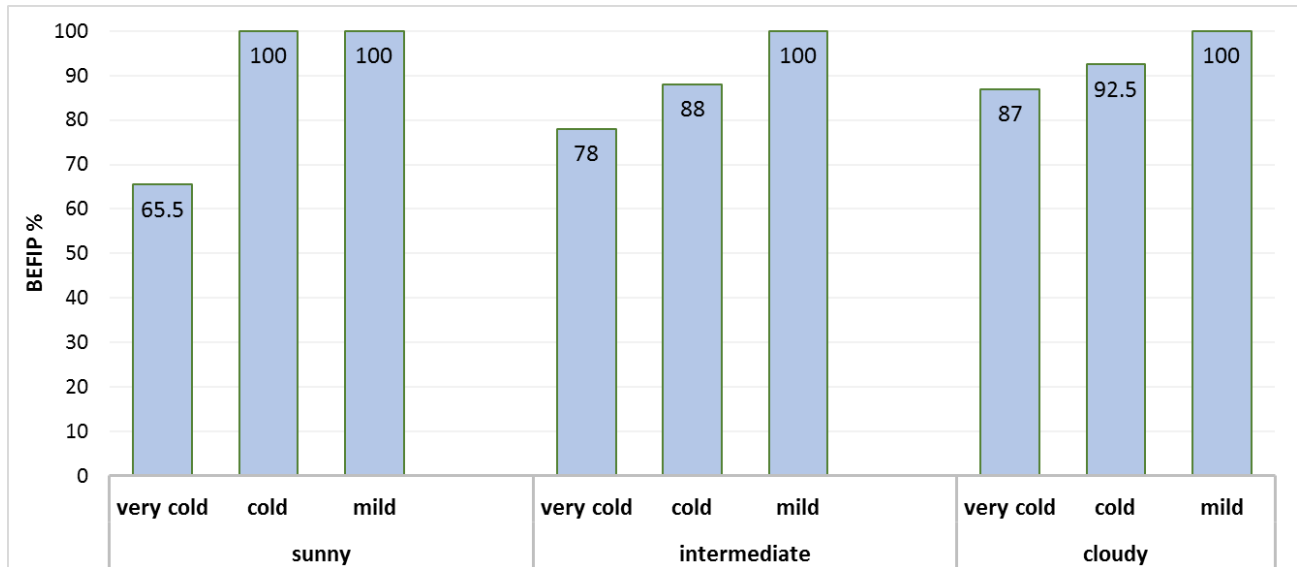


Figure 4-25: Resultant BEFIP % for all 9 scenarios under energy flexibility strategy.

Table 4-4 below compares the control strategies in terms of thermal energy flexibility index, BEFI, for two peak demand periods in Quebec. The results show that with predictive heuristic model-based control strategies with the objective to maximize energy flexibility, it is possible to reduce daily average power demand during 3 hours of the morning and 4 hours of peak period by an average of 90% and 60%, respectively if a building is passively designed and optimally operated.

Table 4-4: BEFI index in kW electrical load under proposed control strategies. % indicates the BEFI relative to the reference average power demand.

Strategy	Sunny		Intermediate		Cloudy	
	Morning peak	Evening peak	Morning peak	Evening peak	Morning peak	Evening peak
<b>Energy Efficiency</b>	46 kW (64%)	-31 kW (-77%)	-17 kW (-21%)	-1.5 kW (-2%)	-6 kW (-7%)	30 kW (30%)
<b>Energy Flexibility</b>	59 kW (83%)	20 kW (48%)	71 kW (90%)	50 kW (66%)	76 kW (95%)	78 kW (75%)

#### 4.5.4 Preheating length analysis

The effect of varying preheating periods for the energy-flexibility strategy on the example of a cloudy day is also investigated. The lengths of 4, 5, 6 and 7 hours of preheating are considered. Table 4-5 presents the BEFI and electrical energy consumption on a very cold cloudy day. Results show that 7 hours of preheating ahead of both peak periods yields significantly higher BEFI, displacing 95% and 78% average power, respectively, at the cost of only 15% increased energy consumption. While for the morning peak, 5 hours of preheating are close to the optimal, for the second peak demand event, 7 hours is recommended.

Table 4-5: BEFI at different preheating lengths alongside daily energy consumption on a very cold cloudy day, January 3, 2018.

Strategy	BEFI		Energy
	Morning peak	Evening peak	
<b>Current</b>	80 kW	99 kW	363 kWh
<b>(Reference)</b>			
<b>4 hours</b>	55 kW (68%)	50 kW (51%)	374 kWh
<b>5 hours</b>	64 kW (83%)	52 kW (53%)	396 kWh
<b>6 hours</b>	69 kW (86%)	55 kW (56 %)	420 kWh
<b>7 hours</b>	76 kW (95%)	78 kW (78%)	442 kWh

## 4.6 Conclusion

This chapter presented heuristic model-based predictive control strategies applied on an archetype institutional NZEB building incorporating active and passive charging of hydronic radiant slab. The methodology for developing and calibrating a control-oriented model derived from the first principles was also investigated. The critical lessons learned from this study include the following:

- It was found that incrementally increasing the complexity of the model with nominal parameters improves the model accuracy. The incorporation of “effective” air node capacitance has a significant effect on the model's short-term indoor air prediction performance. The 10<sup>th</sup> order RC model, which comprised air and wall thermal capacity and nonlinear heat transfer coefficients, can accurately predict the dynamic thermal behaviour of the library (CV-RMSE < 3%). 8<sup>th</sup> order model, which considered indoor objects’ (such as furniture, book stacks and so on) thermal mass effect, was the second-best choice (CV-RMSE of 3.3%).
- It was shown that a building with effective integration of renewable energy technologies (BIPV/T, geothermal) and passive design features could achieve nearly 100% of energy flexibility in the majority of the heating season (cold and mild days) throughout the whole peak demand period.
- On a very cold sunny day, applying a low-temperature setback strategy at night, a smooth transition in a setpoint closer to the library’s opening time and anticipation of the solar gains during the day resulted in 25% energy savings. Using the same approach in the morning but preheating the slab 5.5 hours before the peak demand event displaced approximately 65% of average power over the two peak periods. Considering the library's

energy generating capacity, the bulk of displaced energy was replaced by on-site PV production, resulting in only a 15% rise in heating energy consumption.

- Simple reactive controls with a fixed night setback result in a strongly underheated building on a design day. The use of predictive controls allows initiation of the heating at the right time and power intensity to meet the thermal comfort conditions of the building. A predictive control strategy also prevents the potential overheating on sunny days by anticipating solar gains and taking appropriate actions to reduce the heating loads.
- It was shown that it is possible to displace approximately 85 % of the peak demand on cold cloudy days by preheating the slab 5 hours before morning peak and 7 hours before evening peak demand event or reduce the energy consumption by more than 15% considering the optimal preheating period, smooth morning transition, projected operation of heating equipment and occupancy.
- Using onsite PV production data at 9 am and noon and comparing it with the projected value can be an effective strategy to alleviate the uncertainties associated with the weather prediction and effectively choose a predeveloped model-based predictive control strategy.

Results show that a heuristic MPC can be a successful alternative to the fully optimized MPC as a solution to significantly improve energy efficiency, enhance energy flexibility, enhance load management and thermal comfort while reducing computational needs. The proposed strategy combines the benefits of numerical MPC for using the building model and RBC for practicality and cost-effectiveness of implementation to minimize the energy consumption and maximize the energy flexibility provided to the grid.

# Chapter 5

## BIPV/T modelling, design and optimization

### 5.1 Archetype system analysis

When zero-energy buildings are considered, it is referred to buildings that incorporate energy-saving measures and renewable energy technologies to meet their energy needs. Therefore, integrating PV systems into buildings becomes critical. To enhance energy flexibility and push energy efficiency even further, upgrading the BIPV system to BIPV/T can be a viable solution, especially in a heating-dominated climate. Besides acting as a generation system, they can store heat in a manifold, couple with heat pumps and any active storage technology such as hot water storage or ventilated slab. As was discussed in Chapter 2, there are not many large-scale applications of the BIPV/T currently in practice. One of such archetype systems is installed in the Varennes Library as a prototype. Approximately 1/6<sup>th</sup> portion of the roof is covered with the BIPV/T, integrated with the AHU to preheat the ventilation air during the heating period. It serves as an excellent archetype system to analyze the collected data and provide a methodology for control-oriented modelling to study alternative design and control options. The arrangement of the BIPV/T installed on the roof of the Varennes library is shown in Figure 5-1.

The air passing through the BIPV/T cavity enters the Air Handling Unit (AHU) to preheat the ventilation air if there is a demand for heating; otherwise, it exhausts outside. When the air enters the AHU, it mixes with the incoming outdoor fresh air, followed by proceeding through the heat recovery unit (Figure 5-2). The heat recovery unit installed is the Heat Wheel modulated between 0% and 100% with nominal efficiency of 40%. It recovers heat from the return air

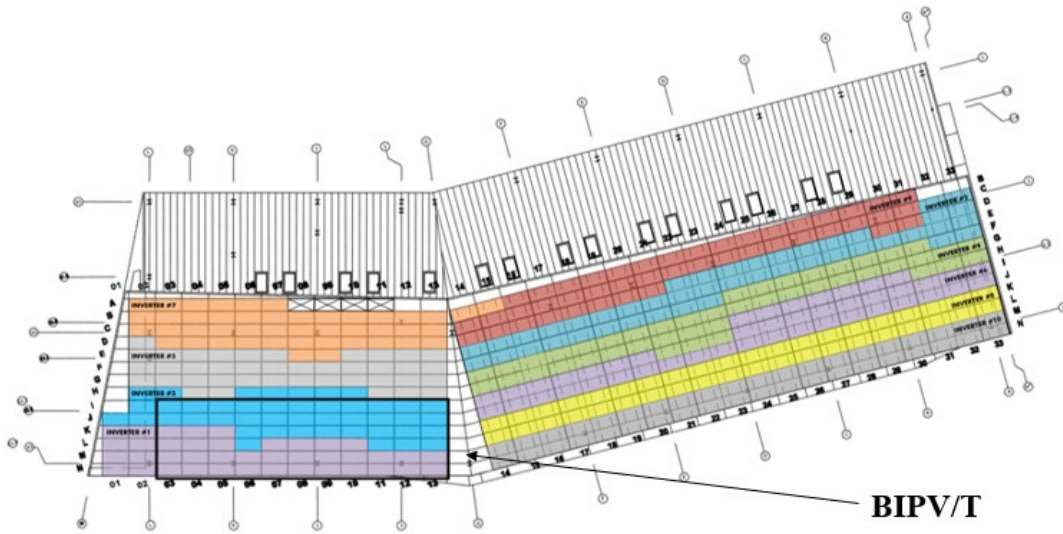


Figure 5-1: BIPV/T layout on the south-facing roof of the Varennes Library.

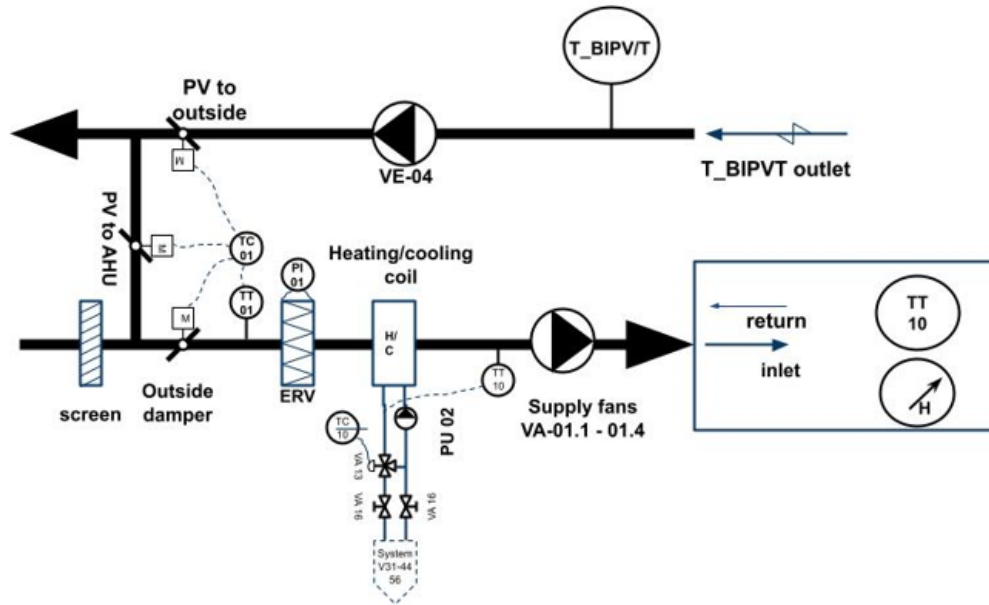


Figure 5-2: Mechanical arrangement of the BIPV/T and AHU.

stream and terminates when the return temperature is lower than the supply temperature or when the system demands cooling.

Sensors in the AHU continuously record the data every 15 minutes, including BIPV/T, mixture, supply, exhaust temperatures; the state of BIPV-to-outside, BIPV/T-to-AHU, outdoor air dampers; the modulation of all supply and exhaust fans and the modulation of the valve in

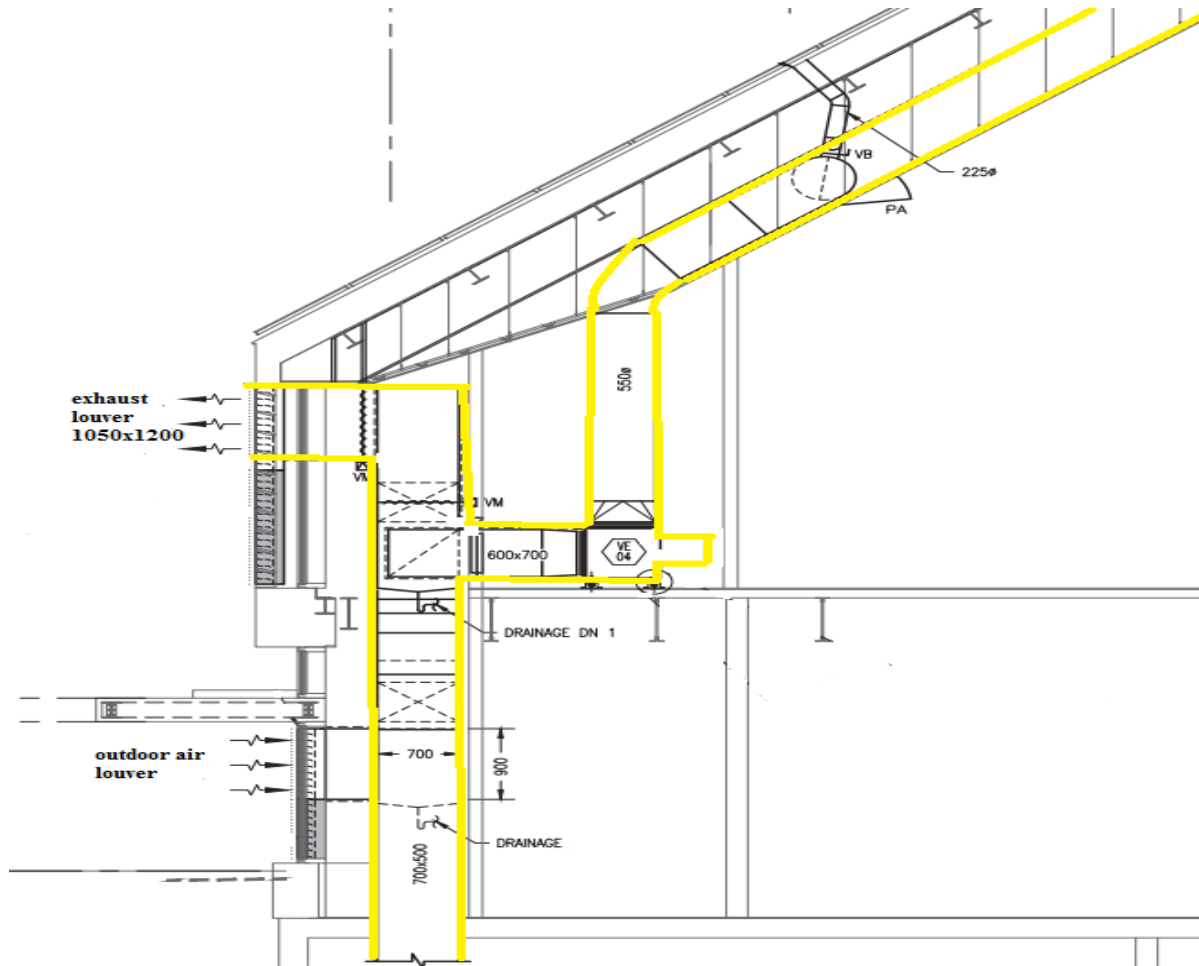


Figure 5-3: Cross-sectional view of the air stream from the BIPV/T. Air from the BIPV/T either enters the AHU or exhausts outside.

heating /cooling coils. The detailed view of the BIPV/T system configuration is shown in Figure 5-3. To analyze the operation and performance of the system, two cold (ambient temperature around -10 °C) sunny days are selected: February 5<sup>th</sup> and March 20<sup>th</sup> (Figure 5-4). Solar irradiation data is obtained from the CanmetENERGY-Varenes PV research measurement station, whereas hourly wind velocity data is acquired from the L'Assomption weather station. The recovery fan (VE04 fan from Figure 5-2), which ventilates the PV cells of BIPV/T, has a flowrate capacity of 1142 L/s.

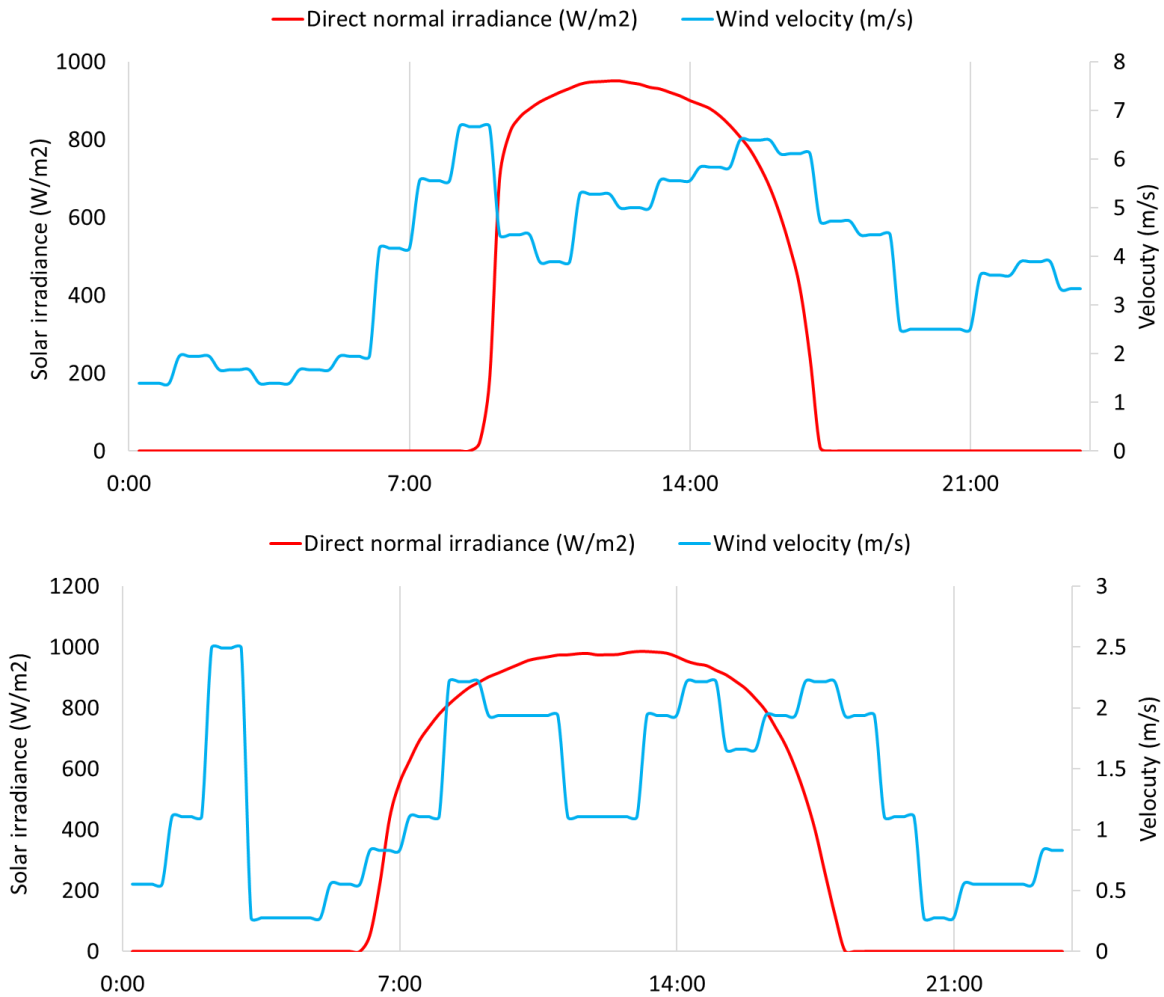


Figure 5-4: Direct Normal Irradiance and wind velocity on February 5 (top) and March 20 (bottom).

The speed of the BIPV/T fan is controlled by the outlet temperature from the air channel of the BIPV/T only. The overriding control of the fan is based on the energy generation of the overlying BIPV system. When there is no energy production, the fans are stopped, and the BIPV/T-to-AHU damper is closed. When there is an energy generation and if there is a demand for heating, the BIPV/T-to-AHU damper opens, followed by the start of the BIPV/T fan (VE-04 fan). The BIPV/T fan operates sequentially; once ON, its capacity is discretely modulated between 33% or 80% to maintain the outlet temperature from BIPV/T under 25°C. When the outlet temperature of the air is below 25°C for more than 60 minutes, the fan switches its speed

from 80% to 33%. The modulation algorithms of the BIPV/T recovery fan and thermal wheel are summarized as follows:

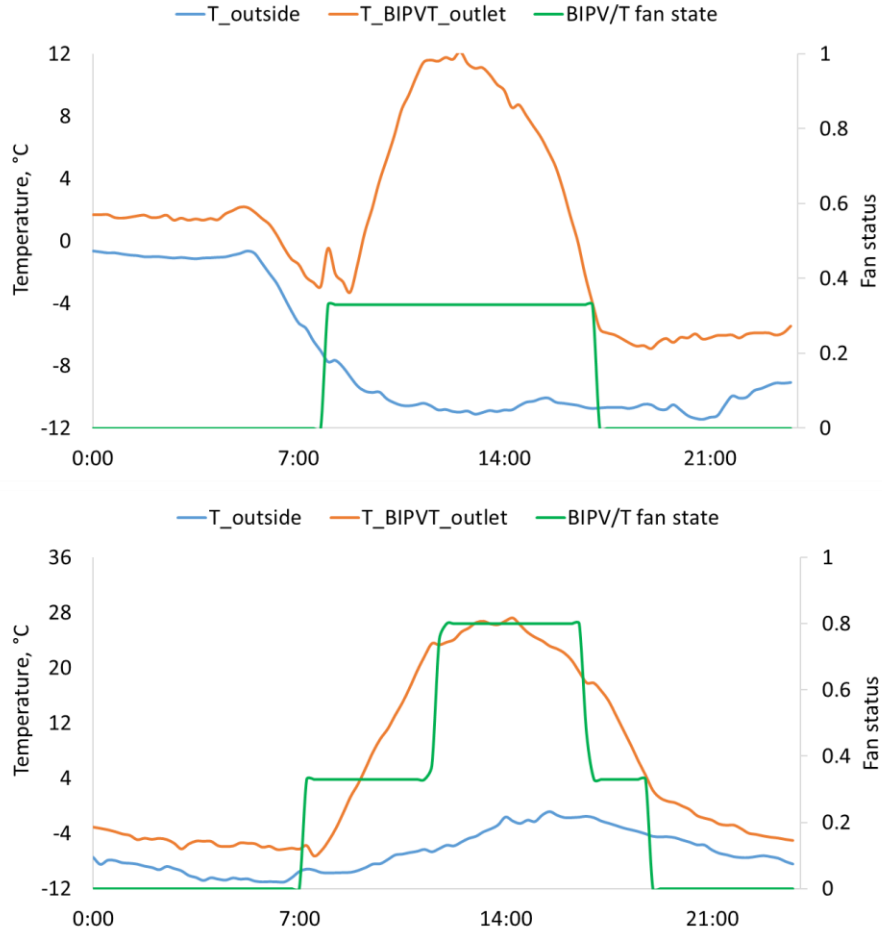


Figure 5-5: Daily fan operation, BIPV/T outlet and outside temperatures (°C) on February 5 (top) and March 20 (bottom).

$$BIPV/T\_fan_{modulation} = \begin{cases} 0.33 & \text{if } T_{outlet} < 25^{\circ}\text{C} \\ 0.8 & \text{if } T_{outlet} \geq 25^{\circ}\text{C} \end{cases}; \quad \Delta t_{deadband} = 60 \text{ min} \quad (5-1)$$

$$Heat\_wheel_{modulation} = \begin{cases} 0 & \text{if } T_{return} - T_{mix} \leq 0^{\circ}\text{C} \\ 1 & \text{if } T_{return} - T_{mix} > 0^{\circ}\text{C} \end{cases}; \quad \Delta t_{deadband} = 30 \text{ min} \quad (5-2)$$

where,

$T_{outlet}$  – outlet air temperature from the BIPV/T, °C,

$T_{return}$  – temperature of the return airstream, °C,

$T_{mix}$  – temperature of the mixture of air from the BIPV/T and unconditioned outside air, °C,

$\Delta t_{deadband}$  – bidirectional delay in the controlled VFD; if the controlled variables are outside of setpoint by more than  $\Delta t_{deadband}$ , the control action is taken; otherwise, modulation does not change.

This is well illustrated in Figure 5-5 above. On a clear cold windy day, February 20, the outlet temperature from the BIPV/T fluctuates between -6°C and 12°C and the recovery fan operates at 33% modulation unless there is no energy generation. On March 20, however, when the weather is more moderate, the temperature of the BIPV/T channel reaches 28°C. Once the temperature exceeds 25°C for more than 60 minutes, the fan modulates from 33% to 80%. One of the challenges associated with this integrated system was identifying the actual amount of air incoming from each source: outdoor air and recovered BIPV/T air. Having the measured data, the total incoming flow rate and individual fresh air and BIPV/T outlet air temperatures and temperature of the mixture before passing through the heat wheel made this task straightforward. The total incoming flow rate equals the total exhaust air from the building, which is recorded in the dataset. Then, the following equation of the mixture's temperature can be used (Equation 5-3).

$$T_{mix} = \frac{T_{BIPVT} * V_{BIPVT} + T_{outdoor} * V_{outdoor}}{V_{exhaust}} \quad (5-3)$$

Figure 5-6 below shows the proportion of the BIPV/T flowrate out of the total volumetric flow passing through the AHU on the two selected days. It can be observed that the fraction of the BIPV/T flow is consistently above 75%, even when the recovery fan operates at only 33% of the capacity. This implies that the general supply fans, VA-01.1-VA01.4, significantly contribute to air suction from the BIPV/T channel once the BIPV-to-AHU damper is open. One of the possible

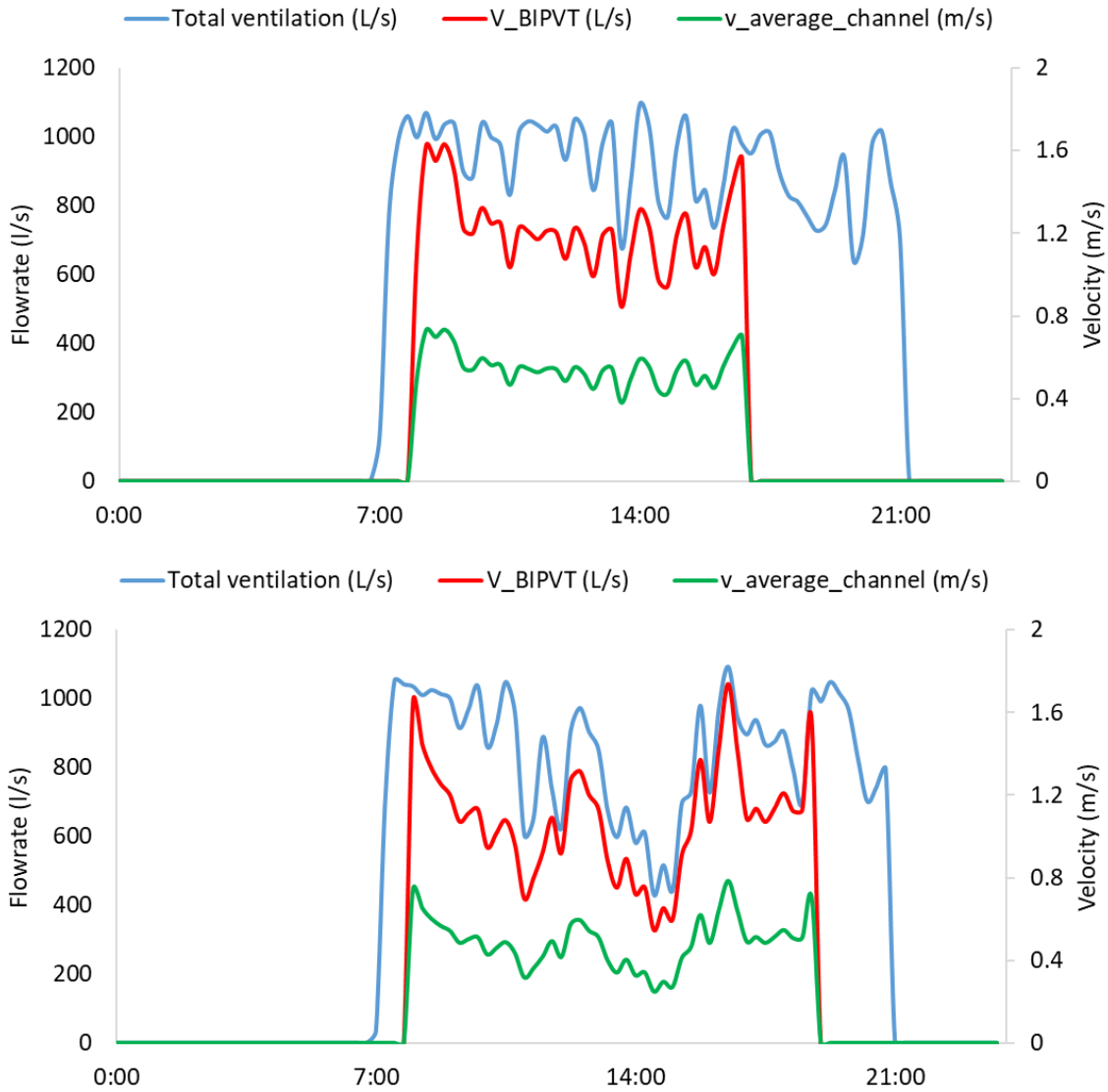


Figure 5-6: Total ventilation, BIPV/T flowrate (L/s) and average velocity over the channel (m/s) on February 5 (top) and March 20 (bottom).

reasons is that the outside damper is not 100% open, and the discrete recordings of the sensor at the gates do not fully represent the complete picture of the damper state. The velocity in the air channel fluctuates between 0.3 m/s and 0.8 m/s. The effect of the heat wheel on the supply air temperature is shown in Figure 5-7. It can be seen that on March 20<sup>th</sup>, the supply temperature due to recovered heat from the BIPV/T approaches the inside temperature, after which heat recovery stops its operation. The temperature after the heat wheel is calculated by the following relationship (Equation 5-4).

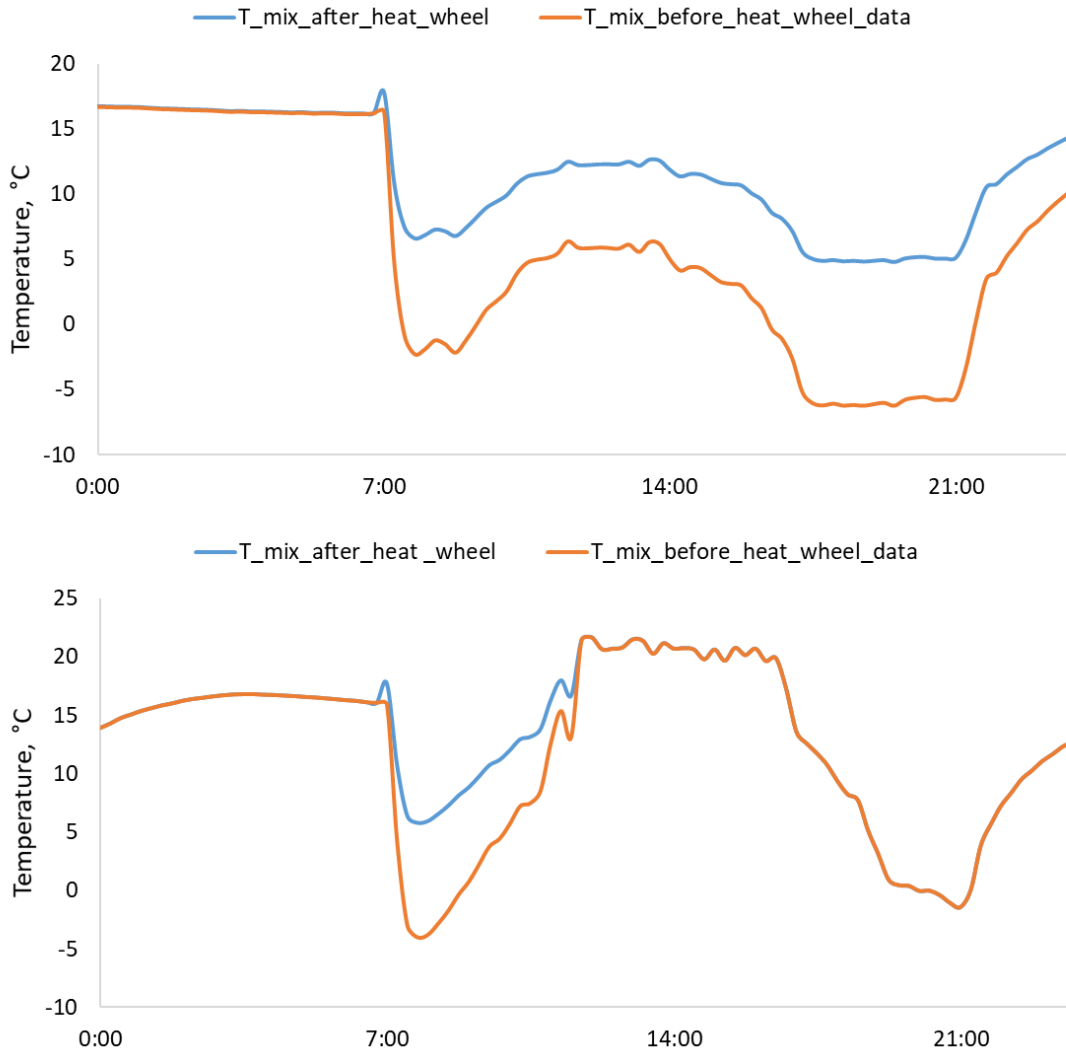


Figure 5-7: Temperature of mixed air from BIPV/T outlet and outdoor air before and after passing through thermal wheel (°C) on February 5 (top) and March 20 (bottom).

$$\eta = \frac{T_{out} - T_{in}}{T_{return} - T_{in}} \quad (5-4)$$

The thermal performance of the BIPV/T on two clear days is shown in Figure 5-8 below. On a sunny windy day (February 5), the heat recovered by the BIPV/T significantly contributes to preheating the ventilation air by supplying peak thermal power of 20 kW from 10 am to 2 pm and outweighing the additional heat provided by the heating coil most of the time. On a still clear

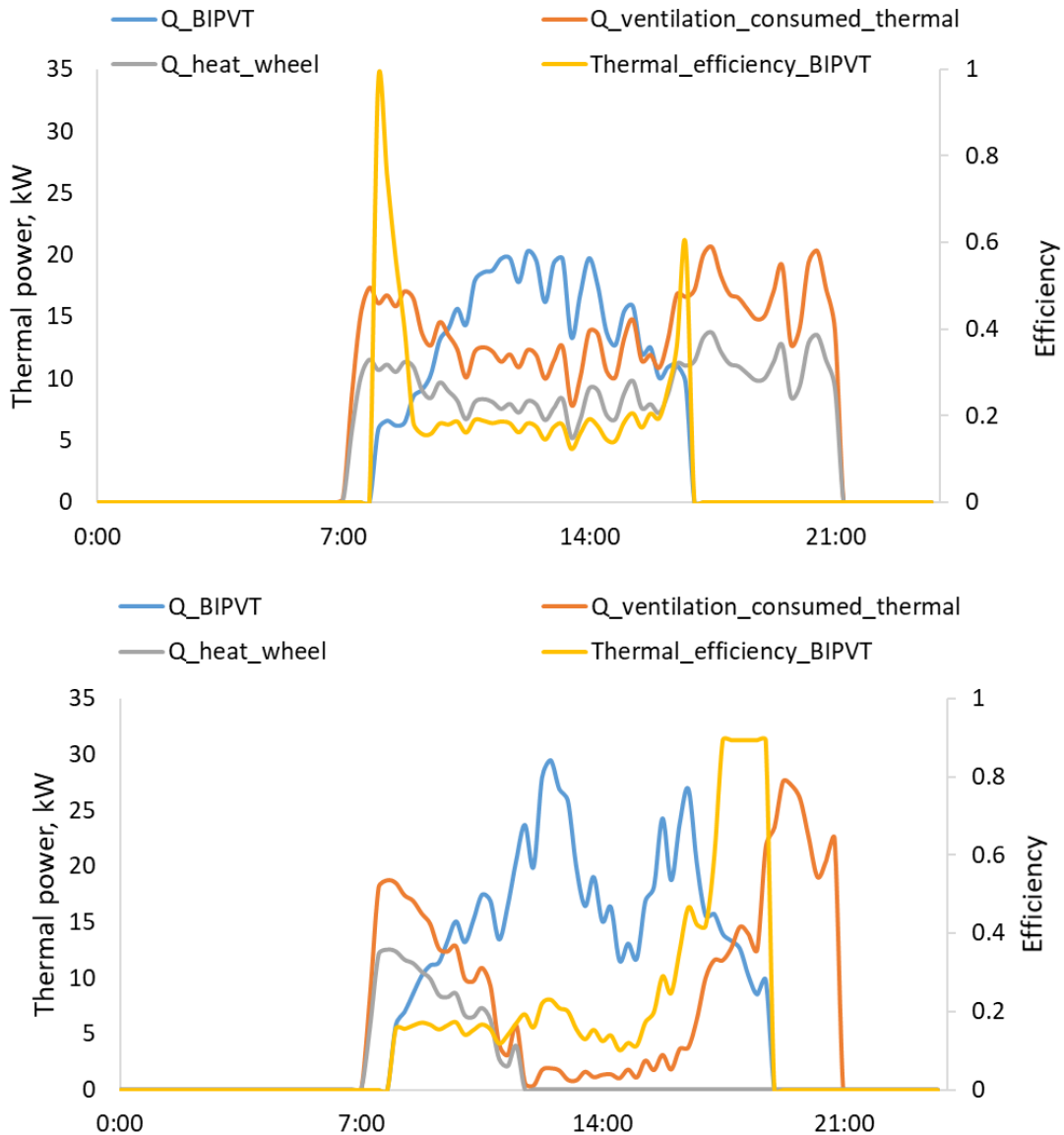


Figure 5-8: Heat recovered by the BIPV/T and thermal wheel (kW), heat added to bring the ventilation air to indoor air temperature (kW) and thermal efficiency of the BIPV/T on February 5 (top) and March 20 (bottom).

day (March 20), heat provided by the BIPV/T entirely displaces the ventilation load from 11:45 am till 5 pm, after which the recovered thermal energy gradually drops till 7 pm. Thermal efficiency in the morning and evening periods is skewed by the day before preheated AHU and unrealistically aims for infinity. The practical thermal efficiency identified at stable conditions throughout the day fluctuates between 20 – 25%. Considering the electricity production, the

combined efficiency of the installed BIPV/T system, if coupled with an air-source heat pump (ASHP), is potentially above 80%. Overall, the thermal energy recovered on February 5 and March 20 equals 127 kWh and 180 kWh. The following section will cover a wind-driven convective transfer correlation study and control-oriented model development. This will be followed up with the alternative design and control suggestions and conclusion.

## 5.2 Control-oriented model development

To evaluate the thermal behaviour of the BIPV/T, the RC thermal network model is used (Figure 5-9). The network comprises a BIPV panel, the air in the cavity below the PV layer, bottom insulation and ambient which interaction achieves a steady state in a relatively short term due to insignificant thermal capacitance of the PV panel. As air flows through the BIPV/T channel, heat is extracted from both the top and bottom surfaces of the cavity. Air is heated as it flows through the channel, and its temperature increases along the flow route. To model this phenomenon, the roof is discretized into 100 one-dimensional control volumes in a streamwise direction. Each control volume is divided into 100 points to model the subsection. The outlet

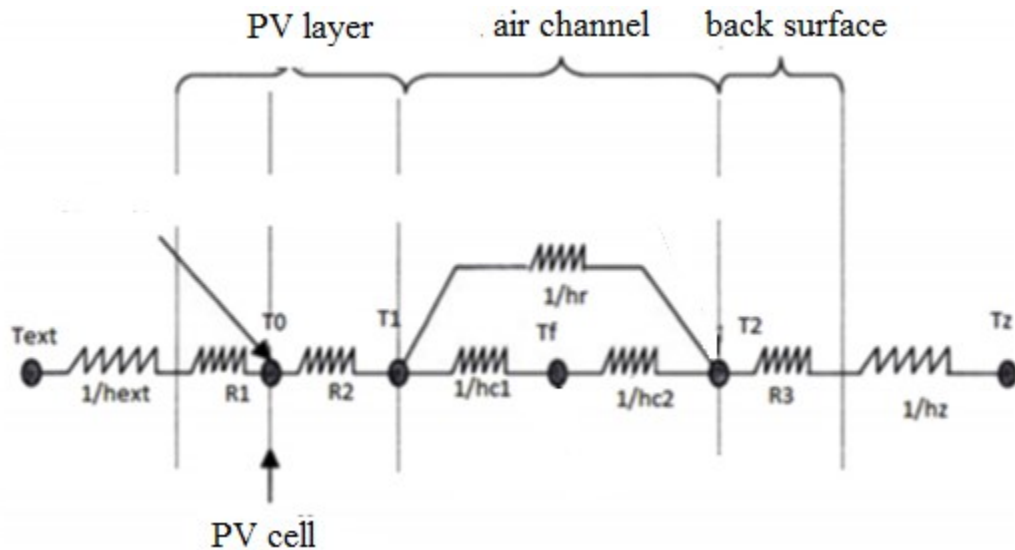


Figure 5-9: RC thermal network representing the PV later, air channel beneath it and back surface insulation.

temperature of each control volume is equal to the inlet temperature for the following one. In both vertical and horizontal directions, 1D heat transfer and steady-state are assumed. As several studies showed, the temperature difference across the PV layer can be significant (Amori & Abd-AlRaheem, 2014; Candanedo, 2010), conduction heat transfer through the module is thus considered. The model was developed and simulated in MATLAB.

Air in each control volume extracts a total amount of thermal energy given by Equation 5-5:

$$Q_{air} = \dot{m}c_p(T_{exit} - T_{in}) \quad (5-5)$$

Where,

$Q_{air}$  – heat gained by air while passing through the channel of the BIPV/T, W,

$\dot{m}$  - mass flowrate of air through the channel, kg/s,

$c_p$  – specific heat capacity, J/(K kg),

$T_{exit}$  – outlet temperature of the air from the BIPV/T, °C,

$T_{in}$  – inlet temperature of the air, °C.

For PV surface, air channel and bottom insulation, the following energy balance equations are defined (Equations 5-6, 5-7, 5-8):

$$S_{PV} = \frac{A\sigma(T_{PV}^4 - T_{ins}^4)}{\frac{1}{\epsilon_{PV}} + \frac{1}{\epsilon_{ins}} - 1} + Ah_{amb}(T_{pv} - T_{amb}) + Ah_{top}(T_{pv} - T_{air}) \quad (5-6)$$

Where,

$S_{PV}$  – total heat gained by the PV surface, W,

$A$  – area of the PV layer, m<sup>2</sup>,

$\sigma$ – Stefan-Boltzmann constant,  $5.67 \times 10^{-8} \text{ W/m}^2 \text{ K}^4$ ,

$T_{PV}$ ,  $T_{ins}$ ,  $T_{amb}$ ,  $T_{air}$ – respective average PV layer surface, insulation surface, ambient air and channel air temperatures, °C,

$h_{amb}$ ,  $h_{top}$  – convective heat transfer coefficients between ambient and PV surface; a top surface of the channel and flowing air in the channel respectively,  $\text{W/K m}^2$ ,

$\varepsilon_{PV}$ ,  $\varepsilon_{ins}$  – total hemispherical emissivity of the PV and insulation layers, respectively.

$$\dot{m}c_p(T_{exit} - T_{in}) = Ah_{top}(T_{pv} - T_{air}) + Ah_{bot}(T_{ins} - T_{air}) \quad (5-7)$$

$$\frac{A\sigma(T_{PV}^4 - T_{ins}^4)}{\frac{1}{\varepsilon_{PV}} + \frac{1}{\varepsilon_{ins}} - 1} = Ah_{bot}(T_{ins} - T_{air}) \quad (5-8)$$

The interior convective heat transfer coefficient,  $h_{top}$ , is calculated based on the local Nusselt number. A Nusselt number is a dimensionless number that is defined as a ratio of convective heat transfer to conduction within the flow (Equation 5-9):

$$Nu = \frac{hL}{k} \quad (5-9)$$

Where,

$h$  – convective heat transfer coefficient,  $\text{W/K m}^2$ ,

$L$  – characteristic length of the flow, the diameter of the pipe, m,

$k$  – thermal conductivity of the air,  $\text{W/K m}$ .

Reynolds and Prandtl numbers are conventionally used to calculate the Nusselt number for the forced convection. Many studies in the literature suggest different Nu correlations under various conditions for BIPV/T, the Dittus-Boelter equation (Dittus & Boelter, 1985) is commonly used

by researchers. However, in a multi-inlet system considered in this thesis, the Dittus-Boelter equation underpredicts the Nu number due to the additional entrance and turbulence effects (Rounis, 2020).

Yang & Athienitis (2015b), thus, experimentally developed correlation for the Nusselt number between the rear surface of the PV layer and the channel air for the two-inlet systems (Equations 5-10 and 5-11):

$$1^{\text{st}} \text{ inlet: } Nu_{pv-air} = 0.0149Re^{0.9}Pr^{0.43} \quad 1453 < Re < 14322 \quad (5-10)$$

$$2^{\text{nd}} \text{ inlet: } Nu_{pv-air} = 1.451Re^{0.44}Pr^{0.4} \quad 3600 < Re < 19034 \quad (5-11)$$

Where,

Re – Reynolds number, the dimensionless number which equates to the ratio of inertial to viscous forces; characterizes the flow patterns in the channel of fluid flow,

Pr – Prandtl number, the dimensionless number which equates to the ratio of momentum diffusivity to thermal diffusivity.

For the original one-inlet system, the calculated Reynold number in the channel is equal to 3270, indicating the turbulent fully mixed flow. Since the turbulent flow reaches the fully developed conditions fast enough, the average Nu equation can be used. Thus, the average Nu correlation for both the top and bottom surface of the air channel developed experimentally by Candanedo et al., (2011) is used.

The next step is to identify the exterior convective heat transfer coefficient driven by wind. For that, several correlations available in the literature are tested, and their effect on the outlet

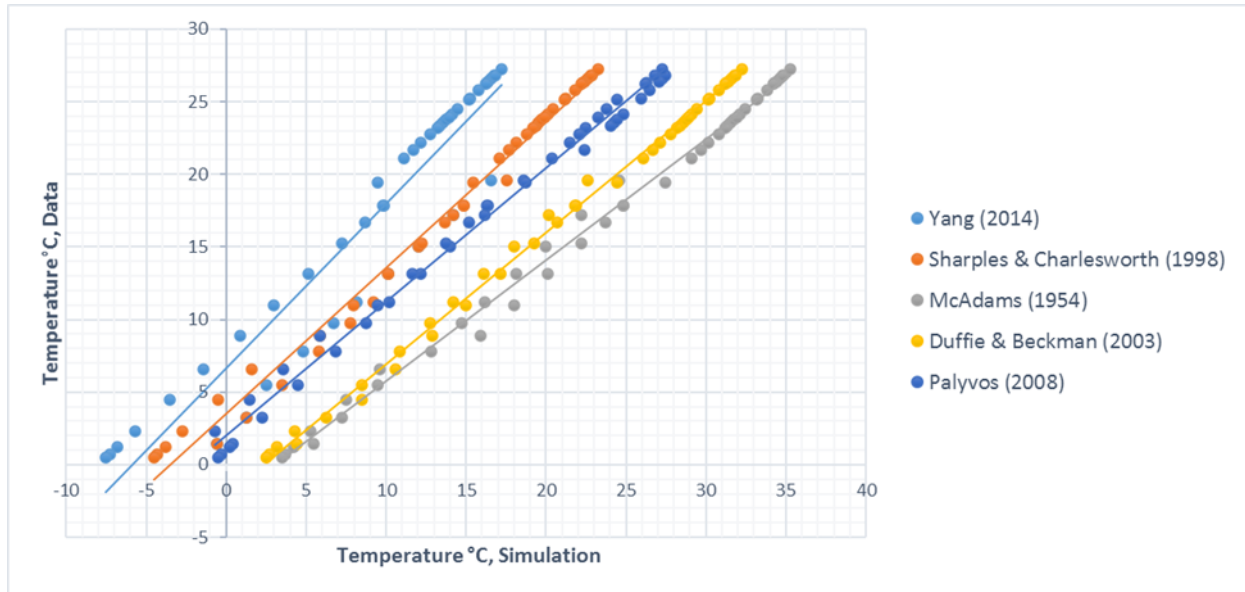


Figure 5-10: Comparison of outlet temperature predictions with different exterior convective heat transfer coefficient correlations with the actual data.

BIPV/T temperature versus collected data is obtained and plotted in Figure 5-10. The exterior convective coefficient developed by Palyvos (2008) yields the most accurate prediction of outlet BIPV/T temperature, followed by the Sharples & Charlesworth correlation. However, this result is specific for this case, and it is possible that the accuracy of wind-driven convection strongly correlated to the Nu number. More detailed research is needed to develop an independent variable that would formulate this relationship. For this study, the correlation developed by Palyvos will be used for the modelling.

To develop a simple control-oriented model, the critical inputs identified based on the virtual experiment with a more detailed model are solar irradiance (S), outside temperature ( $T_o$ ), flowrate over the channel (Q) and wind velocity (W). The challenge is to identify whether there is a need to include variable wind speed and wind direction, given that wind data is unavailable from the nearest weather station. The assumption of a single average wind velocity in Quebec

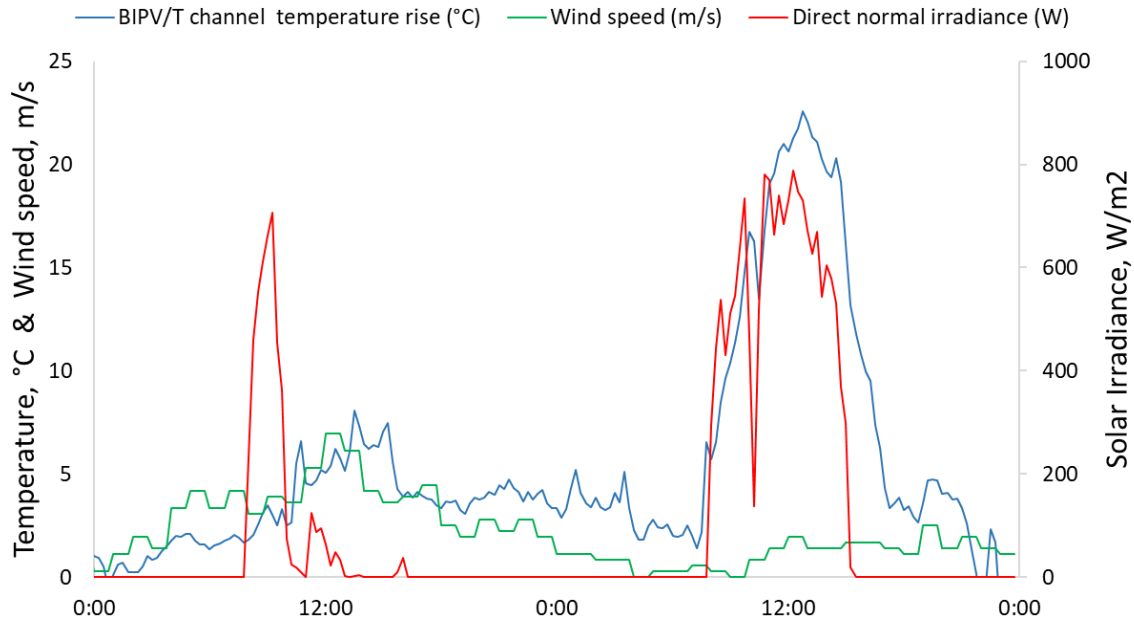


Figure 5-11: Channel air temperature rise over two consecutive days with variable wind speed but similar irradiance intensity. The impact of wind speed on outlet temperature can be observed. 9-10 January, 2018.

(around 3.5 m/s) yielded a significant simulation error. The wind data from the L'Assomption weather station, which is 10 km away from Varennes, was inspected for correlation with BIPV/T temperature. The results are plotted in Figure 5-11. The relationship between temperature rise across the channel and wind speed is evident. At the same time, the wind direction did not show a strong correlation and was ignored in this study.

A system identification technique is used after collecting the vectors of input and output data from a more detailed model. A black box regressive model is proposed, where the parameters identified do not hold any physical significance. If the measured output from the developed model is denoted as  $y$ , the prediction of the regressive model is defined as  $\hat{y}$  and is represented as follows:

$$\hat{y}(t) = x(t + 1) = ax(t) + bS(t) + cTo(t) + dQ(t) + eW(t) + f \quad (5-12)$$

where,

$\hat{y}(t)$  - is a BIPTV/T outlet temperature, variable that we are trying to predict (°C),

$x(t)$  – previous exit temperature of BIPV/T channel (°C),

$S(t)$  – solar irradiance (W/m<sup>2</sup>),

$T_o(t)$  – outside temperature (°C),

$Q(t)$  – flowrate (m<sup>3</sup>/s),

$W(t)$  – wind speed (m/s).

The resulting objective function is then defined as:

$$J(y_1, \hat{y}_1, y_i, \hat{y}_i) = \min \sum_1^{n=i} \|y_n - \hat{y}_n\| \quad (5-13)$$

This optimization problem is solved using MATLAB Optimization Toolbox, and parameters are identified.

The conditions of applicability of the model were chosen iteratively by varying the training dataset, and the best fit was achieved when the inputs were narrowed down to the following constraints:

$$600 < S < 1000;$$

$$0.7 < Q < 1.142;$$

$$1 < W < 4.$$

The model was trained using acquired data between January 13 and January 20, 2018, and tested with the measured data between January 23 and January 26, 2018. The performance of the regressive model on the test dataset is shown in Figure 5-12 below. As shown in the graph, over three consecutive days from 24<sup>th</sup> to 26<sup>th</sup> January, the prediction of the channel outlet temperature accurately matches the measured data from the BIPV/T system. However, on the first day of test data, 23 January, the model overpredicts the outlet temperature from BIPV/T. The possible reason is non-compliance with the applicable conditions of the model specified above, both in terms of solar irradiation and wind speed, which is one of the limitations of the approach.

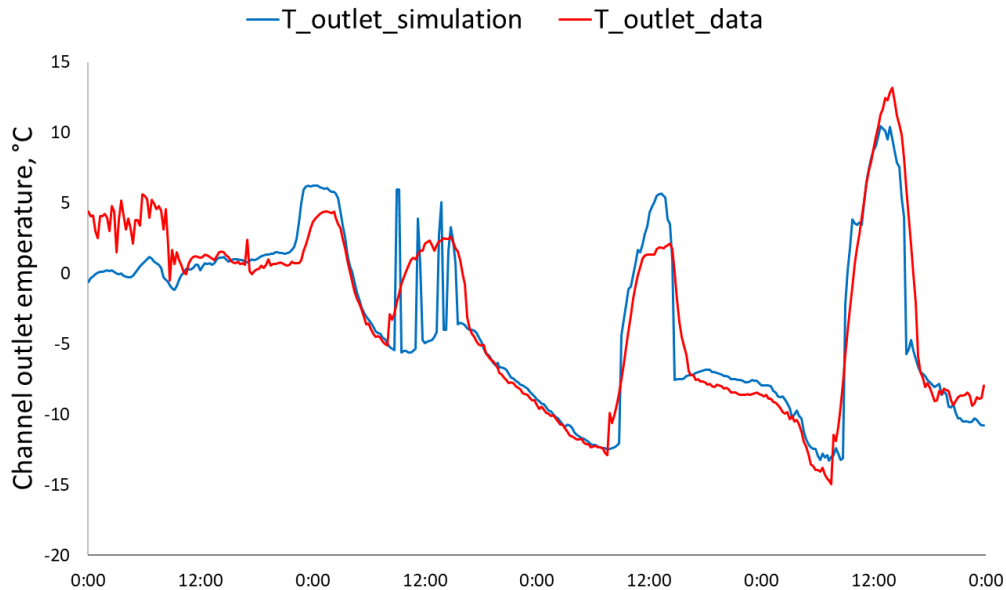


Figure 5-12: Performance of regressive control-oriented model in predicting of outlet air temperature from BIPV/T on a test set over four consecutive days. 23-27 January, 2018.

Overall, it can be concluded that the regressive model with the static parameters has a limited predictive capacity and cannot fully describe a daily variation; several models must be developed for different sets of conditions. More complex models, which can capture nonlinearities, such as deep neural networks, may also describe this behaviour.

### 5.3 Design and control suggestions

With a new reality set by the COVID – 19 pandemics, the importance of enhanced ventilation is emphasized more than before. An optimally designed and controlled BIPV/T system can effectively enhance ventilation with little to no disturbance to the building energy profile. The BIPV/T system installed in the Varennes library provides one of the first large-scale prototype examples demonstrating how this system could potentially operate and the efficiency it can achieve. Since it is one of the pioneers of large-scale installation, it is designed and operated far from optimal manner while providing invaluable data and insights about the operation. Due to being a novice technology and resultant natural concern of involved stakeholders during the

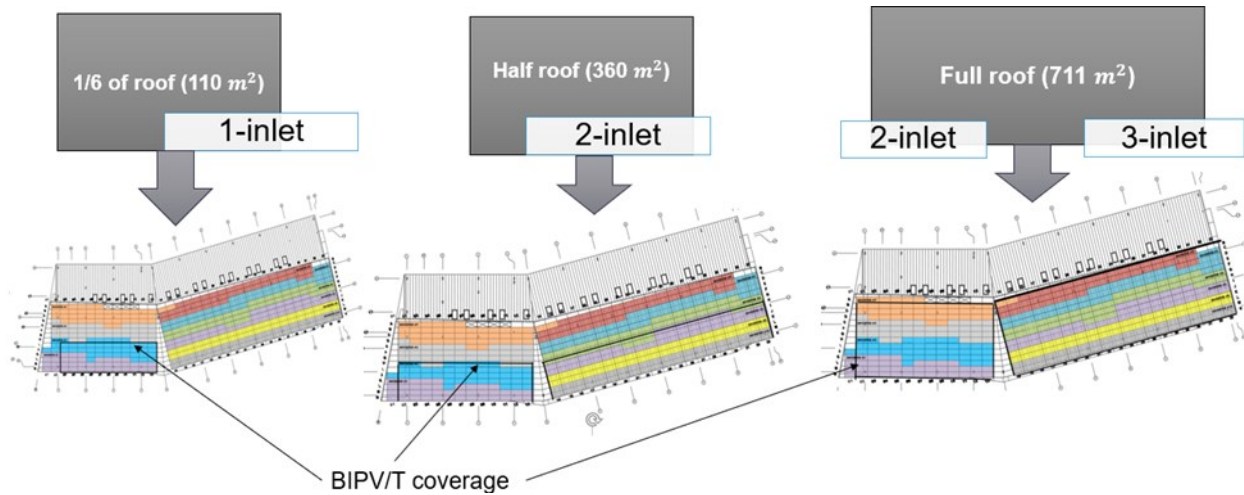


Figure 5-13: Alternative design configurations in terms of BIPV/T area coverage.

Table 5-1: Alternative design configuration cases of BIPV/T.

Area (m <sup>2</sup> )	Design (number of inlets)	Maximum Fan speed (m/s)	Maximum Flowrate (L/s)
110 (1/6 of the roof, original)	1-inlet	1	1142
360 (half roof)	2-inlet	1	3240
711 (full roof)	2 - inlet	1	3470
	3 - inlet		

design phase, the only one-sixth portion of the roof was covered with a BIPV/T. One of the first design alternatives inspected in this study is to examine the potential performance of different coverage areas of BIPV/T, namely half roof and entire roof with areas of 360 m<sup>2</sup> and 711 m<sup>2</sup>, respectively, which can potentially increase the energy flexibility available in the building. As a thermal enhancement option, multi-inlet systems are proposed. In double-inlet design, the size of the second inlet is assumed to be 1/3<sup>rd</sup> of the original channel gap size (which is 7 mm), whereas in triple-inlet, each inlet is sized as 1/10<sup>th</sup> to avoid the significant heat loss while still benefiting from the entrance effects. Energy and mass balance are conserved. Figure 5-13 above illustrates

configurations of the considered cases. The detailed parameters of the design cases are shown in Table 5-1. Another modification suggested is the fan control strategy. Currently, the BIPV/T fan speed is controlled by the temperature of the BIPV/T outlet only. As was mentioned at the beginning of the chapter, if the outlet temperature is above 25°C, the fan modulates to 80%; otherwise, it sequences back to 33% unless there is no electricity generation. When considering BIPV/T for preheating the ventilation air applications, the alternative strategy of the control sequence of the BIPV/T fan is to link the fan speed to the current occupancy. Dynamic occupancy demand is defined as **exhaust rate (m<sup>3</sup>/s)/total exhaust capacity (m<sup>3</sup>/s)**, where both of the variables are known from the collected dataset. Then, the proposed fan speed control algorithm is the following:

Strategy 1: both occupational needs and BIPV/T surface temperature are considered:

$$\text{Fan speed control modulation}_{occ} = v_{max}c_1c_2 \quad (5-14)$$

where  $v_{max}$  – maximum speed of the fan, m/s

$$c_1 = \begin{bmatrix} 0.33 \text{ if } T_{outlet} \leq 25^\circ\text{C} \\ 0.5 \text{ if } 25^\circ\text{C} < T_{outlet} \leq 30^\circ\text{C} \\ 0.6 \text{ if } 30^\circ\text{C} < T_{outlet} \leq 35^\circ\text{C} \\ 0.7 \text{ if } 35^\circ\text{C} < T_{outlet} \leq 40^\circ\text{C} \\ 0.8 \text{ if } T_{outlet} > 40^\circ\text{C} \end{bmatrix}$$

$$c_2 = \frac{\text{exhaust flowrate (m}^3\text{/s)}}{1.142 \text{ (m}^3\text{/s)}}$$

Strategy 2: Only BIPV/T temperature is considered, same equation as before but  $c_2 = 0$ .

The results of the performance of all cases are shown in Figures 5-14, 5-15 and Table 5-2 below.

Overall, it can be concluded that when occupancy is taken into account, less total heat is recovered; however, the fraction of the useful heat (when  $T_{outlet} > 20^\circ\text{C}$ ) is substantially

higher, so it can be directly used for space heating applications or integration with air-to-air heat pumps.

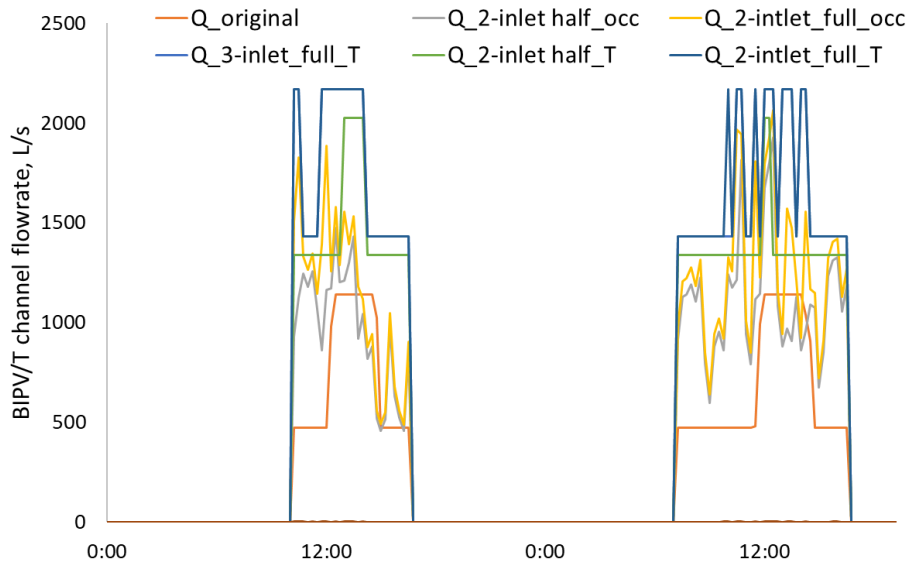


Figure 5-14: The resulting flowrate (L/s) of all cases. “half”, “full” in the legend bar imply the BIPV/T portion of the roof coverage. “T”, “occ” indicate temperature-based control (Strategy 2) and occupancy + temperature-based control (Strategy 1), respectively. 18-19 January, 2018.

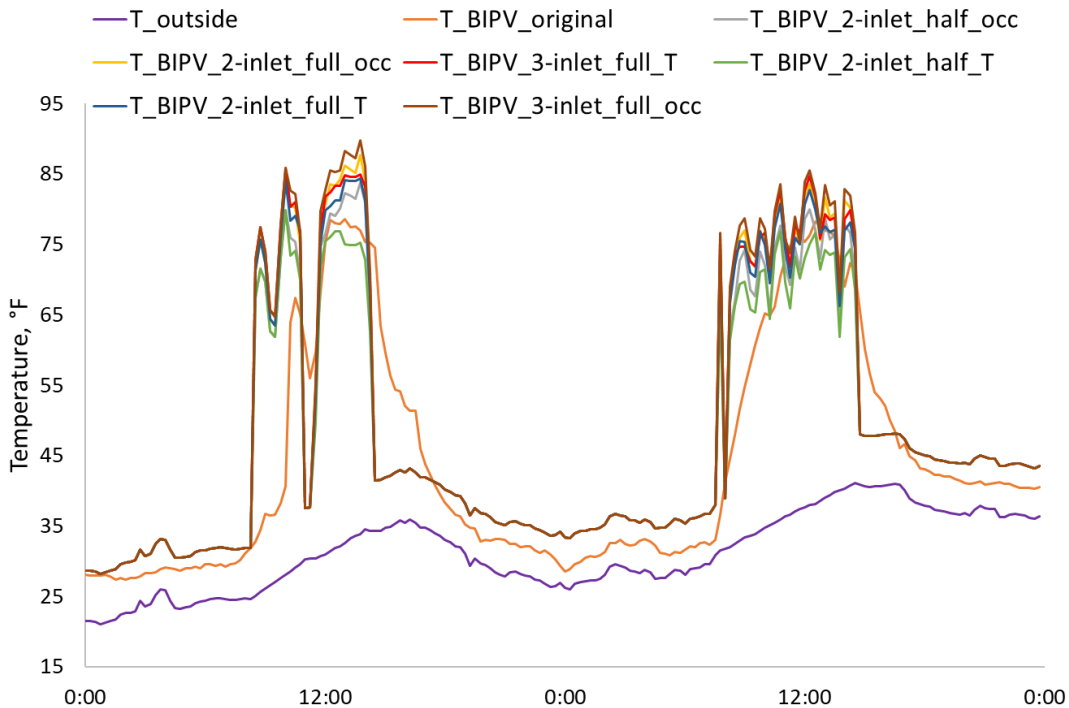


Figure 5-15: The resulting BIPV/T outlet temperature (°F) of all cases. “half”, “full” in the legend bar imply the BIPV/T portion of the roof coverage. “T”, “occ” indicate temperature-based control (Strategy 2) and occupancy + temperature-based control (Strategy 1) respectively. 18-19 January, 2018.

Table 5-2: Performance of suggested 8 alternative cases in terms of total recovered heat, useful heat and flowrate. Useful heat assumes heat extracted above 20°C.

<b>Cases</b>	<b>Recovered heat (kWh)</b>	<b>Average flowrate (L/s)</b>	<b>% of useful heat</b>	<b>Useful heat (kWh)</b>
<b>Current</b>	2454	413	5.7	141
<b>Current, T controlled</b>	2310	396	8.2	192
<b>Current, T + occupancy controlled</b>	1894	280	17	343
<b>Half roof, 2-inlet, T controlled</b>	7099	1131	8.7	617
<b>Half roof, 2-inlet, T + occupancy controlled</b>	5743	814	16.1	928
<b>Full roof, 2-inlet, T controlled</b>	8512	1223	13.72	1167
<b>Full roof, 2-inlet, T + occupancy controlled</b>	6704	883	20.03	1343
<b>Full roof, 3-inlet, T controlled</b>	8829	1237	14.9	1316
<b>Full roof, 3-inlet, T + occupancy controlled</b>	6919	887	21.4	1481

## 5.4 Conclusion

To increase the energy flexibility in the building, a BIPV/T system that can generate, store, and enhance HVAC efficiency can be a viable solution if optimally designed and operated. In this chapter, a detailed analysis of the installed large-scale BIPV/T system was followed by the control-oriented data-driven model development, concluding with the study on alternative design and control options that can potentially increase building energy flexibility. The modelling approach used a data-verified detailed thermal network-based grey-box model with physical parameters to visualize the real system. The relevant input parameters were then identified, and different wind-driven convective heat transfer correlations were tested. Exterior convective heat loss in the BIPV/T system has the most significant effect on the energy balance, and its accurate description is critical for adequate evaluation. After creating an accurate visualization of the BIPV/T system and identifying critical input parameters, a black-box regressive model was proposed with parameters of no physical significance. Upon verification, the model performed satisfactorily ( $\pm 1.5^{\circ}\text{C}$ ) when the input constraints were met and underperformed in the other cases. Overall, the black-box modelling technique is a promising solution in modelling BIPV/T and other more comprehensive models that can capture nonlinearities, such as those incorporating deep-neural networks, can be more robust. This chapter is wrapped up with the alternative design and fan control strategy proposal. Multi-inlet design and occupancy-based control for ventilation air preheat resulted in more than 20% higher useful heat extraction than the current baseline case. Whereas baseline yielded the most recovered heat due to a higher flow rate, 94.3% of it is delivered at a temperature less than  $18^{\circ}\text{C}$ . The integration with an air source heat pump can make the proposed strategy for energy flexibility even more effective.

# Chapter 6

## Conclusion

### 6.1 Summary and future work

**This thesis** presented heuristic model-based predictive control techniques developed for an institutional NZEB archetype example with an active and passive hydronic radiant slab system. A rigorous step-by-step generic control-oriented modelling methodology and calibration was proposed. A heuristic MPC combined the benefits of numerical MPC by using the building model and RBC for practicality and cost-effectiveness of implementation to minimize the energy consumption and/or maximize energy flexibility in the building. The heuristic MPC drastically eased the computational requirements of the model while still necessitating generic methodology of model development. Albeit the generalization of the approach was a priority, specific inherent features of each building remained unique and required an indoor temperature analysis to identify the structure of the model. Several modelling approaches were attempted, and the RC thermal network-based grey-box 10<sup>th</sup> order model with physics-based parameters showed promising results in capturing the basic thermal behaviour in the institutional NZEB archetype. The incorporation of “effective” air capacitance, which considers the effects of furniture and book stacks, had resulted in a significant improvement in model accuracy. Next, the concept of heuristic MPC was introduced, and step-by-step development of near-optimal strategies to maximize energy efficiency and/or energy flexibility was demonstrated. Anticipated types of days were classified into very cold, cold, mild and sunny, semi-cloudy, and cloudy clusters. For every 9 combinations of weather scenarios, 2 sets of heating setpoint profiles were developed. Nearly 100% of BEFIP was achieved on cold and mild days, while this value was around 80%

for very cold days. Results showed that heuristic MPC could be a successful alternative to a traditional MPC as a solution to significantly improve energy efficiency, enhance energy flexibility, enhance load management and thermal comfort while reducing computational needs.

The thesis concluded with a small study focused on the increasing energy flexibility potential through the enhanced BIPV/T design. After an exhaustive analysis of the collected data from the installed BIPV/T system in the Varennes library, a simple black-box regressive model was derived. The parameters were calibrated through optimization techniques with constrained input conditions. Upon verification, the model performed satisfactorily ( $\pm 1.5^{\circ}\text{C}$ ), concluding that the black-box modelling technique is a promising solution in control-oriented modelling of BIPV/T and models trained by more sophisticated system identification techniques can potentially be more robust. This was followed up by the alternative design and fan control proposal, where multi-inlet design and occupancy-based control for preheating ventilation air resulted in a more than 20% higher useful heat extraction than the current baseline.

**As future work**, the proposed predictive control strategy to maximize energy flexibility is expected to be practically applied to the BAS of the library for test purposes in December. To avoid possible discomfort and visitors' dissatisfaction, the initial plan is to test the control algorithm on holidays when the library is unoccupied. After better understanding the impacts of proposed control strategies on the system from the tests, the next step is to refine the control algorithm further by considering more clustered cases and the cooling season. For instance, the intermediate days can be subdivided into two further categories: semi-sunny and semi-cloudy days. Having more predefined cases allows the strategy to be more robust since the cost of the error in the prediction is minimized.

Moreover, the control strategies developed in this study are based on the weather forecast only; however, another major driver of the future demand in buildings is occupancy behaviour, which was not considered in this thesis. The impact of various occupancy behaviour on energy flexibility must be quantified; the relation of the occupants on the selection of control algorithms in the available literature is significantly unexplored. Lastly, the proposed 10<sup>th</sup> order model did not include the air conductance between the zones. Incorporation and calibration of that effect must be further studied.

This work is also a part of a research incentive by the International Energy Agency's (IEA) Energy in Buildings and Communities (EBC) Annex 81 "Data-driven Smart Buildings" program where the Varennes library has been modelled in the Modelica software (Appendix D) and is expected to be introduced to the framework for simulation-based testing and comparison of building advanced control strategies, called BOPTEST - Building Optimization Performance Test. The primary advantage of Modelica over other component-based modelling software such as Simulink and TRNSYS is that the Modelica supports multidomain modelling, which means it can define and link model components corresponding to objects from a variety of domains, including electrical, mechanical, thermodynamic, hydraulic, biological, and control applications. Also, Modelica relies heavily on equations rather than assignment statements. Since equations do not define a particular data-flow direction, this allows acausal modelling, enabling greater class reuse and enhanced modelling flexibility compared to Simulink. The ultimate objective of this project is to make Varennes Library the first Canadian building accepted as a case study in the BOPTEST emulator, which will serve as an institutional NZEB archetype so that different advanced control and modelling strategies can be tested, which will establish and benchmark the

state-of-the-art performance of control for building energy systems by avoiding the challenges of individualized studies and cost of developing a building emulator.

## 6.2 Contributions

The main contributions of this thesis can summarize as follows:

- 1) The generic and step-by-step methodology for control-oriented model development with little to no required data was shown. The addition of “effective” air capacitance ensures increased accuracy in the short-term response as buildings usually contain mass objects inside, which yield an accumulative thermal mass effect. Linearization of the 6<sup>th</sup> order RC model, especially the convective coefficients, can significantly affect short-scale temperature prediction.
- 2) The thesis showed the formulation of a unique rule-based MPC technique as an alternative to the numerical MPC. Results showed it might significantly enhance energy flexibility, improve load management and energy efficiency, and ensure thermal comfort while decreasing computing requirements of traditional MPC and providing predictive capacity and effectiveness to the RBC.
- 3) Prediction uncertainty and robustness are innovatively handled through the verification with on-site PV production data. The appropriate corrections are applied if the verification test does not pass and the best matching temperature setpoint profile is selected.
- 4) Introduction of a BEFIP index to estimate the flexibility in terms of percentage that the buildings can provide to the grid. It was shown that buildings with effective integrated

technologies and passive design features could achieve nearly 100% of energy flexibility in the majority of the heating season throughout the peak demand period.

- 5) Detailed data analysis and control-oriented model development for installed large-scale BIPV/T technology from the original nonlinear system formulation. The computing cost of a black-box model, such as linear regression, is significantly lower than that of a comprehensive white-box and can be used for whole-building and subsystem MPC development.
- 6) Based on the study proposed in this thesis, one conference paper has been written and presented at the international conference of Sustainable Development of Energy, Water and Environment Systems 2021 (SDEWES 2021). A journal paper based on this work is also planned and has already received an invitation from the Energies journal.:
  - Jalilov, E. and Athienitis, A. K. (2021). "Heuristic model-based predictive control strategies for an institutional net-zero energy building", Abstract submitted to 16th Conference on Sustainable Development of Energy, Water, and Environment Systems, Dubrovnik, Croatia, October 10 – 15 (Accepted).

## References

Aelenei, L., & Gonçalves, H. (2014). From Solar Building Design to Net Zero Energy Buildings: Performance Insights of an Office Building. *Energy Procedia*, 48, 1236–1243.

<https://doi.org/10.1016/j.egypro.2014.02.140>

Ahmed-Dahmane, M., Malek, A., & Zitoun, T. (2018). Design and analysis of a BIPV/T system with two applications controlled by an air handling unit. *Energy Conversion and Management*, 175, 49–66. <https://doi.org/10.1016/j.enconman.2018.08.090>

Amara, F., Dermardiros, V., & Athienitis, A. K. (2019). Energy Flexibility for an Institutional Building with Integrated Solar System: Case Study Analysis. 2019 IEEE Electrical Power and Energy Conference (EPEC). <https://doi.org/10.1109/epec47565.2019.9074815>

American Society of Heating, Ventilating, and Air Conditioning Engineers (ASHRAE). Guideline 14-2014, Measurement of Energy and Demand Savings; Technical Report; American Society of Heating, Ventilating, and Air Conditioning Engineers: Atlanta, GA, USA, 2014

Amori, K. E., & Abd-ALRaheem, M. A. (2014). Field study of various air-based photovoltaic/thermal hybrid solar collectors. *Renewable Energy*, 63, 402–414.

<https://doi.org/10.1016/j.renene.2013.09.047>

ASHRAE (2016). ANSI/ASHRAE Standard 55-2016: Thermal Environmental Conditions for Human Occupancy. ASHRAE. 19

Athienitis, A. K., Bambara, J., O'Neill, B., & Faille, J. (2011). A prototype photovoltaic/thermal system integrated with transpired collector. *Solar Energy*, 85(1), 139–153.

<https://doi.org/10.1016/j.solener.2010.10.008>

Athienitis, A., & O'Brien, W. (2015). *Modeling, Design, and Optimization of Net-Zero Energy Buildings (Solar Heating and Cooling)* (1st ed.). Ernst & Sohn.

Athienitis, A., Dumont, E., Morovat, N., Lavigne, K., & Date, J. (2020). Development of a dynamic energy flexibility index for buildings and their interaction with smart grids. Conference: 2020 Summer Study on Energy Efficiency in BuildingsAt: California, USA

Athienitis, A.K. (1988). A predictive control algorithm for massive buildings. *ASHRAE Transactions* **94**, 1050-1068

Avci, M., Erkoc, M., Rahmani, A., & Asfour, S. (2013). Model predictive HVAC load control in buildings using real-time electricity pricing. *Energy and Buildings*, *60*, 199–209.

<https://doi.org/10.1016/j.enbuild.2013.01.008>

Behl, M., Smarra, F., & Mangharam, R. (2016). DR-Advisor: A data-driven demand response recommender system. *Applied Energy*, *170*, 30–46.

<https://doi.org/10.1016/j.apenergy.2016.02.090>

Bünning, F., Huber, B., Heer, P., Aboudonia, A., & Lygeros, J. (2020). Experimental demonstration of data predictive control for energy optimization and thermal comfort in buildings. *Energy and Buildings*, *211*, 109792. <https://doi.org/10.1016/j.enbuild.2020.109792>

Candanedo, J. A., & Athienitis, A. K. (2011). Predictive control of radiant floor heating and solar-source heat pump operation in a solar house. *HVAC&R Research*, *17*(3), 235–256.

<https://doi.org/10.1080/10789669.2011.568319>

Candanedo, J. A., and Athienitis, A. K., 2010. Investigation of Anticipatory Control Strategies in a Net-Zero Energy Solar House. *ASHRAE Trans* *116* (1), 246–259.

Candanedo, J. A., Dehkordi, V. R., Saberi-Derakhtenjani, A., & Athienitis, A. K. (2015). Near-optimal transition between temperature setpoints for peak load reduction in small buildings.

*Energy and Buildings*, 87, 123–133. <https://doi.org/10.1016/j.enbuild.2014.11.021>

Candanedo, L. M., Athienitis, A., & Park, K. W. (2011). Convective Heat Transfer Coefficients in a Building-Integrated Photovoltaic/Thermal System. *Journal of Solar Energy Engineering*,

133(2). <https://doi.org/10.1115/1.4003145>

Carvalho, A. D., Moura, P., Vaz, G. C., & de Almeida, A. T. (2015). Ground source heat pumps as high efficient solutions for building space conditioning and for integration in smart grids.

*Energy Conversion and Management*, 103, 991–1007.

<https://doi.org/10.1016/j.enconman.2015.07.032>

Chen, B., Cai, Z., & Bergés, M. (2020). Gnu-RL: A Practical and Scalable Reinforcement Learning Solution for Building HVAC Control Using a Differentiable MPC Policy. *Frontiers in Built Environment*, 6. <https://doi.org/10.3389/fbuil.2020.562239>

*Built Environment*, 6. <https://doi.org/10.3389/fbuil.2020.562239>

Chen, Y., Galal, K., & Athienitis, A. (2010). Modeling, design and thermal performance of a BIPV/T system thermally coupled with a ventilated concrete slab in a low energy solar house:

Part 2, ventilated concrete slab. *Solar Energy*, 84(11), 1908–1919.

<https://doi.org/10.1016/j.solener.2010.06.012>

Chowdhury, M. S., Rahman, K. S., Chowdhury, T., Nuthammachot, N., Techato, K.,

Akhtaruzzaman, M., Tiong, S. K., Sopian, K., & Amin, N. (2020). An overview of solar photovoltaic panels' end-of-life material recycling. *Energy Strategy Reviews*, 27, 100431.

<https://doi.org/10.1016/j.esr.2019.100431>

Clauß, J., Stinner, S., Sartori, I., & Georges, L. (2019). Predictive rule-based control to activate the energy flexibility of Norwegian residential buildings: Case of an air-source heat pump and direct electric heating. *Applied Energy*, 237, 500–518.

<https://doi.org/10.1016/j.apenergy.2018.12.074>

Dar, U. I., Sartori, I., Georges, L., & Novakovic, V. (2014). Advanced control of heat pumps for improved flexibility of Net-ZEB towards the grid. *Energy and Buildings*, 69, 74–84.

<https://doi.org/10.1016/j.enbuild.2013.10.019>

Dar, U. I., Sartori, I., Georges, L., & Novakovic, V. (2014). Advanced control of heat pumps for improved flexibility of Net-ZEB towards the grid. *Energy and Buildings*, 69, 74–84.

<https://doi.org/10.1016/j.enbuild.2013.10.019>

Date, J., Athienitis, A. K., & Fournier, M. (2015). A Study of Temperature Set Point Strategies for Peak Power Reduction in Residential Buildings. *Energy Procedia*, 78, 2130–2135.

<https://doi.org/10.1016/j.egypro.2015.11.289>

Date, J., J. A. Candanedo, and A. K. Athienitis. 2016. Control-oriented modelling of thermal zones in a house: A multi-level approach. Proceedings of the 4th International High-Performance Buildings Conference at Purdue University

Date, J., Candanedo, J. A., Athienitis, A. K., & Lavigne, K. (2020). Development of reduced order thermal dynamic models for building load flexibility of an electrically-heated high temperature thermal storage device. *Science and Technology for the Built Environment*, 26(7), 956–974. <https://doi.org/10.1080/23744731.2020.1735260>

De Coninck, R., Baetens, R., Saelens, D., Woyte, A., & Helsens, L. (2013). Rule-based demand-side management of domestic hot water production with heat pumps in zero energy

neighbourhoods. *Journal of Building Performance Simulation*, 7(4), 271-288.

doi:10.1080/19401493.2013.801518

de Salis, R. T., Clarke, A., Wang, Z., Moyne, J., & Tilbury, D. (2014). Energy storage control for peak shaving in a single building. *2014 IEEE PES General Meeting | Conference & Exposition*.

Published. <https://doi.org/10.1109/pesgm.2014.6938948>

Debbarma, M., Sudhakar, K., & Baredar, P. (2017). Comparison of BIPV and BIPVT: A review.

*Resource-Efficient Technologies*, 3(3), 263–271. <https://doi.org/10.1016/j.refit.2016.11.013>

Delcroix, B., Kummert, M., & Daoud, A. (2014). Experimental assessment of a phase change material in walls for heating and cooling applications. Conference: ESim 2014At: Ottawa, ON, Canada. Published.

Dermardiros V., Athienitis A.K. and Bucking S. (2019). “Energy Performance, Comfort and Lessons Learned from an institutional building designed for Net-Zero Energy”. *ASHRAE Transactions* Vol. 125 (1).

Dermardiros, V. (2020). *Data-Driven Optimized Operation of Buildings with Intermittent Renewables and Application to a Net-Zero Energy Library*. Montreal / Concordia University.

Dermardiros, V., Bucking, S., & Athienitis, A. K. (2019). A Simplified Building Controls Environment with a Reinforcement Learning Application. *Proceedings of Building Simulation 2019: 16th Conference of IBPSA*. Published. <https://doi.org/10.26868/25222708.2019.211427>

Dittus, F., & Boelter, L. (1985). Heat transfer in automobile radiators of the tubular type.

*International Communications in Heat and Mass Transfer*, 12(1), 3–22.

[https://doi.org/10.1016/0735-1933\(85\)90003-x](https://doi.org/10.1016/0735-1933(85)90003-x)

Duffie, J. A., Beckman, W. A., & Worek, W. M. (1994). Solar Engineering of Thermal Processes, 2nd ed. *Journal of Solar Energy Engineering*, 116(1), 67–68.

<https://doi.org/10.1115/1.2930068>

Finck, C., Li, R., & Zeiler, W. (2019). Economic model predictive control for demand flexibility of a residential building. *Energy*, 176, 365–379. <https://doi.org/10.1016/j.energy.2019.03.171>

Gautam, K. R., & Andresen, G. B. (2017). Performance comparison of building-integrated combined photovoltaic thermal solar collectors (BiPVT) with other building-integrated solar technologies. *Solar Energy*, 155, 93–102. <https://doi.org/10.1016/j.solener.2017.06.020>

Gholami, H., Nils Røstvik, H., Manoj Kumar, N., & Chopra, S. S. (2020). Lifecycle cost analysis (LCCA) of tailor-made building integrated photovoltaics (BIPV) façade: Solsmaragden case study in Norway. *Solar Energy*, 211, 488–502. <https://doi.org/10.1016/j.solener.2020.09.087>

Halfmann, F., Alhaider, F., Wendiggensen, J., & Gerhard, S. (2017). A Predictive Control Strategy for Battery Energy Storage Systems to combine Peak Shaving with Primary Frequency Control. NEIS Conference 2016, 113–118. [https://doi.org/10.1007/978-3-658-15029-7\\_18](https://doi.org/10.1007/978-3-658-15029-7_18)

Hida, Y., Yokoyama, R., Shimizukawa, J., Iba, K., Tanaka, K., & Seki, T. (2010). Load following operation of NAS battery by setting statistic margins to avoid risks. IEEE PES General Meeting. Published. <https://doi.org/10.1109/pes.2010.5588170>

Hottel, H. C., *Solar Energy*, 18, 129 (1976). “A Simple Model for Estimating the Transmittance of Direct Solar Radiation Through Clear Atmospheres.

Houghton, J. (2017). *Global warming: the complete briefing*. Cambridge University Press

IEA EBC Annex 67 “Energy Flexible Buildings”. <http://www.annex67.org>

IEA (2020). Tracking Buildings 2020 – Analysis. IEA. <https://www.iea.org/reports/tracking-buildings-2020>

IPCC (2014) AR5 Synthesis Report: Climate Change. (n.d.). <https://www.ipcc.ch/report/ar5/syr/>

IPCC (2019) *Climate Change and Land*. Special Report on Climate Change and Land. <https://www.ipcc.ch/srccl/>

IRENA. (2018, April). *Renewable Energy Policies in a Time of Transition*.

<https://www.irena.org/publications/2018/apr/renewable-energy-policies-in-a-time-of-transition>

IRENA. (2019, November). *Future of solar photovoltaic. Deployment, investment, technology, grid integration and socio-economic aspects*. IRE. [https://irena.org/-/media/Files/IRENA/Agency/Publication/2019/Nov/IRENA\\_Future\\_of\\_Solar\\_PV\\_2019.pdf](https://irena.org/-/media/Files/IRENA/Agency/Publication/2019/Nov/IRENA_Future_of_Solar_PV_2019.pdf)

Jadhav, N. Y. (2018). *Green and Smart Buildings: Advanced Technology Options (Green Energy and Technology)* (Softcover reprint of the original 1st ed. 2016 ed.). Springer.

Jain, A., Behl, M., & Mangharam, R. (2016). Data Predictive Control for Building Energy Management. Proceedings of the 3rd ACM International Conference on Systems for Energy-Efficient Built Environments. Published. <https://doi.org/10.1145/2993422.2996410>

Kontes, G., Giannakis, G., Sánchez, V., de Agustin-Camacho, P., Romero-Amorrortu, A., Panagiotidou, N., Rovas, D., Steiger, S., Mutschler, C., & Gruen, G. (2018). Simulation-Based Evaluation and Optimization of Control Strategies in Buildings. *Energies*, 11(12), 3376. <https://doi.org/10.3390/en11123376>

Kontes, G., Giannakis, G., Sánchez, V., de Agustin-Camacho, P., Romero-Amorrortu, A., Panagiotidou, N., Rovas, D., Steiger, S., Mutschler, C., & Gruen, G. (2018). Simulation-Based

Evaluation and Optimization of Control Strategies in Buildings. *Energies*, 11(12), 3376.

<https://doi.org/10.3390/en11123376>

Lamnatou, C., & Chemisana, D. (2017). Photovoltaic/thermal (PVT) systems: A review with emphasis on environmental issues. *Renewable Energy*, 105, 270–287.

<https://doi.org/10.1016/j.renene.2016.12.009>

Lawrence Berkley National Laboratory. (2017, March). *Electric Load Shape Benchmarking for Small- and Medium-Sized Commercial Buildings*. Energy Technologies Area.

[https://simulationresearch.lbl.gov/sites/all/files/t\\_hong\\_-\\_electric\\_load\\_shape\\_benchmarking\\_for\\_small-\\_and\\_medium-sized\\_commercial\\_buildings.pdf](https://simulationresearch.lbl.gov/sites/all/files/t_hong_-_electric_load_shape_benchmarking_for_small-_and_medium-sized_commercial_buildings.pdf)

Lee, K., Joo, M., & Baek, N. (2015). Experimental evaluation of simple thermal storage control strategies in low-energy solar houses to reduce electricity consumption during grid on-peak periods. *Energies*, 8(9), 9344–9364. doi:10.3390/en8099344

Liu, T., Yang, X., Chen, W., Li, Y., Xuan, Y., Huang, L., & Hao, X. (2019). Design and Implementation of High Efficiency Control Scheme of Dual Active Bridge Based 10 kV/1 MW Solid State Transformer for PV Application. *IEEE Transactions on Power Electronics*, 34(5), 4223–4238. <https://doi.org/10.1109/tpel.2018.2864657>

Lu, F., Yu, Z., Zou, Y., & Yang, X. (2021). Cooling system energy flexibility of a nearly zero-energy office building using building thermal mass: Potential evaluation and parametric analysis. *Energy and Buildings*, 236, 110763. <https://doi.org/10.1016/j.enbuild.2021.110763>

Mařík, K., Rojíček, J., Stluka, P., & Vass, J. (2011). Advanced HVAC Control: Theory vs. Reality. *IFAC Proceedings Volumes*, 44(1), 3108–3113. <https://doi.org/10.3182/20110828-6-it-1002.03085>

- May-Ostendorp, P., Henze, G. P., Corbin, C. D., Rajagopalan, B., & Felsmann, C. (2011). Model-predictive control of mixed-mode buildings with rule extraction. *Building and Environment*, 46(2), 428–437. <https://doi.org/10.1016/j.buildenv.2010.08.004>
- McAdams, W. H. (2021). *Heat transmission (McGraw-Hill series in chemical engineering)* (3rd Edition). McGraw-Hill Book Company, Inc.
- Mirakhorli, A., & Dong, B. (2018). Model predictive control for building loads connected with a residential distribution grid. *Applied Energy*, 230, 627–642. <https://doi.org/10.1016/j.apenergy.2018.08.051>
- Mirzaei, P. A., & Carmeliet, J. (2013). Influence of the underneath cavity on buoyant-forced cooling of the integrated photovoltaic panels in building roof: a thermography study. *Progress in Photovoltaics: Research and Applications*, 23(1), 19–29. <https://doi.org/10.1002/pip.2390>
- Moghimi, M., Leskarac, D., Bennett, C., Lu, J., & Stegen, S. (2016). Rule-based Energy Management System in an Experimental Microgrid with the Presence of Time of Use Tariffs. *MATEC Web of Conferences*, 70, 10011. <https://doi.org/10.1051/mateconf/20167010011>
- Palyvos, J. (2008). A survey of wind convection coefficient correlations for building envelope energy systems' modeling. *Applied Thermal Engineering*, 28(8–9), 801–808. <https://doi.org/10.1016/j.applthermaleng.2007.12.005>
- Péan, T. Q., Salom, J., & Costa-Castelló, R. (2019). Review of control strategies for improving the energy flexibility provided by heat pump systems in buildings. *Journal of Process Control*, 74, 35–49. <https://doi.org/10.1016/j.jprocont.2018.03.006>

Pedersen, T. H., Hedegaard, R. E., & Petersen, S. (2017). Space heating demand response potential of retrofitted residential apartment blocks. *Energy and Buildings*, *141*, 158–166.

<https://doi.org/10.1016/j.enbuild.2017.02.035>

Plan for a Green Economy 2030. (2020, November 15). Gouvernement Du Québec.

<https://www.quebec.ca/en/government/policies-orientations/plan-green-economy>

Prívarová, S., Cigler, J., Váňa, Z., Oldewurtel, F., Sagerschnig, C., & Žáčková, E. (2013).

Building modeling as a crucial part for building predictive control. *Energy and Buildings*, *56*, 8–22. <https://doi.org/10.1016/j.enbuild.2012.10.024>

Radziemska, E., & Klugmann, E. (2002). Thermally affected parameters of the current–voltage characteristics of silicon photocell. *Energy Conversion and Management*, *43*(14), 1889–1900.

[https://doi.org/10.1016/s0196-8904\(01\)00132-7](https://doi.org/10.1016/s0196-8904(01)00132-7)

Reed, S. (2017, December 25). Power Prices Go Negative in Germany, a Positive for Energy Users. *The New York Times*. <https://www.nytimes.com/2017/12/25/business/energy-environment/germany-electricity-negative-prices.html>

Reynolds, J., Rezgui, Y., Kwan, A., & Piriou, S. (2018). A zone-level, building energy optimization combining an artificial neural network, a genetic algorithm, and model predictive control. *Energy*, *151*, 729–739. <https://doi.org/10.1016/j.energy.2018.03.113>

Rounis, E. D., Athienitis, A. K., & Stathopoulos, T. (2016). Multiple-inlet Building Integrated Photovoltaic/Thermal system modelling under varying wind and temperature conditions. *Solar Energy*, *139*, 157–170. <https://doi.org/10.1016/j.solener.2016.09.023>

Rounis, E. D., Athienitis, A., & Stathopoulos, T. (2021). Review of air-based PV/T and BIPV/T systems - Performance and modelling. *Renewable Energy*, *163*, 1729–1753.

<https://doi.org/10.1016/j.renene.2020.10.085>

Rounis, E. D., Ioannidis, Z., Dumoulin, R., Kruglov, O., Athienitis, A., & Stathopoulos, T. (2018). Design and Performance Assessment of a Prefabricated BIPV/T Roof System Coupled with a Heat Pump. *Proceedings of EuroSun 2018*. Published.

<https://doi.org/10.18086/eurosun2018.02.06>

Ruus, R., Cao, S., Manrique Delgado, B., & Hasan, A. (2019). Direct quantification of multiple-source energy flexibility in a residential building using a new model predictive high-level controller. *Energy Conversion and Management*, *180*, 1109–1128.

<https://doi.org/10.1016/j.enconman.2018.11.026>

Sathe, T. M., & Dhoble, A. (2017). A review on recent advancements in photovoltaic thermal techniques. *Renewable and Sustainable Energy Reviews*, *76*, 645–672.

<https://doi.org/10.1016/j.rser.2017.03.075>

Schibuola, L., Scarpa, M., & Tambani, C. (2015). Demand response management by means of heat pumps controlled via real time pricing. *Energy and Buildings*, *90*, 15–28.

<https://doi.org/10.1016/j.enbuild.2014.12.047>

Sharples, S., & Charlesworth, P. (1998). Full-scale measurements of wind-induced convective heat transfer from a roof-mounted flat plate solar collector. *Solar Energy*, *62*(2), 69–77.

[https://doi.org/10.1016/s0038-092x\(97\)00119-9](https://doi.org/10.1016/s0038-092x(97)00119-9)

The causes and effects of negative power prices. (2018, November 26). Clean Energy Wire.

<https://www.cleanenergywire.org/factsheets/why-power-prices-turn-negative>

The state of energy in Quebec 2021 (2021, January 28). Chaire de gestion du secteur de l'énergie. <https://energie.hec.ca/eeq/>

UNEP (2019) - *UN Environment Programme*. (n.d.). <https://www.unep.org/>

UNFCCC, 2015 – Adoption of the Paris agreement.

<https://unfccc.int/resource/docs/2015/cop21/eng/109r01.pdf>

Vallianos, C., Athienitis, A., & Rao, J. (2019). Hybrid ventilation in an institutional building: Modeling and predictive control. *Building and Environment*, 166, 106405.

<https://doi.org/10.1016/j.buildenv.2019.106405>

Vrettos, E., Lai, K., Oldewurtel, F., & Andersson, G. (2013). Predictive Control of buildings for Demand Response with dynamic day-ahead and real-time prices. *2013 European Control Conference (ECC)*. Published. <https://doi.org/10.23919/ecc.2013.6669762>

Waqas, A., & Jie, J. (2018). Effectiveness of Phase Change Material for Cooling of Photovoltaic Panel for Hot Climate. *Journal of Solar Energy Engineering*, 140(4).

<https://doi.org/10.1115/1.4039550>

Yamaguchi, Y., N. Shigei, and H. Miyajima (2015). Air Conditioning Control System Learning Sensory Scale Based on Reinforcement Learning. In *Proceedings of the International MultiConference of Engineers and Computer Scientists*, Volume 1. 33

Yang, T., & Athienitis, A. K. (2012). A Study of Design Options for a Building Integrated Photovoltaic/thermal (BIPV/T) System with Glazed Air Collector and Multiple Inlets. *Energy Procedia*, 30, 177–186. <https://doi.org/10.1016/j.egypro.2012.11.022>

Yang, T., & Athienitis, A. K. (2015). Experimental investigation of a two-inlet air-based building integrated photovoltaic/thermal (BIPV/T) system. *Applied Energy*, 159, 70–79.

<https://doi.org/10.1016/j.apenergy.2015.08.048>

Yin, R., Kara, E. C., Li, Y., DeForest, N., Wang, K., Yong, T., & Stadler, M. (2016).

Quantifying flexibility of commercial and residential loads for demand response using setpoint changes. *Applied Energy*, 177, 149–164. <https://doi.org/10.1016/j.apenergy.2016.05.090>

# Appendix

## 1.4 A.

Varenes Library was modelled in TRNSYS to provide a twin model of the Library. It was used to analyze alternative design options such as removal of the east-west partition wall, effect of coupling air-source heat pump with BIPV/T and its control strategy and impact of motorized shading

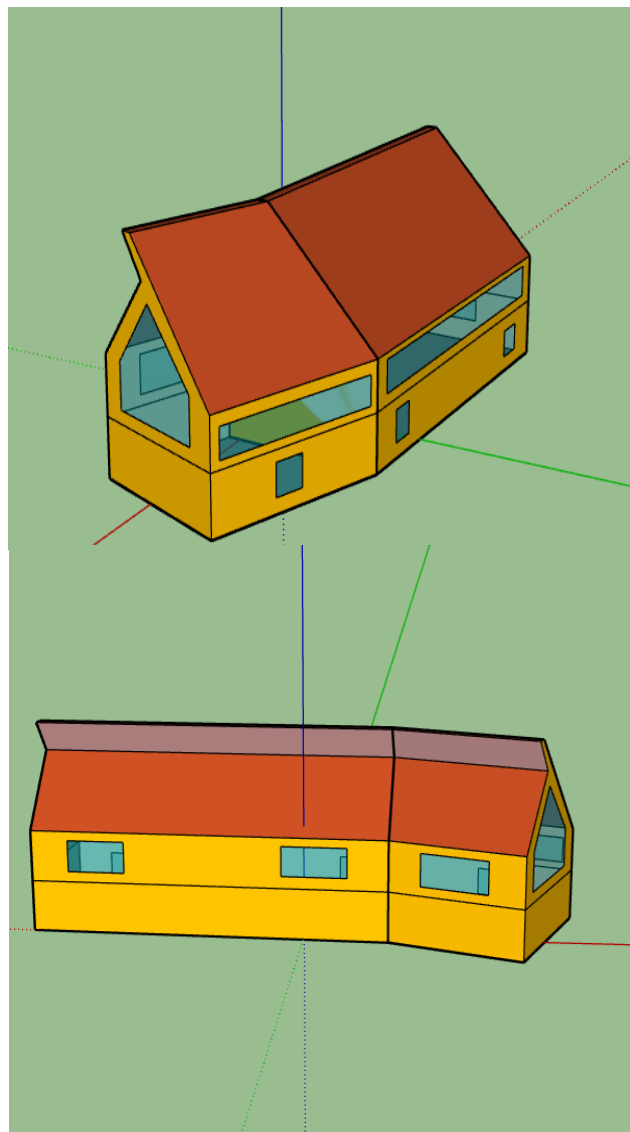


Figure A-1: 3D model of the Varenes Library

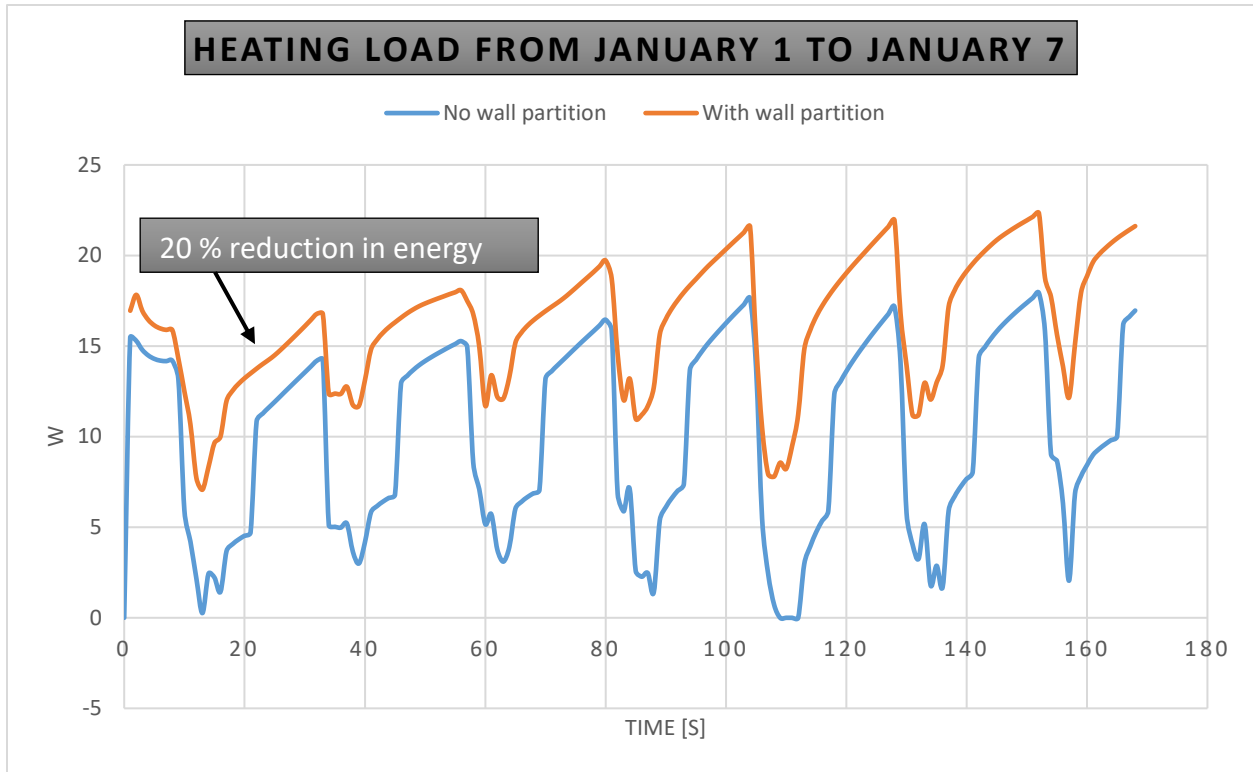


Figure A-2: Effect of removal of internal wall partition between east and west portions of the envelope on the heating load in the 1-week winter period



**60 Degree High Cop and Low Noise 11kw-250kw Heating /Hot Water Air Source Heat Pump**

Get Latest Price > Chat with Supplier.

Min. Order / Reference FOB Price  
1 Piece **US \$1,200/ Piece**

Port: Huangpu, China @

Production Capacity: 5000000000000000 Units/Year

Payment Terms: L/C, T/T, D/P, Western Union, Paypal

Energy Efficiency Grade: One

Heat Temperature: 50-70°C

Work Environment: Common Heat Pump

Heat Source: Air-source

Heating Type: Circulating Heat

Application: Villa Family, Sauna and Swimming Pool, Hotels, Factory Hospital, Student Apartments, Beauty Salons

60 degree high cop and low noise 11kw-250kw heating or hot water air source heat pump

Air to water heat pump cycle type

Model No.	Unit	MG-030KFXRS	MG-050KFXRS	MG-030KFXRS	MG-050KFXRS	MG-080KFXRS	MG-100KFXRS	MG-120KFXRS	MG-150KFXRS	
Heating Capacity	KW	10.8	18	10.8	18	28.8	38	43.2	72	
Power Input	KW	2.7	4.5	2.7	4.5	7.2	9.6	10.8	18	
Largest Current	A	5.9	5.9	5.9	5.9	9	11.2	17.6	36	
Rated Water Temp.	°C	55								
Highest Water Temp.	°C	60								
Power Supply		220V/1P/60Hz			380V/60Hz					
Anti-electric Shock Type		I								

Figure A-3: Air-source heat pump selection based on heating and cooling loads

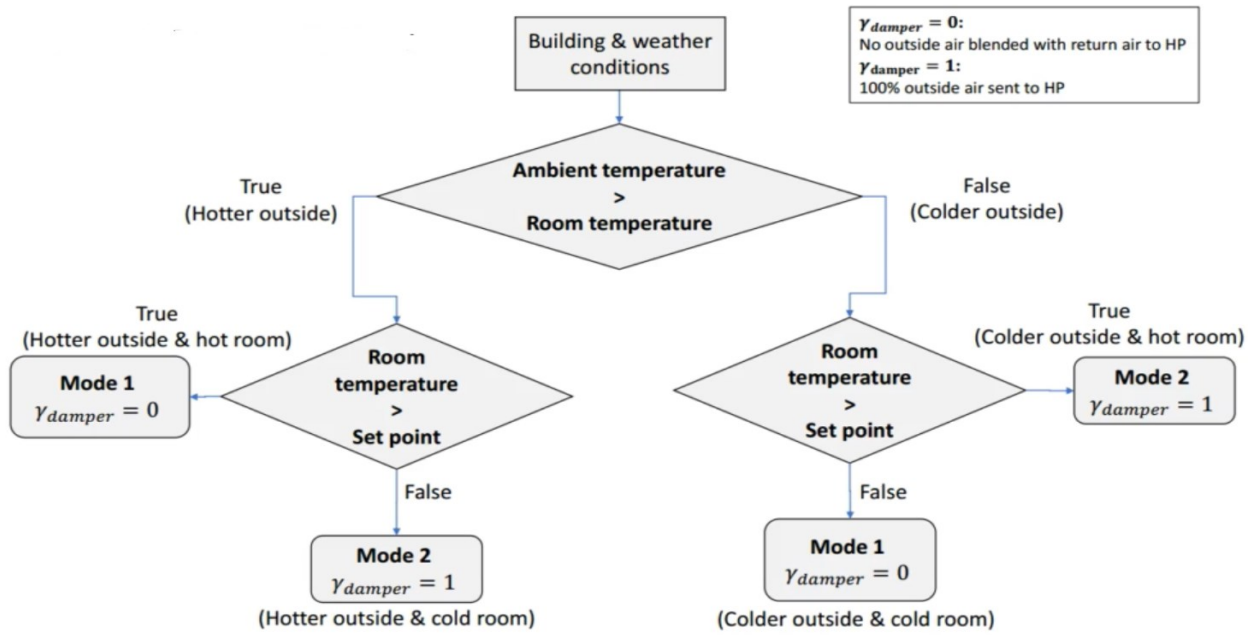


Figure A-4: Air damper control strategy of the ASHP

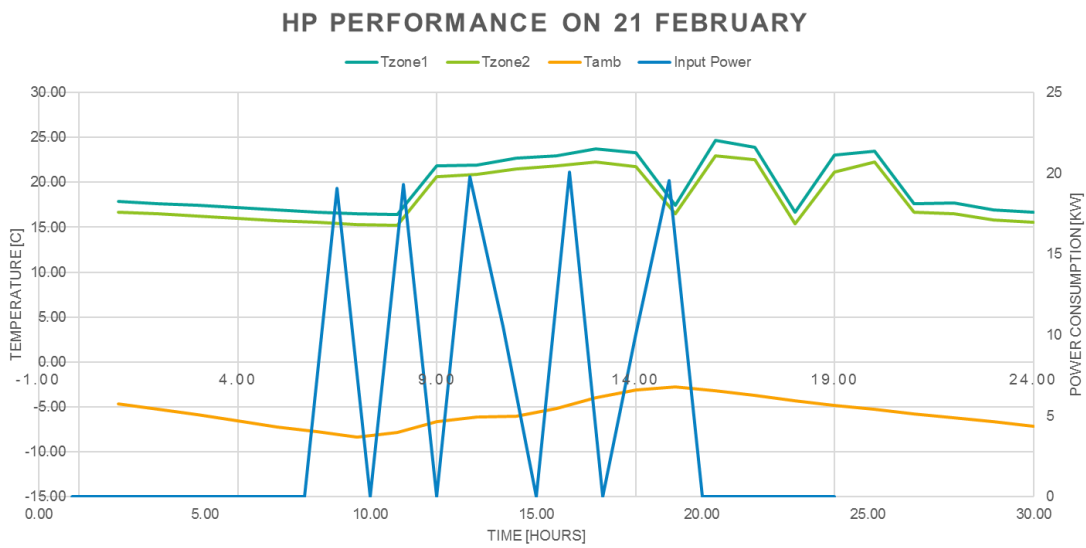


Figure A-5: Performance of air-source HP on 21<sup>st</sup> February

### Summer Performance (June 1<sup>st</sup> to August 31<sup>st</sup>)

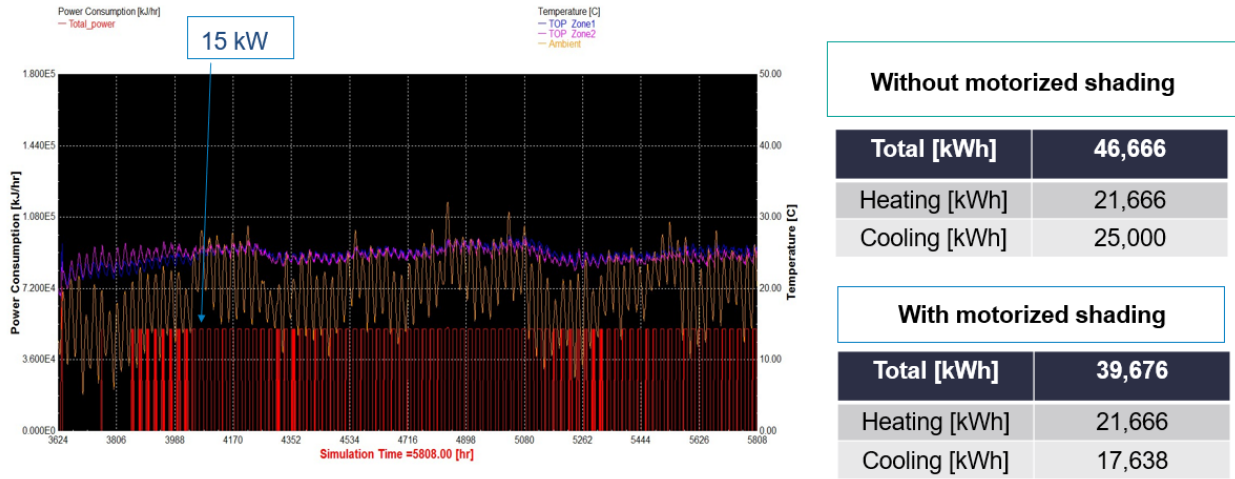


Figure A-6: Power consumption on Summer period with air-source HP and the studied effect of motorized shading

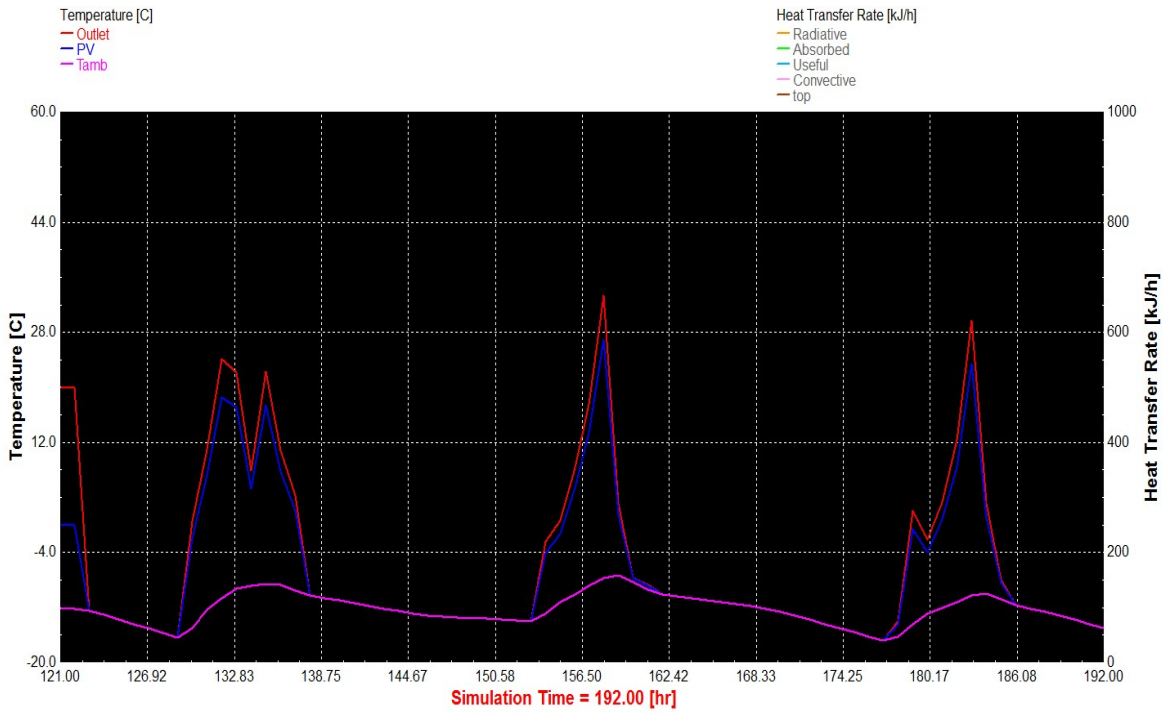


Figure A-7: BIPV/T performance in winter period after coupling with Air source HP

# 1.5 B

## Floor slab thickness analysis

The original floor thickness was decreased from 12.5 cm down to 8 cm, and the results are compared below. When the capacity of the hydronic heating system is undersized for the thickness, it is more efficient to have a thinner slab rather than thicker on extremely cold days.

This stems from the higher temperature difference between slab and interior

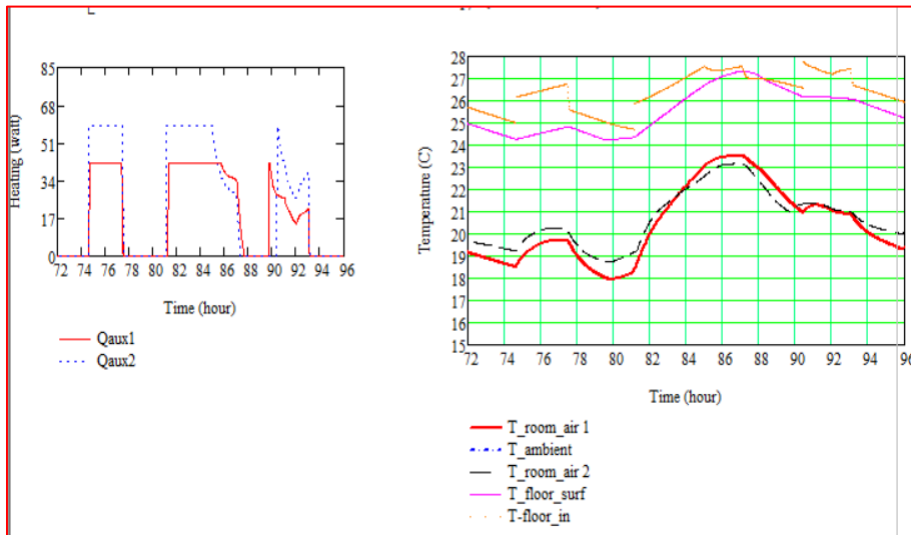


Figure B-1: Thermal slab; thickness 12.5 cm; thermal load 1011 kWh;  $T_{\text{ambient}} \sim -15 - -20 \text{ }^\circ\text{C}$

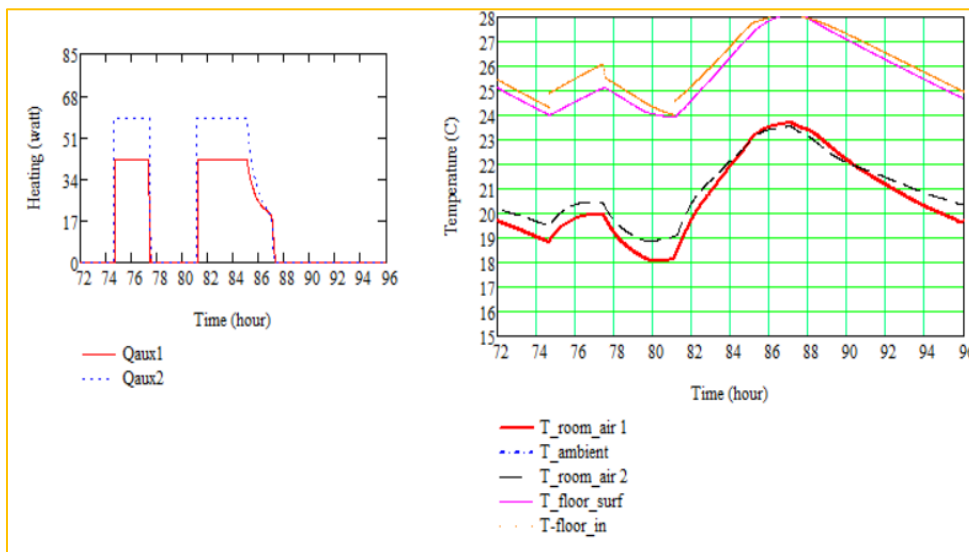


Figure B-2: Thermal slab; thickness 8 cm; thermal load 792 kWh;  $T_{\text{ambient}} \sim -15 - -20 \text{ }^\circ\text{C}$

# 1.6 C

## Proposed control strategy - results

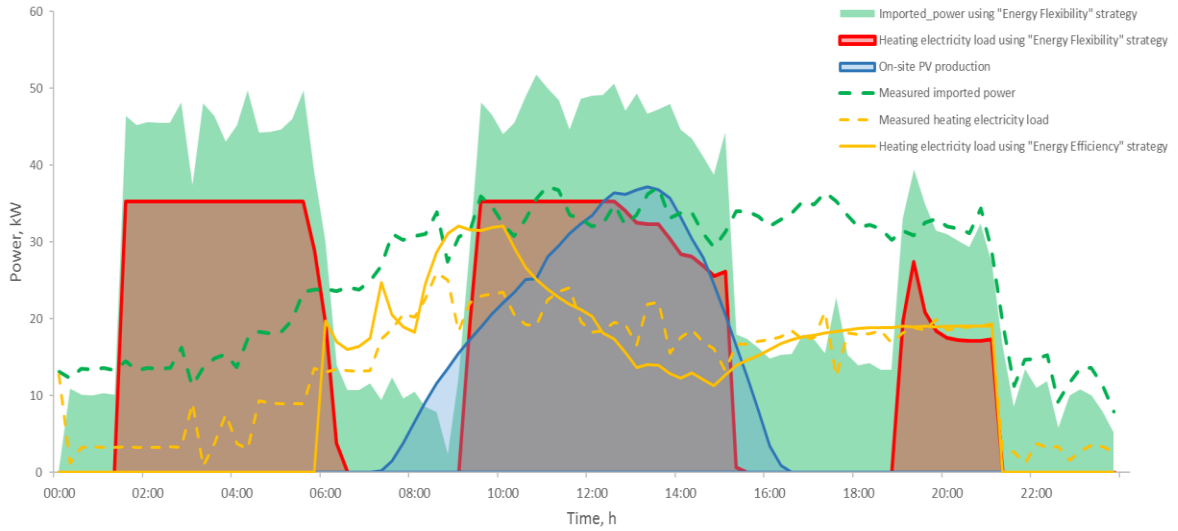


Figure C-1: Energy balance over very cold semi-cloudy day under proposed controls strategies, January 13, 2018

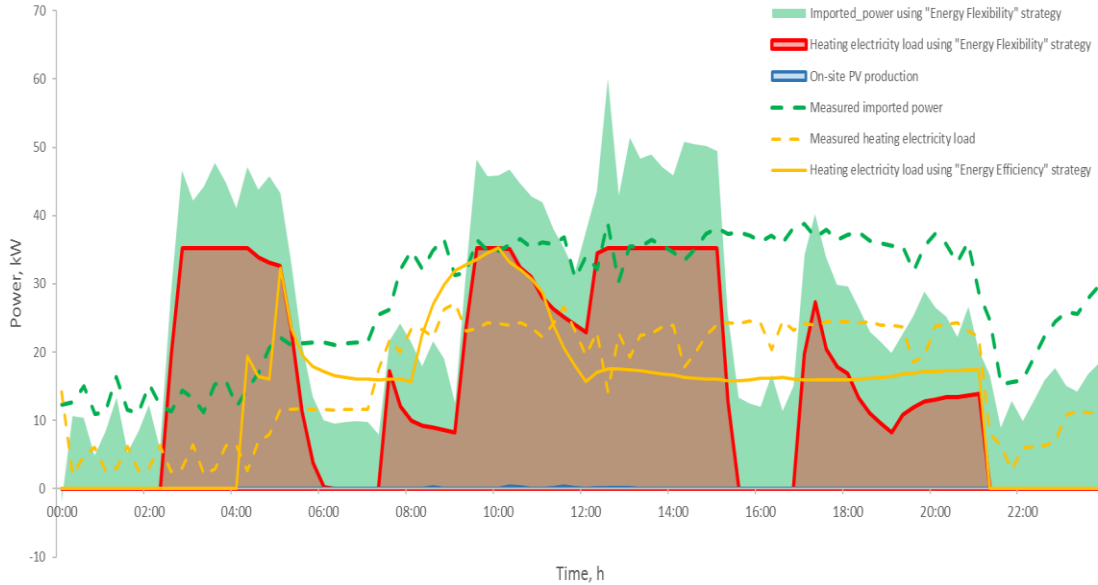


Figure C-2: Energy balance over very cold -cloudy day under proposed controls strategies, January 3, 2018

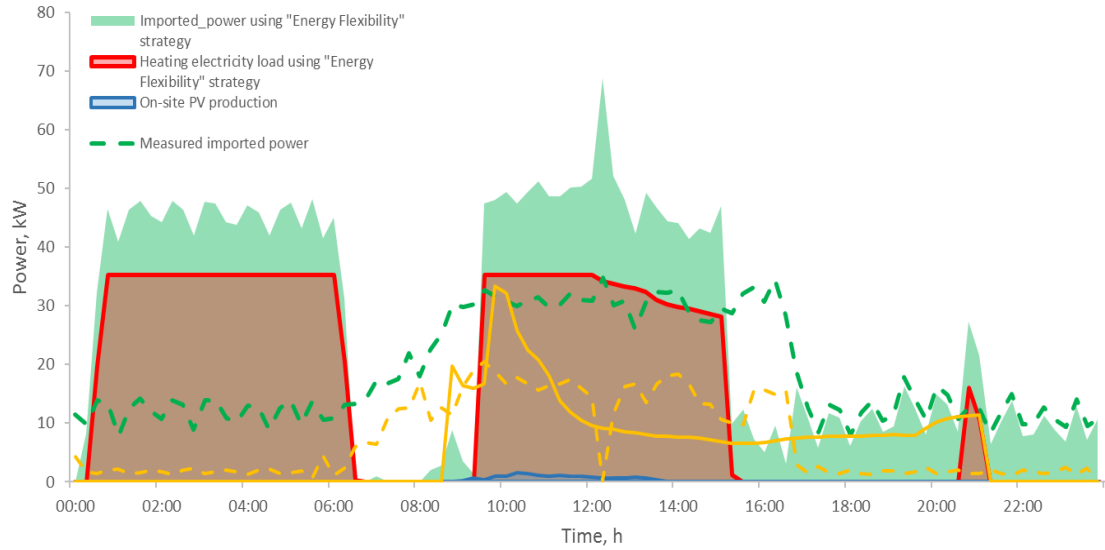


Figure C-3: Energy balance over cold cloudy day under proposed controls strategies, February 10, 2018

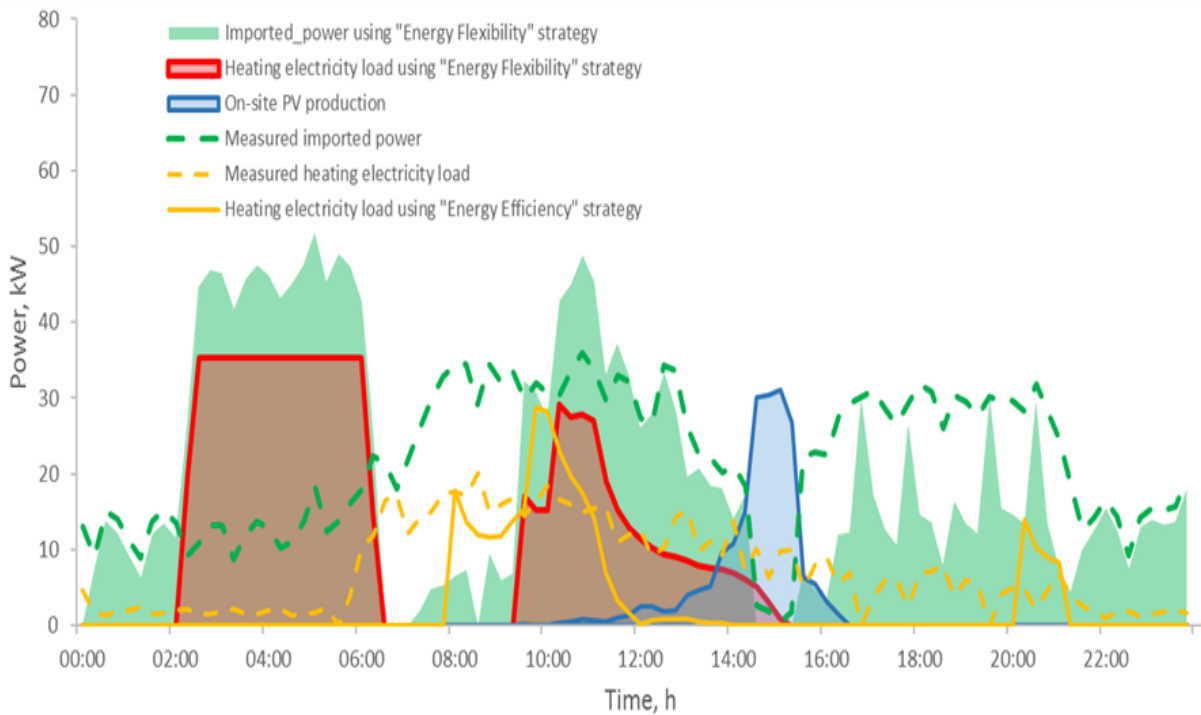


Figure C-4: Energy balance over cold semi-cloudy day under proposed controls strategies, February 1, 2018

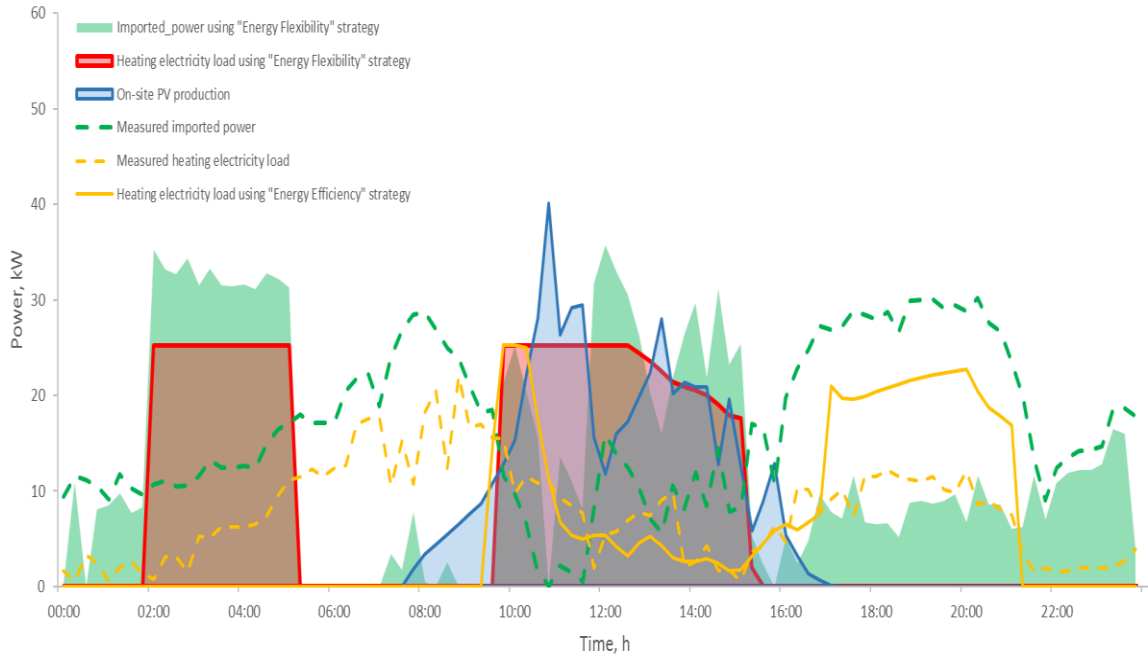


Figure C-5: Energy balance over cold sunny day under proposed controls strategies, February 12, 2018

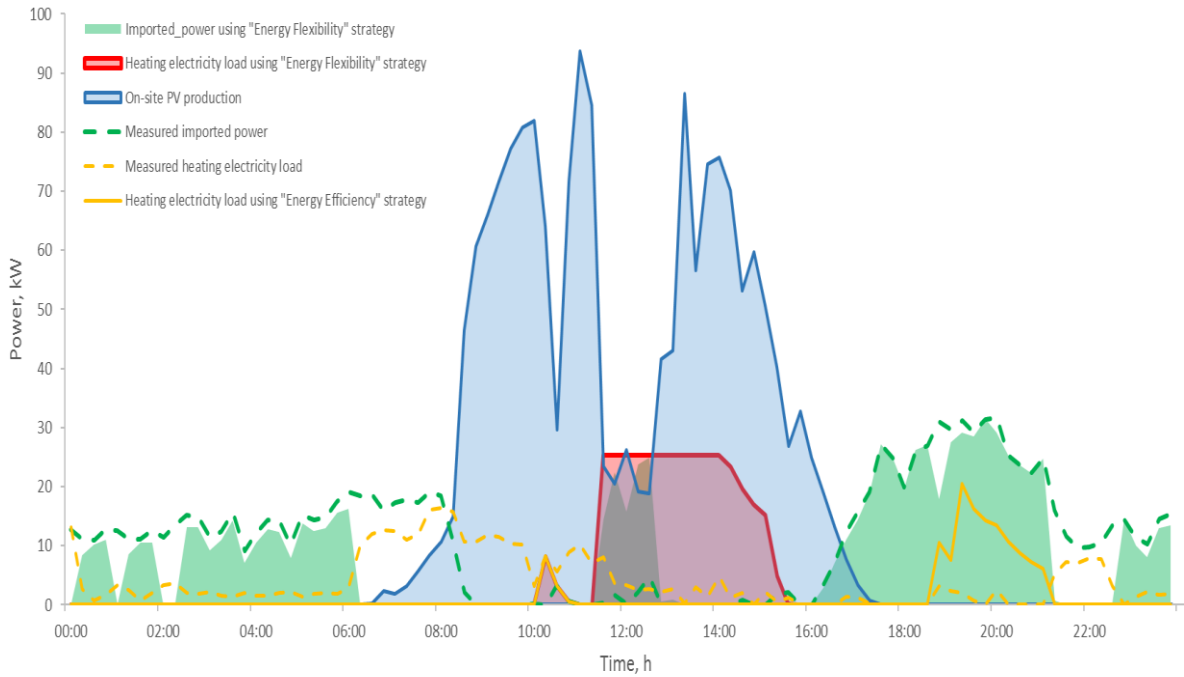


Figure C-6: Energy balance over mild sunny day under proposed controls strategies, February 26, 2018

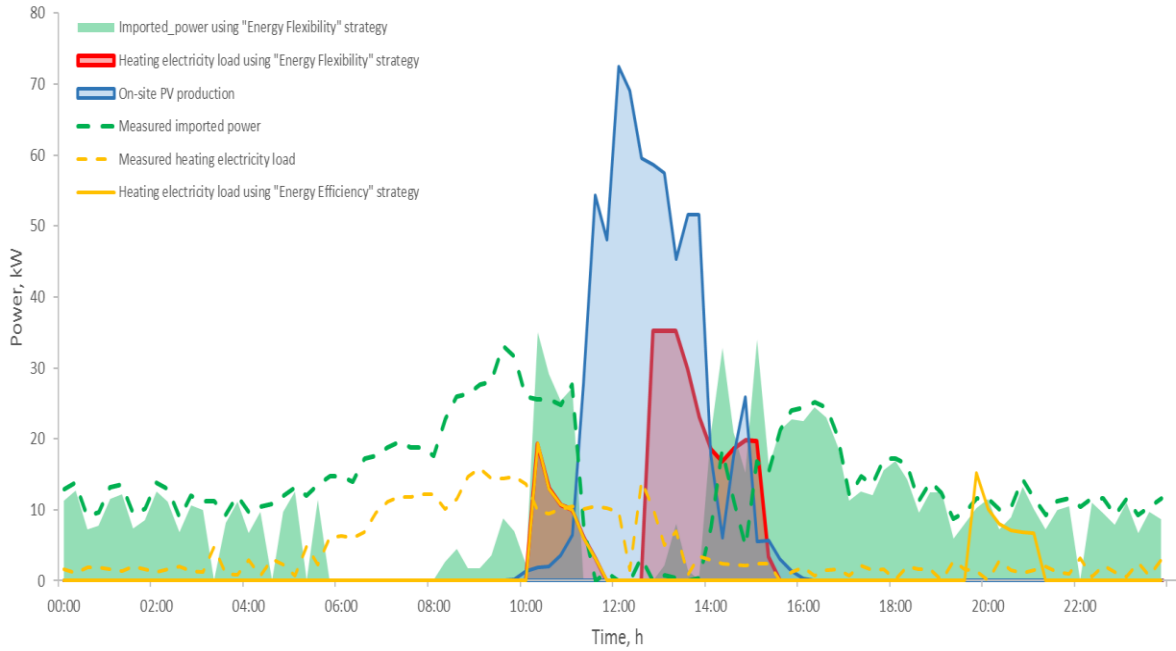


Figure C-7: Energy balance over a mild semi-cloudy day under proposed controls strategies, January 20, 2018

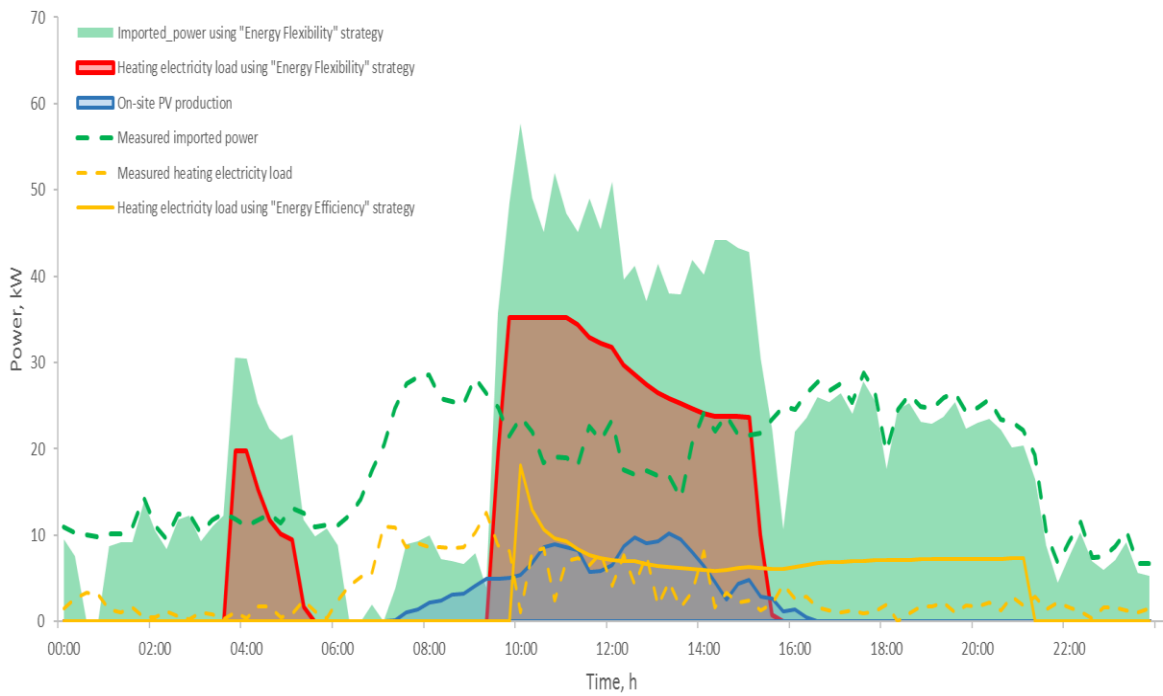


Figure C-8: Energy balance over a mild semi-cloudy day under proposed controls strategies, February 20, 2018

# 1.7 D.

## Modelica Model

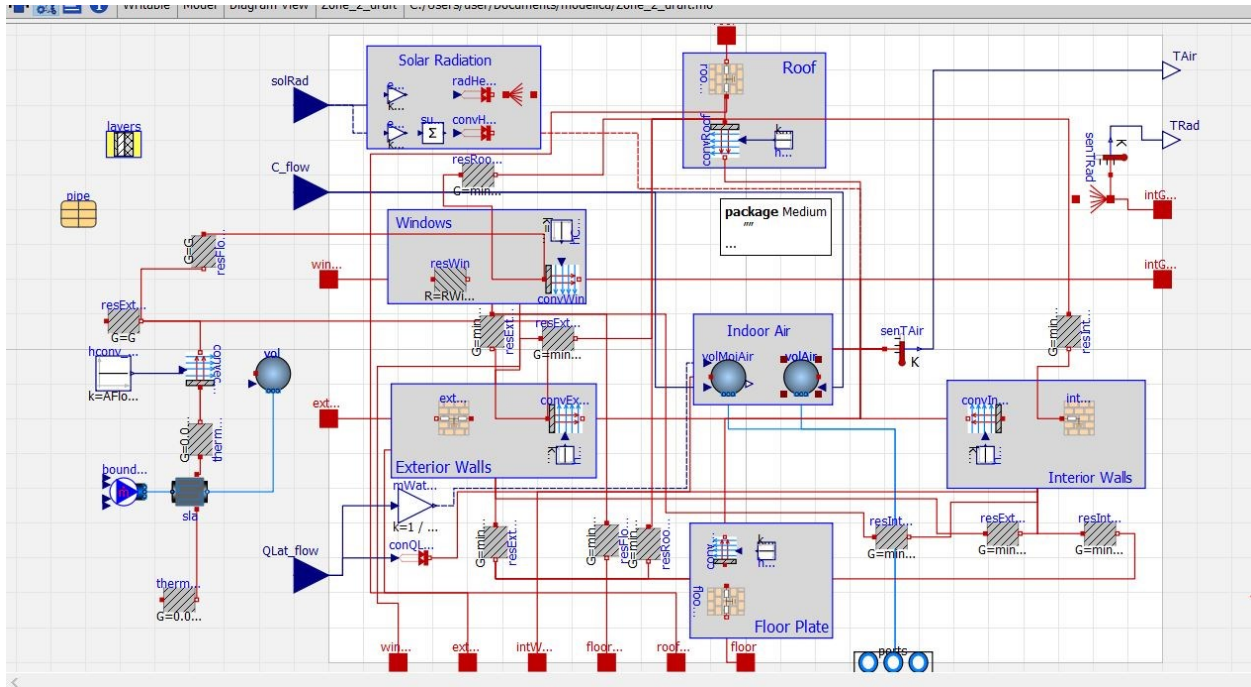


Figure D-1 Bottom floor-zone detailed model in Modelica

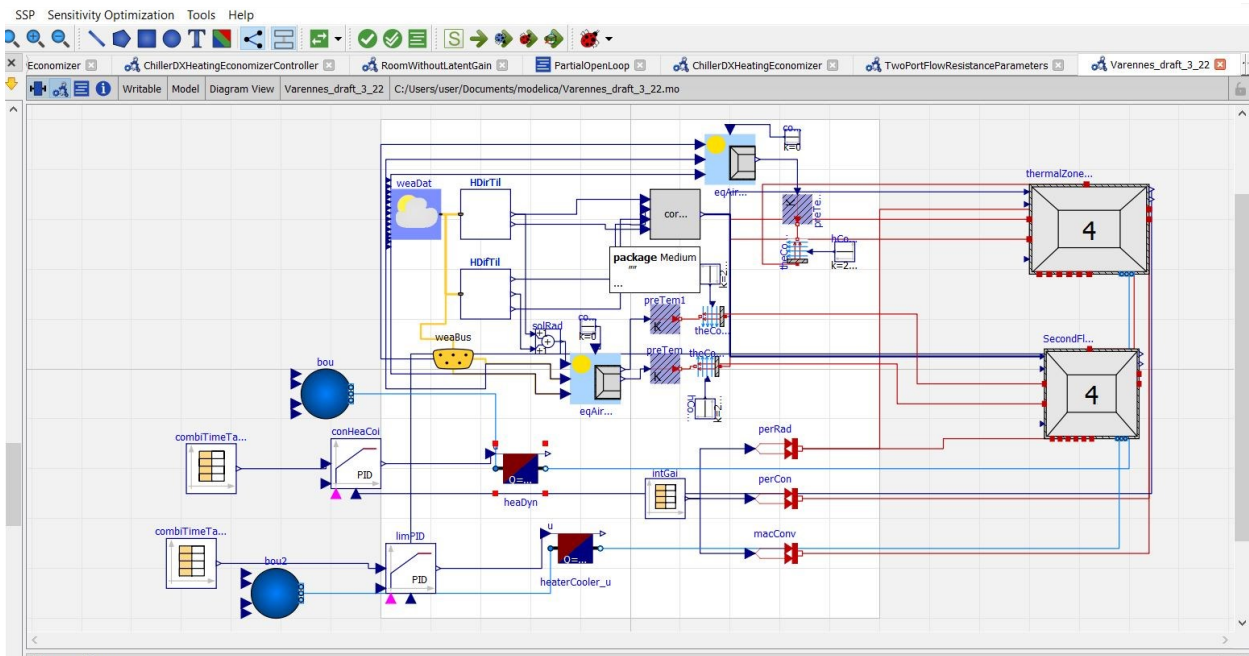


Figure D-2: Whole-building level model comprised of two zones and detailed solar irradiance calculations

## 1.8 E.

### Matlab Codes

#### #State-Space representation of Building model

```
U06=1000/6.21;  
U01=1000/1.458;  
U61=100000/5.93;  
U67=10000/2.367;  
U62=10000/2.367;  
U17=100000/8.607;  
U12=100000/8.607;  
U23=100000/3.713;  
U78=100000/4.774;  
U34=100000/7.426;  
U810=1000/1.626;  
U45=100000/7.426;  
U510=1000/3.719;  
U015=0.012;  
U010=1000/1.363;  
U1516=10000/2.367;  
U1510=10000/1.359;  
U1511=10000/2.367;  
U1016=100000/8.607;  
U1011=100000/8.607;  
U1617=100000/4.774;  
U1112=100000/3.713;  
U1213=100000/7.426;  
U1314=100000/7.426;  
C1=0.01;  
C2=0.01;  
C3=3.346*10^7;  
C4=0.01;  
C5=3.346*10^7;  
C6=0.01;  
C7=0.01;  
C8=1.562*10^8;  
C10=0.01;  
C11=0.01;  
C12=3.346*10^7;  
C13=0.01;  
C14=3.346*10^7;
```

```

C15=0.01;
C16=0.01;
C17=1.562*10^8;
A=[-(U61+U01+U17+U12)/C1 U12/C1 0 0 0 U61/C1 U17/C1 0 0 0 0
0 0 0 0 0;
    U12/C2 -(U12+U23+U62)/C2 U23/C2 0 0 U62/C2 0 0 0 0 0 0
0 0 0 0;
    0 U23/C3 -(U34+U23)/C3 U34/C3 0 0 0 0 0 0 0 0 0 0 0 0;
    0 0 U34/C4 -(U34+U45)/C4 U45/C4 0 0 0 0 0 0 0 0 0 0 0;
    0 0 0 U45/C5 -(U45+U510)/C5 0 0 0 U510/C5 0 0 0 0 0 0
0;
    U61/C6 U62/C6 0 0 0 -(U06+U61+U67+U62)/C6 U67/C6 0 0 0
0 0 0 0 0 0;
    U17/C7 0 0 0 0 U67/C7 -(U67+U17+U78)/C7 U78/C7 0 0 0 0
0 0 0 0;
    0 0 0 0 0 U78/C8 -(U78+U810)/C8 U810/C8 0 0 0 0 0 0
0;
    0 0 0 0 U510/C10 0 0 U810/C10 -
(U810+U510+U1016+U1011+U1510+U010)/C10 U1011/C10 0 0 0
U1510/C10 U1016/C10 0;
    0 0 0 0 0 0 0 U1011/C11 -(U1011+U1112+U1511)/C11
U1112/C11 0 0 U1511/C11 0 0;
    0 0 0 0 0 0 0 0 U1112/C12 -(U1112+U1213)/C12
U1213/C12 0 0 0 0;
    0 0 0 0 0 0 0 0 0 U1213/C13 -(U1213+U1314)/C13
U1314/C13 0 0 0;
    0 0 0 0 0 0 0 0 0 0 U1314/C14 -(U1314)/C14 0 0 0;
    0 0 0 0 0 0 0 0 U1510/C15 U1511/C15 0 0 0 -
(U015+U1516+U1510+U1511)/C15 U1516/C15 0;
    0 0 0 0 0 0 0 U1016/C16 0 0 0 0 U1516/C16 -
(U1516+U1016+U1617)/C16 U1617/C16;
    0 0 0 0 0 0 0 0 0 0 0 0 0 U1617/C17 -U1617/C17];
B=[U01/C1 1/C1 0 0;
    0 0 0 0.08/C2;
    0 0 0 0;
    0 0.876/C4 0 0;
    0 0 0 0;
    U06/C6 0 0 0.15/C6;
    0 0 0 0.27/C7;
    0 0 0 0;
    U010/C10 0 0.124/C10 0;
    0 0 0 0.08/C11;
    0 0 0 0;
    0 0 0.876/C13 0;

```

```

    0 0 0 0;
    0 0 0 0.15/C15;
    0 0 0 0.27/C16;
    0 0 0 0];

C=[1 0 0 0 0 0 0 0 0 0 0 0 0 0 0 0;
    0 0 0 0 0 0 0 0 0 1 0 0 0 0 0 0

    ];
D=[0 0 0 0;
    0 0 0 0

    ];
sys = ss(A,B,C,D);
% step(sys)
data2=xlsread('Input_3_wi.xlsx','A:D');
data1=xlsread('Output_3','A:D');
x0 = ones(16,1)*10;
sys1 = chgTimeUnit(sys,'minutes');
[y_out, time] = lsim(sys1,data2,0:15:5745,x0);
figure(1)
p1=plot(time,y_out(1:end,1))
title('air T')
hold on
y1 = data1(1:end,1);
d1=plot(time,y1)
h=[p1; d1];
legend(h,'Simulation','Data');
hold off

% plot(t,y)
% lsim(sys,data2,0:288)
% t = 0:300;
%initial condition of system states
% [y,x] = lsim(A,B,C,D,data2,t); %do the simulation
% plot(t,y,t,u)
% legend('Response','Input')

```

### #Explicit representation of 10<sup>th</sup> order model with ADEs

```
% define energy balance model
function dTdt =
Heat_test_original_pure_air(t,var,To_inp,Q1_inp,Q2_inp,S_in
p,Tg_inp)
To = interp1(1:900:86400*4,To_inp,t);
Q1 = interp1(1:900:86400*4,Q1_inp,t);
Q2 = interp1(1:900:86400*4,Q2_inp,t);
S = interp1(1:900:86400*4,S_inp,t);
Tg=interp1(1:900:86400*4,Tg_inp,t);
T1=var(1);
T2=var(2);
T3=var(3);
T4=var(4);
T5=var(5);
T6=var(6);
T7=var(7);
T8=var(8);
T10=var(9);
T11=var(10);
T12=var(11);
T13=var(12);
T14=var(13);
T15=var(14);
T16=var(15);
T17=var(16);
U06=2.09;
c2=1.2*1.3;
c1=0.8*2.9;
c=2;
U01=6.3216*0.7*c2*1.1;
U61=abs(433)*6;
U67=0.56*1056*6;
U62=0.44*1056*6;
% U17=abs(0.56*1056)*4;
U17=abs((0.56*1056)*(1.52*(T7-T1)^(1/3)));
% U17=20000;
% U12=abs(0.44*1056)*4;
U12=abs((0.44*1056)*(1.52*(T2-T1)^(1/3)));
% U12=20000;
U23=3.9525;
U78=1.676;
U34=1.975;
```

```

U810=( (0.56*1056) * (1.01*(abs (T10-T8)) ^ (1/3))) ;
U45=1.9751;
U510=( (0.44*1056) * (1.01*(abs (T10-T5)) ^ (1/3))) ;
U015=8.5623;
U010=6.3216*0.7*c1;
U1516=0.75*1056*6;
U1510=(433) *6;
U1511=0.25*1056*6;
% U1016=abs (0.75*1056) *4;
% U1011=abs (0.25*1056) *4;
U1016=abs ( (0.75*1056) * (1.52*(T16-T10) ^ (1/3))) ;
U1011=abs ( (0.25*1056) * (1.52*(T11-T10) ^ (1/3))) ;
% U1016=20000;
% U1011=20000;
U1617=2.2447;
U1112=2.2447;
U1213=1.12;
U1314=1.12;
C3=6.98*c;
C5=6.98*c;
C8=1.774*c;
C12=3.962*c;
C14=3.96*c;
C17=2.38*c;
C1=4.22;
C10=4.22;
kef=1.3;
C6=5.3;
C15=5.3;
scf2=1.2*1.2;
scf1=1;

dTdt (1,1) = (1.0/(C1*6e+6)) * ((T6-T1) *U61+(To-
T1) *U01*100+(T7-T1) *U17+(T2-T1) *U12+0.5*Q2) ;
dTdt (2,1)=(T1*U12+T3*U23*10000+T6*U62+0.154*S*scf2) / (U12+U2
3*10000+U62) -T2;
dTdt (3,1) = (1.0/(kef*C3*1e+7)) * ((T4-T3) *U34*10000+(T2-
T3) *U23*10000) ;
dTdt (4,1)=(T3*U34*10000+T5*U45*10000+0.625*Q1) / (U34*10000+U
45*10000) -T4;
dTdt (5,1)=(1/(kef*C5*1e+7)) * ((T4-T5) *U45*10000+(T10-
T5) *U510) ;
dTdt (6,1)=(1.0/(kef*C6*6e+6)) * ((To-T6) *U06*100+(T1-
T6) *U61+(T7-T6) *U67+(T2-T6) *U62+0.15*S*scf2)

```

```

dTdt(7,1)=(T6*U67+T1*U17+T8*U78*10000+0.196*S*scf2)/(U67+U1
7+U78*10000)-T7;
dTdt(8,1)=(1/(kef*C8*1e+8))*((T7-T8)*U78*10000+(T10-
T8)*U810);
dTdt(9,1)=(1/(C10*6e+6))*((T8-T10)*U810+(T5-
T10)*U510+(T16-T10)*U1016+(T11-T10)*U1011+(T15-
T10)*U1510+(To-T10)*U010*100+0.5*Q2);
dTdt(10,1)=-
T11+(T10*U1011+T12*U1112*10000+T15*U1511+0.08*S*scf1)/(U101
1+U1112*10000+U1511);
dTdt(11,1)=(1/(kef*C12*1e+7))*((T11-T12)*U1112*10000+(T13-
T12)*U1213*10000);
dTdt(12,1)=(T12*U1213*10000+T14*U1314*10000+0.375*Q1)/(U121
3*10000+U1314*10000)-T13;
dTdt(13,1)=(1/(kef*C14*1e+7))*((T13-T14)*U1314*10000+(To-
T14+6)*0*U010/2);
dTdt(14,1)=(1/(kef*C15*1e+6))*((To-T15)*U015*10+(T16-
T15)*U1516+(T10-T15)*U1510+(T11-T15)*U1511+0.15*S*scf1);
dTdt(15,1)=(T15*U1516+T10*U1016+T17*U1617*10000+0.27*S*scf1
)/(U1516+U1016+U1617*10000)-T16;
dTdt(16,1)=(1/(kef*C17*1e+8))*((T16-T17)*U1617*10000+(To-
T16+6)*0*U010/2);
end

```

### #Simulation of above-mentioned model

```

range = [1:900:86400*4];
data2=xlsread('Input_3_2','A:D');
data1=xlsread('Output_3','A:D');
a=3;
b=5;
ICs=[data1(1,1),data1(1,3)+a,data1(1,3)+a+b,data1(1,3)+a+b,
data1(1,3),data1(1,1),data1(1,3)+a,data1(1,3)+a,data1(1,2),
data1(1,4)+a,data1(1,4)+a+b,data1(1,4)+a+b,data1(1,4)+a+b,d
ata1(1,2),data1(1,4)+a,data1(1,4)+a];
To_inp=data2(1:end,1);
Q1_inp=data2(1:end,2);
Q2_inp=data2(1:end,3);
S_inp=data2(1:end,4);
Tg_inp=data2(1:end,1)+7;
% opts = odeset('MaxStep',300)

```

```

[t,T]=ode15s(@(t,var)
Heat_test_wall_air_draft2(t,var,To_inp,Q1_inp,Q2_inp,S_inp,
Tg_inp),range,ICs);
figure(1)
x = t(1:end);
y1 = T(1:end,1);
p1=plot(x,y1);
title('2nd floor air T')
hold on

x = t(1:end);
y1 = data1(1:end,1);
d1=plot(x,y1)
h=[p1; d1];
legend(h,'Simulation','Data');
hold off

figure(2)
x = t(1:end);
y1 = T(1:end,9);
p2=plot(x,y1)
title('1st floor air T')
hold on
x = t(1:end);
y1 = data1(1:end,2);
d2=plot(x,y1)
d=[p2; d2];
legend(d,'Simulation','Data');
hold off

```

**#BIPV/T 2-inlet model with different wind and channel CHTC, 100 CVs each with 10 subdivisions**

```

%%
clear all
clc
%%
Tamb = 2.797;
G =514;
m_kg_hr = 15000;
Tzone = 20;
V_w = 3.6;
Tamb_K = Tamb+273.15;

```

```

Tsky = 284.15;
F_sky = 1;
Tsur = Tamb+273.15;
F_sur = 1;

m = m_kg_hr/3600;

wind_mode = 6;
ho_mode = 1;
Nu_mode = 1;

Nu_expression = 1;

c = 1000
rho = 1.2;
mi = 18*10^(-6);
k = 0.0247;
Pr = c*mi/k;
sigma = 5.67E-8;

L = 13;
W = 55.4;
D = 0.07;
A = W*L;
Ac = W*D;
Dh = 2*Ac/(W+D);

ab = 0.95;
h0 = 0.061;
e1 = 0.9;
e2 = 0.8;
e_glass = 0.8;

tg = 0.95;

Rtop = 0.0042;
Rbot = 0.0072;
Rins = 100;

Q = m/rho;
V = Q/Ac;

```

```

Re = rho*V*Dh/mi;

if Re>2800
    f = (0.79*log(Re)-1.64)^(-2);
else
    f = 64/Re;
end
w_outlet = W;
h_outlet = 0.07;
A_outlet = w_outlet * h_outlet;
V_outlet = V*Ac/A_outlet;
K_entrance = 0.5;

DP_entrance = K_entrance*rho*(V_outlet^2)/2;

e_glass = 0.0015;
e_mullion = 0.035;
e_back = 0.15;

e_average = (e_glass*W + e_mullion*2*D +
e_back*W)/(2*W+2*D);
numb = -1.8*log(6.9/Re+(e_average/(3.7*Dh))^1.11);
f = 1/(numb^0.5);

DP_friction = f*(L/Dh)*rho*(V^2)/2;

DP_total = DP_friction + DP_entrance;

W_pumping = Q*DP_total;

n = 100;
dx = L/n;
i = 1:n;
x = i*dx;

Acv = W*dx;

l = 10;
j = 1:l;

Vwind = 0.1307.*((x-dx/2).^4)-1.053.*((x-
dx/2).^3)+3.219.*((x-dx/2).^2)-4.525.*((x-dx/2))+3.759;
ho_Yang = 13.45.*Vwind;
Vwind_avg_Yang = sum(Vwind)/n;

```

```

ho_Yang_avg = sum(ho_Yang)/n;

if wind_mode == 1
    ho = ho_Yang;
elseif wind_mode == 2
    ho = ones(1,n)*(13.42*V_w);
elseif wind_mode == 3
    ho = ones(1,n)*(11.9+2.2*V_w);
elseif wind_mode == 4
    ho = ones(1,n)*(3.8*V_w);
elseif wind_mode == 5
    ho = ones(1,n)*(3*V_w+2.8);
elseif wind_mode == 6
    ho = ones(1,n)*(4*V_w+7.4);
end

ho_avg = sum(ho)/n;

    if Re<2300
        Nu_PV_Yang = 0.6883*((Re)^0.7)*(Pr^0.8).*exp((- (x-
dx/2).^ (0.3))/(6.45*Dh))+0.0124*((Re)^0.7)*(Pr^0.8));
    else
        Nu_PV_Yang = 8.188*((Re)^0.77)*(Pr^3.85)*exp((- (x-
dx/2).^ (0.2))/(2.8*Dh))+0.061*((Re)^0.77)*(Pr^3.85));
    end

    if Re<2300
        Nu_ins_Yang = 50*((Re)^0.5)*(Pr^0.2)*exp((- (x-
dx/2).^ (0.3))/(1.37*Dh))+0.428*(Re^0.5)*(Pr^0.2);
    else
        Nu_ins_Yang = 4.02*((Re)^1.09)*(Pr^19.3)*exp((- (x-
dx/2).^ (0.2))/(14*Dh))+0.005*(Re^1.09)*(Pr^19.3);
    end

    if Re<2400
        Nu_PV_Cand = 0.039*(Re^0.78)*(Pr^0.4).*exp((- (x-
dx/2).^ (0.2))/(20*Dh))+0.034*((Re)^0.78)*(Pr^0.4));
    else
        Nu_PV_Cand = 0.012*(Re^0.78)*(Pr^0.4).*exp((- (x-
dx/2).^ (0.2))/(9.09*Dh))+0.049*((Re)^0.78)*(Pr^0.4));
    end

```

```

    if Re<2400
        Nu_ins_Cand = Nu_PV_Cand;
    else
        Nu_ins_Cand = Nu_PV_Cand;
    end

Nu_PV_avg_Yang = sum(Nu_PV_Yang)/n;
Nu_ins_avg_Yang = sum(Nu_ins_Yang)/n;

Nu_PV_avg_Cand = 0.052*(Re^0.78)*(Pr^0.4);
Nu_PV_avg_Cand_check = sum(Nu_PV_Cand)/n;
Nu_ins_avg_Cand = 1.017*(Re^0.471)*(Pr^0.4);

Nu_PV_avg_DB = 0.023*(Re^0.8)*(Pr^0.4);
Nu_ins_avg_DB = Nu_PV_avg_DB;

Nu_PV_Ath_1 = 0.014*((Re*2/3)^0.9)*(Pr^0.43);
Nu_PV_Ath_2 = 1.451*((Re*1)^0.44)*(Pr^0.4);

if Nu_expression == 1
    Nu_PV = Nu_PV_Yang;
    Nu_ins = Nu_ins_Yang;
elseif Nu_expression == 2
    Nu_PV = Nu_PV_Cand;
    Nu_ins = Nu_ins_Cand;
elseif Nu_expression == 3
    Nu_PV = ones(1,n) * Nu_PV_avg_Cand;
    Nu_ins = ones(1,n) * 1.017*(Re^0.471)*(Pr^0.4);
elseif Nu_expression == 4
    Nu_PV = ones(1,n) * Nu_PV_avg_DB;
    Nu_ins = ones(1,n) * Nu_PV_avg_DB;
elseif Nu_expression == 5
    Nu_PV = ones(1,n) *
0.0158*(Re^0.8)+(0.00181*Re+2.92)*exp(-0.0379*(L/Dh));
    Nu_ins = ones(1,n) *
0.0158*(Re^0.8)+(0.00181*Re+2.92)*exp(-0.0379*(L/Dh));
elseif Nu_expression == 6
    Nu_PV = ones(1,n) * (((Re-
1000)*Pr*(f/8))/(1+12.7*((f/8)^0.5)*((Pr^(2/3))-
1)))*(1+(Dh/L)^(2/3));
    Nu_ins = ones(1,n) * (((Re-
1000)*Pr*(f/8))/(1+12.7*((f/8)^0.5)*((Pr^(2/3))-
1)))*(1+(Dh/L)^(2/3));
elseif Nu_expression == 7

```

```

    Nu_PV = ones(1,n)*(12*V+3)*Dh/k;
    Nu_ins = ones(1,n)*(12*V+3)*Dh/k;
elseif Nu_expression==8 & i>n/2
    Nu_PV=ones(1,n)*Nu_PV_Ath_1;
    Nu_ins=Nu_PV;
elseif Nu_expression==8 & i>n/2
    Nu_PV=ones(1,n)*Nu_PV_Ath_2;
    Nu_ins=Nu_PV;
end

```

```

TPV = zeros(1,n);
Tb = zeros(1,n);
T = zeros(1,n);
Ttop = zeros(1,n);
Tlow = zeros(1,n);
E_el_cv = zeros(1,n);
S_pv_cv = zeros(1,n);
E_th_cv = zeros(1,n);
E_th_check = zeros(1,n);
h = zeros(1,n);
hrad = zeros(1,n);
hrad_sky = zeros(1,n);
hrad_sur = zeros(1,n);
Tma = zeros(1,n);
Ten = zeros(1,n);
Tm1 = zeros(1,n);
Tm_sky = zeros(1,n);
Tm_sur = zeros(1,n);
Uo = zeros(1,n);
U1 = zeros(1,n);
U2 = zeros(1,n);
Urad = zeros(1,n);
Urad_sky = zeros(1,n);
Urad_sur = zeros(1,n);

```

```

for i = 1:n;
    if i<20
        Re = 2/3*rho*V*Dh/mi;
        x(1,i) = i*dx;
        m1=m*2/3;
    else
        Re=rho*V*Dh/mi;
        x(1,i) = (i-19)*dx;
    end
end

```

```

        m1=m;
    end

    if Re<2300
        Nu_PV_Yang = 0.6883*((Re)^0.7)*(Pr^0.8).*exp((- (x-
dx/2).^0.3)/(6.45*Dh))+0.0124*((Re^0.7)*(Pr^0.8));
    else
        Nu_PV_Yang = 8.188*((Re)^0.77)*(Pr^3.85)*exp((- (x-
dx/2).^0.2)/(2.8*Dh))+0.061*((Re^0.77)*(Pr^3.85));
    end

    if Re<2300
        Nu_ins_Yang = 50*((Re)^0.5)*(Pr^0.2)*exp((- (x-
dx/2).^0.3)/(1.37*Dh))+0.428*(Re^0.5)*(Pr^0.2);
    else
        Nu_ins_Yang = 4.02*((Re)^1.09)*(Pr^19.3)*exp((- (x-
dx/2).^0.2)/(14*Dh))+0.005*(Re^1.09)*(Pr^19.3);
    end

    Nu_PV = Nu_PV_Yang;
    Nu_ins = Nu_ins_Yang;

    hc_PV = Nu_PV*k/Dh;
    hc_ins = Nu_ins*k/Dh;
    hc = (hc_PV+hc_ins)/2;

    hc_PV_avg = sum (hc_PV)/n;
    hc_ins_avg = sum(hc_ins)/n;
    hc_avg = sum(hc)/n;

    a1 = m1*c./(W.*hc);
        TPV(1,i) = Tamb
        Ttop(1,i) = Tamb;
        Tlow(1,i) = Tamb;
        Tb(1,i) = Tamb;
        if i==1;
            Ten(1,i) = Tamb;
        elseif i==20;
            Ten(1,i)=0.66*(T(1,i-1))+0.34*(Tamb);
        else
            Ten(1,i) = T(1,i-1);
        end
    error_toll = 0.001;

```

```

while abs(error_toll)>=0.0001
    Tprevious = TPV(1,i);
    I_total = G;
    h(1,i) = h0*(1-0.0045*(TPV(1,i)-25));
    S_tot_cv = tg*ab*Acv*I_total;
    E_el_cv(1,i) = h(1,i)*Acv*I_total;
    S_pv_cv(1,i) = S_tot_cv - E_el_cv(1,i);

    Tm1(1,i) =
((Tlow(1,i)+273.15)^2+(Tb(1,i)+273.15)^2).*(Tlow(1,i)+273.1
5+Tb(1,i)+273.15);
    F = 0.78;
    hrad(1,i) = sigma.*F*Tm1(1,i)/((1/e1)+(1/e2)-
1);

    Tm_sky(1,i) =
((Ttop(1,i)+273.15)^2+(Tsky)^2).*(Ttop(1,i)+273.15+Tsky);
    hrad_sky(1,i) =
sigma.*F_sky.*Tm_sky(1,i).*e_glass;

    Tm_sur(1,i) =
((Ttop(1,i)+273.15)^2+(Tsur)^2).*(Ttop(1,i)+273.15+Tsur);
    hrad_sur(1,i) =
sigma.*F_sur.*Tm_sur(1,i).*e_glass;

    Uo = ho*Acv;
    U1(1,i) = hc_PV(1,i)*Acv;
    U2(1,i) = hc_ins(1,i)*Acv;
    Urad = hrad*Acv;
    Urad_sky = hrad_sky*Acv;
    Urad_sur = hrad_sur*Acv;

    Rglass = Rtop;
    Uglass = (1/Rglass)*Acv;

    Rmix = Rbot;
    Umix = (1/Rmix)*Acv;
    Uins = (1/Rins)*Acv;

    for j = 1:l;
        xx(j) = j*dx/l;
        T(j,i) =
(hc_PV(1,i).*Tlow(1,i)+hc_ins(1,i).*Tb(1,i))./(hc_PV(1,i)+h

```

```

c_ins(1,i))+(Ten(1,i)-
(hc_PV(1,i).*Tlow(1,i)+hc_ins(1,i).*Tb(1,i))./(hc_PV(1,i)+h
c_ins(1,i))).*exp(-
W.*(xx(j)).*(hc_PV(1,i)+hc_ins(1,i))./(m*c)));
    end
    Tma(1,i) = sum(T(1:l,i))/l;

    Tb(1,i) =
(Tma(1,i).*U2(1,i)+Tlow(1,i).*Urad(1,i)+Uins*Tzone)./(U2(1,
i)+Urad(1,i)+Uins);

TPV(1,i)=(Uo(1,i).*Tamb+U1(1,i).*Tma(1,i)+Urad(1,i).*Tb(1,i
)+S_pv_cv(1,i))./(Uo(1,i)+Urad(1,i)+U1(1,i));
    Tlow(1,i) =
(Umix.*TPV(1,i)+U1(1,i).*Tma(1,i)+Urad(1,i).*Tb(1,i))./(Umi
x+U1(1,i)+Urad(1,i));

    E_th_cv(1,i) = m*c*(T(1,i)-Ten(1,i));

    E_th_check(1,i) = (U1(1,i)*(TPV(1,i)-
Tma(1,i))+U2(1,i)*(Tb(1,i)-Tma(1,i)));
    error_toll = (TPV(1,i)-Tprevious)/Tprevious
    end
end

hrad_sky_avg = sum(hrad_sky)/n;
hrad_sur_avg = sum(hrad_sur)/n;
hrad_avg_sur = hrad_sky_avg+hrad_sur_avg;

TPV_avg = sum(TPV)/n;
Tb_avg = sum(Tb)/n;
Tma_avg = sum(Tma)/n;
Tma_max = max(Tma);
T_out = T(1,n)-2;
T_out

```

## 1.9 F.

# Data used

Date	Import (kW)	Export (kW)	Production (kW)	T_slab (°C)	heating_total (kW)	T_int (°C)	DNI (kW)	Outside Temp (°C)
23.01.2018 00:00	11.2	0	0	21.809	19.489	20.415	0.026	-4.61
23.01.2018 00:15	8.4	0	0	21.799	7.845	20.388	0.095	-4.327
23.01.2018 00:30	12.8	0	0	21.762	5.478	20.364	0	-4.217
23.01.2018 00:45	13.2	0	0	21.732	6.81	20.324	0	-4.063
23.01.2018 01:00	10.4	0	0	21.693	8.06	20.28	0	-3.94
23.01.2018 01:15	8.8	0	0	21.649	7.096	20.25	0.081	-3.88
23.01.2018 01:30	12	0	0	21.607	4.689	20.189	0.011	-3.863
23.01.2018 01:45	12.8	0	0	21.558	7.138	20.163	0	-3.803
23.01.2018 02:00	9.6	0	0	21.533	8.137	20.124	0	-3.767
23.01.2018 02:15	9.6	0	0	21.478	5.832	20.095	0	-3.837
23.01.2018 02:30	12.8	0	0	21.445	4.609	20.042	0	-3.783
23.01.2018 02:45	12.8	0	0	21.395	7.617	20.033	0	-3.88
23.01.2018 03:00	7.6	0	0	21.35	8.754	19.982	0	-3.96
23.01.2018 03:15	10.4	0	0	21.349	5.61	19.976	0	-4.033
23.01.2018 03:30	13.6	0	0	21.314	5.875	19.939	0	-4
23.01.2018 03:45	11.2	0	0	21.274	7.646	19.908	0	-4.17
23.01.2018 04:00	9.2	0	0	21.224	10.046	19.885	0	-4.22
23.01.2018 04:15	12.8	0	0	21.203	5.46	19.858	0	-4.283
23.01.2018 04:30	12.8	0	0	21.155	6.847	19.812	0	-4.25
23.01.2018 04:45	12.4	0	0	21.139	8.31	19.788	0.034	-4.133
23.01.2018 05:00	12.8	0	0	21.102	7.748	19.781	0	-3.947
23.01.2018 05:15	14	0	0	21.084	7.255	19.779	0	-3.7
23.01.2018 05:30	18	0	0	21.058	6.873	19.776	0	-3.47
23.01.2018 05:45	19.2	0	0	21.027	10.469	19.773	0	-3.313
23.01.2018 06:00	17.6	0	0	21.022	16.834	19.787	0	-3.157
23.01.2018 06:15	17.2	0	0	21.014	34.238	19.812	0	-2.977
23.01.2018 06:30	17.6	0	0	21.02	44.39	19.852	0	-2.843
23.01.2018 06:45	17.2	0	0	21.029	46.869	19.886	0	-2.933
23.01.2018 07:00	23.6	0	0	21.035	50.915	19.941	0	-3.16
23.01.2018 07:15	27.2	0	0	21.047	64.957	19.975	0	-3.253
23.01.2018 07:30	34.4	0	0	21.079	70.999	20.08	0	-3.387
23.01.2018 07:45	32	0	0	21.085	73.114	20.102	0	-3.597
23.01.2018 08:00	29.6	0	0.08	21.09	71.398	20.163	0	-4.27
23.01.2018 08:15	29.6	0	0.56	21.131	73.249	20.264	0	-4.44

23.01.2018 08:30	26.8	0	0.6	21.148	70.892	20.323	0	-4.587
23.01.2018 08:45	31.6	0	0.12	21.166	73.001	20.346	0	-4.84
23.01.2018 09:00	33.6	0	0.12	21.182	69.783	20.374	0	-5.037
23.01.2018 09:15	30	0	1.76	21.202	50.056	20.428	0.014	-5.157
23.01.2018 09:30	27.6	0	1.64	21.212	69.333	20.498	0.149	-4.89
23.01.2018 09:45	30.4	0	1.24	21.23	51.879	20.526	0.069	-4.423
23.01.2018 10:00	30.4	0	1.32	21.255	66.573	20.528	0	-4.08
23.01.2018 10:15	32	0	1.24	21.286	77.028	20.584	0.378	-3.92
23.01.2018 10:30	34.8	0	1.52	21.311	79.45	20.612	0.31	-3.677
23.01.2018 10:45	30.4	0	2.16	21.345	75.459	20.64	0	-3.723
23.01.2018 11:00	29.2	0	2.6	21.358	75.651	20.656	0.012	-3.693
23.01.2018 11:15	23.6	0	2.28	21.39	77.616	20.716	0	-3.58
23.01.2018 11:30	27.2	0	1.2	21.413	53.026	20.764	0.039	-3.377
23.01.2018 11:45	32.8	0	2.12	21.43	55.547	20.807	0.094	-3.367
23.01.2018 12:00	27.2	0	4	21.462	68.762	20.833	0	-3.763
23.01.2018 12:15	23.6	0	6.04	21.47	45.698	20.876	0	-3.51
23.01.2018 12:30	26	0	3.4	21.503	48.765	20.894	0	-3.257
23.01.2018 12:45	28.4	0	2.12	21.536	47.185	20.954	0	-3.297
23.01.2018 13:00	29.2	0	2.24	21.566	69.68	20.922	0	-3.267
23.01.2018 13:15	34.8	0	1.16	21.577	70.532	20.953	0	-3.397
23.01.2018 13:30	37.2	0	0.88	21.601	72.179	20.986	0.135	-3.277
23.01.2018 13:45	30.4	0	2.84	21.625	71.148	20.991	0.341	-2.973
23.01.2018 14:00	29.2	0	2.4	21.63	68.644	20.988	0.001	-2.883
23.01.2018 14:15	27.2	0	2.32	21.656	54.108	21.038	0	-2.87
23.01.2018 14:30	28.4	0	1.56	21.68	52.875	21.104	0	-2.837
23.01.2018 14:45	27.2	0	1.32	21.703	50.447	21.116	0	-3.007
23.01.2018 15:00	29.6	0	0.72	21.737	46.352	21.151	0	-3.13
23.01.2018 15:15	29.6	0	0.68	21.77	44.947	21.145	0	-3.02
23.01.2018 15:30	28	0	1.08	21.771	45.42	21.143	0	-2.997
23.01.2018 15:45	28.4	0	0.88	21.798	44.196	21.136	0	-2.983
23.01.2018 16:00	30	0	0.04	21.819	44.074	21.149	0.165	-2.963
23.01.2018 16:15	31.2	0	0	21.836	44.035	21.155	0	-3.023
23.01.2018 16:30	28.8	0	0	21.84	45.015	21.176	0	-3.053
23.01.2018 16:45	29.2	0	0	21.865	45.174	21.183	0	-3.147
23.01.2018 17:00	28.8	0	0	21.885	46.486	21.21	0	-3.227
23.01.2018 17:15	28.4	0	0	21.9	62.515	21.196	0.372	-3.103
23.01.2018 17:30	26.8	0	0	21.919	46.459	21.172	0.946	-2.987
23.01.2018 17:45	30.4	0	0	21.939	20.992	21.215	0.21	-3.023
23.01.2018 18:00	26.8	0	0	21.954	44.082	21.219	0.231	-2.98
23.01.2018 18:15	28	0	0	21.959	55.857	21.203	0.374	-2.85
23.01.2018 18:30	28	0	0	21.974	55.644	21.189	0.087	-2.773
23.01.2018 18:45	26.8	0	0	21.991	52.363	21.176	0.033	-2.697
23.01.2018 19:00	29.6	0	0	22	51.279	21.175	0	-2.647

23.01.2018 19:15	28	0	0	22.014	45.983	21.175	0	-2.66
23.01.2018 19:30	28.4	0	0	22.021	46.186	21.188	0.002	-2.603
23.01.2018 19:45	28.4	0	0	22.023	46.089	21.19	0	-2.6
23.01.2018 20:00	28.4	0	0	22.028	44.627	21.181	0	-2.483
23.01.2018 20:15	27.2	0	0	22.057	45.257	21.174	0	-2.507
23.01.2018 20:30	28	0	0	22.066	42.968	21.195	0	-2.543
23.01.2018 20:45	28	0	0	22.069	42.927	21.206	0	-2.553
23.01.2018 21:00	25.2	0	0	22.083	41.905	21.193	0	-2.57
23.01.2018 21:15	18.8	0	0	22.081	21.335	21.19	0	-2.567
23.01.2018 21:30	12.8	0	0	22.076	6.164	21.131	0	-2.49
23.01.2018 21:45	9.2	0	0	22.042	7.693	21.061	0	-2.343
23.01.2018 22:00	10	0	0	22.013	5.936	20.991	0	-2.093
23.01.2018 22:15	14.4	0	0	21.979	5.221	20.931	0	-1.54
23.01.2018 22:30	13.2	0	0	21.95	5.75	20.883	0	-0.393
23.01.2018 22:45	8	0	0	21.896	7.624	20.799	0	1.025
23.01.2018 23:00	9.6	0	0	21.871	5.752	20.749	0	1.957
23.01.2018 23:15	13.6	0	0	21.826	4.203	20.732	0	2.193
23.01.2018 23:30	11.6	0	0	21.794	6.985	20.684	0	2.223
23.01.2018 23:45	9.2	0	0	21.758	11.585	20.642	0	2.21
24.01.2018 00:00	12.4	0	0	21.734	6.111	20.597	0	2.26
24.01.2018 00:15	14	0	0	21.682	1.031	20.565	0	2.26
24.01.2018 00:30	10	0	0	21.639	7.473	20.53	0	2.24
24.01.2018 00:45	8	0	0	21.593	7.392	20.517	0	2.143
24.01.2018 01:00	14.4	0	0	21.573	6.041	20.503	0	2.067
24.01.2018 01:15	14	0	0	21.537	5.931	20.491	0	2.047
24.01.2018 01:30	8.4	0	0	21.503	7.701	20.467	0	2.06
24.01.2018 01:45	9.6	0	0	21.471	6.111	20.436	0	1.89
24.01.2018 02:00	14.8	0	0	21.443	4.673	20.41	0	1.823
24.01.2018 02:15	11.6	0	0	21.409	5.873	20.376	0	1.803
24.01.2018 02:30	8	0	0	21.372	8.327	20.351	0	1.673
24.01.2018 02:45	10.4	0	0	21.347	5.944	20.344	0	1.378
24.01.2018 03:00	14	0	0	21.313	2.523	20.333	0	0.409
24.01.2018 03:15	11.2	0	0	21.288	7.126	20.327	0	-0.577
24.01.2018 03:30	8.8	0	0	21.257	6.93	20.252	0	-1.417
24.01.2018 03:45	14.4	0	0	21.23	4.917	20.221	0	-2.653
24.01.2018 04:00	13.6	0	0	21.197	7.218	20.198	0	-3.413
24.01.2018 04:15	12.8	0	0	21.17	7.524	20.14	0	-3.863
24.01.2018 04:30	13.6	0	0	21.155	7.242	20.137	0	-4.603
24.01.2018 04:45	13.6	0	0	21.144	8.264	20.134	0	-5.297
24.01.2018 05:00	13.6	0	0	21.125	7.933	20.136	0	-5.827
24.01.2018 05:15	13.6	0	0	21.108	7.605	20.119	0	-6.387
24.01.2018 05:30	16.8	0	0	21.103	7.734	20.099	0	-6.777
24.01.2018 05:45	17.2	0	0	21.089	10.265	20.113	0	-7.03

24.01.2018 06:00	16.8	0	0	21.097	13.412	20.11	0	-7.243
24.01.2018 06:15	17.6	0	0	21.103	15.766	20.117	0	-7.463
24.01.2018 06:30	18	0	0	21.105	18.946	20.141	0	-7.757
24.01.2018 06:45	17.6	0	0	21.109	40.178	20.161	0	-8.09
24.01.2018 07:00	23.2	0	0	21.121	46.48	20.195	0	-8.2
24.01.2018 07:15	26	0	0	21.126	65.374	20.225	0	-8.263
24.01.2018 07:30	23.6	0	0	21.154	61.602	20.258	0	-8.533
24.01.2018 07:45	32.4	0	0.12	21.168	64.032	20.294	0	-8.643
24.01.2018 08:00	25.2	0	3.6	21.169	71.506	20.361	0.093	-8.94
24.01.2018 08:15	22	0	8.4	21.193	75.692	20.458	43.917	-9.197
24.01.2018 08:30	23.6	0	10.76	21.215	79.812	20.547	557.723	-9.347
24.01.2018 08:45	21.2	0	12.56	21.227	74.323	20.745	693.547	-9.41
24.01.2018 09:00	20	0	14.24	21.254	73.833	20.873	736.643	-9.543
24.01.2018 09:15	18.8	0	15.56	21.297	77.594	21.069	695.347	-9.617
24.01.2018 09:30	22	0	13.96	21.347	77.478	21.184	418.6	-9.59
24.01.2018 09:45	20.4	0	16.16	21.442	66.024	21.298	425.56	-9.477
24.01.2018 10:00	16.4	0	16.96	21.537	72.088	21.385	95.029	-9.5
24.01.2018 10:15	14	0	18.52	21.619	56.123	21.5	38.364	-9.623
24.01.2018 10:30	15.2	0	16.32	21.713	52.326	21.615	65.591	-9.59
24.01.2018 10:45	18.8	0	13.16	21.801	48.517	21.716	117.93	-9.517
24.01.2018 11:00	14.8	0	17.56	21.88	43.673	21.79	474.657	-9.347
24.01.2018 11:15	12	0	18.92	21.979	43.263	21.863	737.943	-9.197
24.01.2018 11:30	13.2	0.22	14.32	22.085	41.925	21.934	522.69	-8.877
24.01.2018 11:45	0.4	1.552	21.08	22.154	37.736	21.956	290.569	-8.713
24.01.2018 12:00	7.6	0.212	18.04	22.218	26.895	22.087	100.18	-8.963
24.01.2018 12:15	7.6	0.14	16.84	22.261	28.906	22.13	17.914	-8.833
24.01.2018 12:30	12.4	0.024	13.36	22.332	14.587	22.172	6.524	-8.777
24.01.2018 12:45	16.4	0	8.44	22.413	25.38	22.197	27.167	-8.73
24.01.2018 13:00	9.6	0	16.6	22.48	24.252	22.137	135.947	-8.51
24.01.2018 13:15	5.6	0	17.32	22.521	10.838	22.155	387.587	-8.177
24.01.2018 13:30	8.4	0	15.52	22.528	21.132	22.171	665.81	-8.017
24.01.2018 13:45	7.6	0	15.64	22.545	20.104	22.238	788.187	-7.943
24.01.2018 14:00	9.6	0	13.48	22.57	20.573	22.289	437.363	-8.013
24.01.2018 14:15	12.8	0	12.28	22.569	19.908	22.327	375.957	-8.017
24.01.2018 14:30	18	0	11.2	22.576	19.425	22.393	621.653	-7.717
24.01.2018 14:45	21.6	0	7.96	22.577	18.334	22.406	724.853	-7.643
24.01.2018 15:00	23.2	0	6	22.576	19.381	22.421	610.193	-7.7
24.01.2018 15:15	23.6	0	6.04	22.576	19.595	22.378	527.923	-7.62
24.01.2018 15:30	24.4	0	3.8	22.586	18.4	22.345	503.71	-7.577
24.01.2018 15:45	27.6	0	1.72	22.587	18.184	22.329	450.907	-7.463
24.01.2018 16:00	30.4	0	0.8	22.586	17.506	22.276	127.269	-7.55
24.01.2018 16:15	29.6	0	0.12	22.578	15.349	22.198	65.997	-7.64
24.01.2018 16:30	25.6	0	0	22.567	16.784	22.123	24.08	-7.857

24.01.2018 16:45	24	0	0	22.557	18.331	22.05	6.262	-7.967
24.01.2018 17:00	23.2	0	0	22.546	17.559	21.974	0	-7.997
24.01.2018 17:15	24.8	0	0	22.525	7.78	21.889	0	-8.043
24.01.2018 17:30	26.4	0	0	22.502	16.586	21.859	0	-8.227
24.01.2018 17:45	25.2	0	0	22.475	21.206	21.788	0	-8.523
24.01.2018 18:00	23.2	0	0	22.45	19.41	21.716	0	-8.807
24.01.2018 18:15	24	0	0	22.433	20.174	21.664	0	-9.3
24.01.2018 18:30	28.4	0	0	22.418	22.477	21.636	0	-9.64
24.01.2018 18:45	31.6	0	0	22.402	30.227	21.544	0	-9.79
24.01.2018 19:00	30.8	0	0	22.368	33.187	21.532	0	-9.977
24.01.2018 19:15	28.8	0	0	22.331	35.332	21.511	0	-10.333
24.01.2018 19:30	28.4	0	0	22.312	36.404	21.513	0	-10.5
24.01.2018 19:45	29.6	0	0	22.285	13.689	21.451	0	-10.333
24.01.2018 20:00	31.2	0	0	22.267	25.673	21.396	0	-10.667
24.01.2018 20:15	27.2	0	0	22.248	40.881	21.36	0	-10.667
24.01.2018 20:30	28	0	0	22.232	42.494	21.346	0	-10.733
24.01.2018 20:45	26.4	0	0	22.201	40.675	21.333	0	-10.833
24.01.2018 21:00	22.4	0	0	22.191	45.044	21.294	0	-11.1
24.01.2018 21:15	20.8	0	0	22.18	11.991	21.242	0	-11.367
24.01.2018 21:30	16.8	0	0	22.146	7.544	21.167	0	-11.467
24.01.2018 21:45	12	0	0	22.121	8.559	21.092	0	-11.6
24.01.2018 22:00	10.8	0	0	22.083	7.385	20.988	0	-11.733
24.01.2018 22:15	14.8	0	0	22.046	4.499	20.887	0	-11.9
24.01.2018 22:30	14.8	0	0	22.012	7.406	20.834	0	-11.933
24.01.2018 22:45	14.4	0	0	21.992	8.164	20.778	0	-12.033
24.01.2018 23:00	14.8	0	0	21.941	8.539	20.723	0	-12.167
24.01.2018 23:15	18.4	0	0	21.905	8.157	20.704	0	-12.367
24.01.2018 23:30	19.2	0	0	21.884	10.83	20.629	0	-12.567
24.01.2018 23:45	19.2	0	0	21.874	15.798	20.633	0	-12.733
25.01.2018 00:00	13.2	0	0	21.846	18.603	20.616	0	-12.933
25.01.2018 00:15	11.6	0	0	21.838	6.822	20.59	0	-13.067
25.01.2018 00:30	14.4	0	0	21.811	4.718	20.529	0	-13.233
25.01.2018 00:45	14.4	0	0	21.77	7.467	20.472	0	-13.267
25.01.2018 01:00	13.2	0	0	21.732	8.544	20.398	0	-13.5
25.01.2018 01:15	9.6	0	0	21.696	8.78	20.345	0	-13.7
25.01.2018 01:30	12.8	0	0	21.659	5.927	20.286	0	-13.8
25.01.2018 01:45	14.4	0	0	21.604	6.468	20.232	0	-14
25.01.2018 02:00	15.2	0	0	21.577	7.884	20.174	0	-14.167
25.01.2018 02:15	14	0	0	21.536	8.64	20.142	0	-14.3
25.01.2018 02:30	9.6	0	0	21.515	8.516	20.101	0	-14.5
25.01.2018 02:45	12.8	0	0	21.455	5.346	20.025	0	-14.7
25.01.2018 03:00	14	0	0	21.429	6.805	19.991	0	-14.867
25.01.2018 03:15	15.6	0	0	21.373	8.123	19.933	0	-14.733

25.01.2018 03:30	14.8	0	0	21.334	8.089	19.875	0	-14.767
25.01.2018 03:45	10.4	0	0	21.294	9.012	19.827	0	-14.933
25.01.2018 04:00	14	0	0	21.253	5.318	19.802	0	-15.267
25.01.2018 04:15	14	0	0	21.216	6.761	19.731	0	-15.467
25.01.2018 04:30	14	0	0	21.17	8.034	19.689	0	-15.533
25.01.2018 04:45	15.6	0	0	21.146	7.811	19.668	0	-15.667
25.01.2018 05:00	15.6	0	0	21.106	11.983	19.637	0	-15.733
25.01.2018 05:15	15.6	0	0	21.078	2.905	19.617	0	-15.833
25.01.2018 05:30	18.8	0	0	21.057	19.149	19.586	0	-15.967
25.01.2018 05:45	18.4	0	0	21.032	13.493	19.569	0	-16.133
25.01.2018 06:00	19.2	0	0	21	16.518	19.582	0	-16.167
25.01.2018 06:15	25.2	0	0	20.99	17.752	19.602	0	-16.167
25.01.2018 06:30	24	0	0	20.995	36.096	19.605	0	-16.267
25.01.2018 06:45	24	0	0	20.989	37.279	19.654	0	-16.333
25.01.2018 07:00	20.8	0	0	20.995	37.22	19.669	0	-16.4
25.01.2018 07:15	26.4	0	0.12	20.998	53.439	19.71	0	-16.4
25.01.2018 07:30	24.8	0	2	21.009	68.84	19.729	0	-16.5
25.01.2018 07:45	29.6	0	4.2	21.027	58.881	19.763	310.843	-16.433
25.01.2018 08:00	26.8	0	6.52	21.018	73.583	19.823	521.52	-16.4
25.01.2018 08:15	19.2	0	8.48	21.026	79.736	19.93	605.97	-16.333
25.01.2018 08:30	19.6	0	10.68	21.039	60.517	20.067	657.19	-16.233
25.01.2018 08:45	18.8	0	12.48	21.048	56.227	20.206	733.8	-16.033
25.01.2018 09:00	18	0	14.16	21.069	75.704	20.358	775.55	-15.9
25.01.2018 09:15	14.8	0	15.64	21.109	82.648	20.611	806.883	-15.8
25.01.2018 09:30	13.2	0	17.08	21.163	51.121	20.786	836.107	-15.8
25.01.2018 09:45	8.4	0	18.36	21.236	56.996	20.915	862.55	-15.633
25.01.2018 10:00	8	0	19.44	21.31	71.089	21.024	882.073	-15.4
25.01.2018 10:15	6.4	0	20.24	21.407	69.159	21.138	895.137	-15.333
25.01.2018 10:30	0.4	0.42	21.08	21.506	50.808	21.277	905.41	-15.2
25.01.2018 10:45	1.2	0.12	21.68	21.599	51.948	21.383	915.363	-14.9
25.01.2018 11:00	3.6	0	22.16	21.699	51.874	21.497	921.85	-14.7
25.01.2018 11:15	7.2	0	22.36	21.8	52.754	21.584	922.083	-14.567
25.01.2018 11:30	6	0	22.24	21.897	50.762	21.677	927.417	-14.233
25.01.2018 11:45	6.4	0	22.36	21.999	45.962	21.723	927.28	-14
25.01.2018 12:00	7.6	0	22.32	22.103	44.212	21.784	929.913	-13.8
25.01.2018 12:15	6.8	0	21.84	22.21	40.121	21.832	932.07	-13.6
25.01.2018 12:30	12	0	21.52	22.285	36.792	21.898	931.237	-13.4
25.01.2018 12:45	14.8	0	20.88	22.357	38.632	21.91	923.143	-12.9
25.01.2018 13:00	10.4	0	20.28	22.431	39.716	21.986	917.47	-12.7
25.01.2018 13:15	12	0	19.2	22.503	24.888	22.04	910.517	-12.467
25.01.2018 13:30	15.2	0	18.36	22.534	16.809	22.081	898.137	-12.267
25.01.2018 13:45	14.4	0	16	22.56	38.522	22.11	884.847	-12
25.01.2018 14:00	12.4	0	14.72	22.573	36.858	22.125	817.927	-11.6

25.01.2018 14:15	16.8	0	13.36	22.574	29.958	22.135	802.273	-11.4
25.01.2018 14:30	23.6	0	6.28	22.58	32.622	22.174	662.733	-11.233
25.01.2018 14:45	23.2	0	2.52	22.589	12.558	22.161	53.043	-11.533
25.01.2018 15:00	22.8	0	1.36	22.588	22.755	22.101	2.754	-11.5
25.01.2018 15:15	23.2	0	1	22.595	26.03	21.991	7.79	-11.5
25.01.2018 15:30	24.4	0	1	22.575	21.672	21.906	6.624	-11.5
25.01.2018 15:45	23.2	0	0.64	22.571	21.596	21.8	0.482	-11.433
25.01.2018 16:00	27.2	0	0.16	22.545	20.704	21.684	7.984	-11.3
25.01.2018 16:15	28.4	0	0	22.522	32.195	21.636	0.464	-11.233
25.01.2018 16:30	27.6	0	0	22.506	33.453	21.553	58.019	-11.2
25.01.2018 16:45	27.6	0	0	22.462	33.123	21.507	7.813	-11.167
25.01.2018 17:00	29.2	0	0	22.464	35.434	21.448	0	-11.067
25.01.2018 17:15	29.2	0	0	22.446	37.232	21.398	0	-11
25.01.2018 17:30	29.2	0	0	22.436	39.049	21.351	0	-10.933
25.01.2018 17:45	28.4	0	0	22.424	43.294	21.333	0	-10.9
25.01.2018 18:00	32	0	0	22.409	45.28	21.306	0	-10.8
25.01.2018 18:15	32.4	0	0	22.392	57.988	21.291	0	-10.833
25.01.2018 18:30	34	0	0	22.38	56.327	21.258	0	-10.833
25.01.2018 18:45	30	0	0	22.385	58.015	21.223	0	-11
25.01.2018 19:00	29.6	0	0	22.379	46.807	21.236	0	-11
25.01.2018 19:15	29.2	0	0	22.37	47.598	21.233	0	-11.033
25.01.2018 19:30	30.4	0	0	22.372	46.784	21.233	0	-11.1
25.01.2018 19:45	32.8	0	0	22.345	47.715	21.222	0	-11.167
25.01.2018 20:00	31.6	0	0	22.333	62.644	21.21	0	-11.3
25.01.2018 20:15	36.8	0	0	22.33	60.093	21.206	0	-11.3
25.01.2018 20:30	33.2	0	0	22.327	61.655	21.227	0	-11.333
25.01.2018 20:45	34	0	0	22.309	61.477	21.218	0	-11.5
25.01.2018 21:00	23.2	0	0	22.311	62.088	21.176	0	-11.5
25.01.2018 21:15	20.8	0	0	22.316	9.656	21.13	0	-11.5
25.01.2018 21:30	19.6	0	0	22.264	7.957	20.995	0	-11.567
25.01.2018 21:45	19.2	0	0	22.221	8.702	20.921	0	-11.533
25.01.2018 22:00	20.4	0	0	22.178	8.993	20.828	0	-11.633
25.01.2018 22:15	20	0	0	22.144	7.998	20.79	0	-11.7
25.01.2018 22:30	16.4	0	0	22.121	8.115	20.747	0	-11.7
25.01.2018 22:45	19.6	0	0	22.096	7.601	20.677	0	-11.667
25.01.2018 23:00	14.8	0	0	22.08	10.353	20.59	0	-11.567
25.01.2018 23:15	18	0	0	22.05	7.775	20.566	0	-11.6
25.01.2018 23:30	18	0	0	22.033	13.053	20.522	0	-11.6
25.01.2018 23:45	18.8	0	0	22.012	16.808	20.514	0	-11.8
26.01.2018 00:00	13.2	0	0	22	18.522	20.478	0	-11.933
26.01.2018 00:15	10.4	0	0	21.988	6.185	20.449	0	-11.933
26.01.2018 00:30	14.4	0	0	21.941	4.727	20.351	0	-11.933
26.01.2018 00:45	14	0	0	21.907	8.091	20.284	0	-11.933

26.01.2018 01:00	13.2	0	0	21.864	8.779	20.229	0	-12
26.01.2018 01:15	10.8	0	0	21.821	8.894	20.189	0	-12.333
26.01.2018 01:30	11.2	0	0	21.777	6.456	20.148	0	-12.433
26.01.2018 01:45	13.6	0	0	21.722	4.772	20.077	0	-12.7
26.01.2018 02:00	13.2	0	0	21.684	8.009	20.033	0	-12.8
26.01.2018 02:15	13.6	0	0	21.619	8.357	19.963	0	-12.7
26.01.2018 02:30	12.4	0	0	21.587	7.994	19.927	0	-12.967
26.01.2018 02:45	8.8	0	0	21.529	9.162	19.865	0	-13.233
26.01.2018 03:00	12.4	0	0	21.499	5.455	19.827	0	-13.533
26.01.2018 03:15	13.6	0	0	21.446	7.778	19.783	0	-14.233
26.01.2018 03:30	13.6	0	0	21.409	7.939	19.73	0	-14
26.01.2018 03:45	13.6	0	0	21.358	7.976	19.695	0	-13.733
26.01.2018 04:00	10.8	0	0	21.321	8.902	19.646	0	-14.1
26.01.2018 04:15	11.2	0	0	21.27	5.543	19.583	0	-14.267
26.01.2018 04:30	13.6	0	0	21.236	6.931	19.529	0	-15.233
26.01.2018 04:45	17.2	0	0	21.194	7.542	19.501	0	-15.8
26.01.2018 05:00	14.4	0	0	21.162	10.464	19.492	0	-16.1
26.01.2018 05:15	16.4	0	0	21.126	6.433	19.461	0	-16.333
26.01.2018 05:30	18	0	0	21.09	12.472	19.437	0	-16.433
26.01.2018 05:45	18.4	0	0	21.071	15.846	19.437	0	-16.433
26.01.2018 06:00	22.8	0	0	21.047	17.426	19.414	0	-16.933
26.01.2018 06:15	23.6	0	0	21.038	36.099	19.435	0	-17.2
26.01.2018 06:30	24	0	0	21.028	37.415	19.46	0	-16.8
26.01.2018 06:45	23.6	0	0	21.03	37.682	19.511	0	-17.033
26.01.2018 07:00	20.4	0	0	21.026	37.546	19.533	0	-16.867
26.01.2018 07:15	22	0	0.24	21.025	54.045	19.556	0	-17.267
26.01.2018 07:30	25.6	0	1.52	21.04	69.226	19.6	0.39	-17
26.01.2018 07:45	25.2	0	3.88	21.027	67.149	19.605	306.033	-16.867
26.01.2018 08:00	25.2	0	6.64	21.031	76.771	19.64	478.293	-16.367
26.01.2018 08:15	22.4	0	9.12	21.025	77.282	19.719	566.29	-16.8
26.01.2018 08:30	20	0	11.56	21.025	77.216	19.874	645.597	-17.233
26.01.2018 08:45	18	0	13.56	21.035	76.604	19.987	700.837	-17.133
26.01.2018 09:00	16	0	15.48	21.064	93.05	20.151	742.023	-17.133
26.01.2018 09:15	12.8	0	17.28	21.102	94.191	20.386	775.977	-15.667
26.01.2018 09:30	11.6	0	19	21.15	93.929	20.616	804.26	-15.033
26.01.2018 09:45	7.2	0	20.6	21.215	59.715	20.795	826.767	-13.9
26.01.2018 10:00	8.4	0	22.12	21.309	79.005	20.908	842.833	-13.533
26.01.2018 10:15	4.4	0	23.48	21.404	77.113	21.024	844.13	-14.267
26.01.2018 10:30	3.6	0	25.16	21.513	73.41	21.115	851.99	-14.767
26.01.2018 10:45	4	0	25.24	21.583	66.714	21.191	812.44	-14.7
26.01.2018 11:00	0	2.28	28.12	21.691	68.068	21.25	832.777	-14.333
26.01.2018 11:15	0	6.64	29.56	21.796	54.07	21.366	867.553	-13.833
26.01.2018 11:30	0	6.328	31.08	21.874	56.49	21.41	874.293	-13.4

26.01.2018 11:45	0	8.392	32.36	21.974	47.65	21.48	878.08	-12.967
26.01.2018 12:00	0	9.804	33.44	22.071	55.758	21.562	881.09	-13.167
26.01.2018 12:15	0	12.796	35.28	22.173	45.214	21.649	869.807	-12.8
26.01.2018 12:30	0	8.744	36.44	22.259	42.193	21.713	878.717	-12.4
26.01.2018 12:45	0	7.168	36.2	22.369	42.508	21.764	829.53	-10.733
26.01.2018 13:00	0	11.412	36.8	22.452	42.366	21.833	828.36	-9.453
26.01.2018 13:15	0	11.052	37.2	22.54	32.793	21.899	813.88	-9.32
26.01.2018 13:30	0	9.52	36.84	22.582	40.561	21.929	781.61	-9.197
26.01.2018 13:45	0	7.856	35.72	22.597	39.07	21.979	809.803	-8.75
26.01.2018 14:00	0	6.136	33.24	22.606	38.448	22.047	791.713	-9.537
26.01.2018 14:15	0	3.256	30.44	22.598	20.748	22.123	748.267	-9.427
26.01.2018 14:30	1.6	0.004	27.96	22.618	18.717	22.162	727.51	-9.647
26.01.2018 14:45	4.4	0	24.56	22.618	23.986	22.165	714.46	-9.387
26.01.2018 15:00	10	0	20.6	22.606	22.315	22.155	657.523	-9.867
26.01.2018 15:15	12	0	16.44	22.602	21.721	22.155	602.337	-9.953
26.01.2018 15:30	10	0	12.44	22.595	20.558	22.143	507.093	-9.73
26.01.2018 15:45	14.4	0	8.12	22.585	17.814	22.076	437.17	-9.363
26.01.2018 16:00	19.6	0	3.48	22.572	16.162	21.991	247.463	-8.73
26.01.2018 16:15	22.8	0	0.88	22.569	15.762	21.88	69.591	-9.483
26.01.2018 16:30	23.6	0	0.04	22.567	15.994	21.785	11.991	-10.027
26.01.2018 16:45	23.6	0	0	22.558	17.705	21.686	10.449	-10.6
26.01.2018 17:00	24.8	0	0	22.528	17.984	21.643	0	-10.967
26.01.2018 17:15	26	0	0	22.506	21.382	21.521	0	-11.1
26.01.2018 17:30	27.2	0	0	22.487	38.044	21.476	0	-11.3
26.01.2018 17:45	27.6	0	0	22.442	37.129	21.389	0	-11.567
26.01.2018 18:00	28.4	0	0	22.45	40.669	21.367	0	-11.7
26.01.2018 18:15	30.4	0	0	22.42	38.124	21.354	0	-11.867
26.01.2018 18:30	24.4	0	0	22.379	52.948	21.283	0	-12.033
26.01.2018 18:45	20.8	0	0	22.365	53.554	21.253	0	-11.967
26.01.2018 19:00	20	0	0	22.361	46.201	21.194	0	-11.833
26.01.2018 19:15	20.4	0	0	22.356	48.245	21.122	0	-12.633
26.01.2018 19:30	26.4	0	0	22.335	47.202	21.055	0	-12.4
26.01.2018 19:45	30.4	0	0	22.324	65.449	21.003	0	-12.533
26.01.2018 20:00	30.4	0	0	22.32	71.07	21	0	-13.467
26.01.2018 20:15	28.4	0	0	22.33	67.062	20.998	0	-13.5
26.01.2018 20:30	26.4	0	0	22.322	66.269	20.985	0	-13.267
26.01.2018 20:45	25.6	0	0	22.3	66.647	20.95	0	-13.9
26.01.2018 21:00	21.6	0	0	22.289	68.321	20.901	0	-14.267
26.01.2018 21:15	14	0	0	22.283	16.896	20.887	0	-14.3
26.01.2018 21:30	14	0	0	22.262	8.435	20.813	0	-14.5
26.01.2018 21:45	13.2	0	0	22.223	8.416	20.686	0	-14.5
26.01.2018 22:00	8.8	0	0	22.188	9.374	20.627	0	-14.5
26.01.2018 22:15	12.4	0	0	22.122	6.121	20.51	0	-14.567

26.01.2018 22:30	13.2	0	0	22.084	7.646	20.42	0	-14.5
26.01.2018 22:45	17.6	0	0	22.037	7.477	20.408	0	-14.3
26.01.2018 23:00	18.8	0	0	22.011	10.741	20.343	0	-14.4
26.01.2018 23:15	18	0	0	21.985	10.012	20.278	0	-14.633
26.01.2018 23:30	19.2	0	0	21.958	14.83	20.28	0	-14.8
26.01.2018 23:45	19.6	0	0	21.95	17.212	20.285	0	-14.8